ELECTROADHESIVE CLUTCHES MADE FROM HIGH DIELECTRIC-CONSTANT POLYMERIC MATERIALS AND FLEXIBLE ELECTRODES

JUN LI

PhD

The Hong Kong Polytechnic University

2021

The Hong Kong Polytechnic University

Institute of Textiles and Clothing

ELECTROADHESIVE CLUTCHES MADE FROM HIGH DIELECTRIC-CONSTANT POLYMERIC MATERIALS AND FLEXIBLE ELECTRODES

JUN LI

A thesis submitted in partial fulfilment of the requirements for the degree of Doctor of Philosophy

January 2021

CERTIFICATE OF ORIGINALITY

I hereby declare that this thesis is my own work and that, to the best of my knowledge and belief, it reproduces no material previously published or written, nor material that has been accepted for the award of any other degree or diploma, expect where due acknowledgement has been made in the text.

_____ (Signed)

LI JUN (Name of student)

ABSTRACT

Electroadhesive clutches based on the electrostatic attraction of the two electroadhesive pads have shown promising application in wearable and haptic systems due to their flexibility, fast response, light weight, low power consumption, easy fabrication as compared with the traditional clutch technologies. Electroadhesive clutches could also be easily integrated into the current electrical or robotic systems. Though the electroadhesive clutches have been investigated for several decades, it remains a challenge to develop clutches with large electroadhesive forces at low driving-voltage. Hence this thesis presents a systematic research towards high-performance clutches with an emphasis on material selection and clutch structure optimization.

Symmetric clutches made from high dielectric constant P(VDF-TrFE-CFE) terpolymers were firstly developed through direct blade coating on Al foil electrodes followed by annealing at 120 ^{o}C overnight. The surface roughness, chemical and dielectric propertiesof the dielectric materials as well as the mechanical properties of the electrodes were systematically investigated. The relationships and response time have been experimentally determined and evaluated including those between the voltage and adhesiveforce, dielectric thickness and force, as well as overlapping area and force. A symmetric-structured electroadhesive clutch could response at 80 V, its electroadhesive force increased dramatically with the increase of applied voltage. A

shear stress over 100 kPa was generated at 120 V (DC) with a power consumption as low as 5.56 μW. A new laboratory-made testing apparatus was established for the response time of the clutch. The engage time and release time were ~25 ms and ~324 ms respectively. Furthermore, the change of bending stiffness of the clutch under different working voltages was investigated. The bending stiffness of the clutch at 120 V was about 2-time higher than the non-engaged clutch. In addition, the clutch response to AC square-wave voltage was evaluated for the first time, which was comparable with the clutch's DC-driving performance.

To evaluate the influence of the charge characteristics of the dielectric materials to the clutch performance, asymmetric clutches made from PU/PTFE and PU/PI were fabricated by blade coating. Their responses to DC voltage were systematically studied. The electroadhesive force was increased when the polarity of the induced charges is the same as the charge characteristics of dielectric materials. The asymmetric PU25/PI5 clutch exhibited a highest shear stress of ~ 200 kPa at 300 V with an engage time of ~ 20 ms and a release time longer than 15 mins. Reversible chemical adhesion due to the formation of abundant hydrogen bonds at the PU/PI interface was attribute to the clutch performance characteristics. A multi-mechanism of the asymmetric PU/PI clutch was postulated to originate from the integration of interfacial H-bonds, electrostatic attraction and charge characteristics of the dielectric materials.

High-*k* polymer composites with tunable dielectric properties were developed with *in situ* thermal reduction of GO in P(VDF-TrFE-CFE) matrix. The linear relationship between the dielectric constant (at 100 Hz) and reduction time was observed for the first time. The GO has been demonstrated to be partially reduced (PRGO) at the relatively low reduction temperature of 120 ^{o}C by using Raman and FTIR spectra. A relative dielectric constant as high as 1480 with a tan δ of 0.283 at 100 Hz was obtained at a doping ratio of 4 wt%. A clutch-type pressure sensor made of the high-*k* PRGO/PVDF-FS composites has been demonstrated. The pressure-current relationship at a constant voltage, current-voltage relationship under a constant pressure and pressure sensing behaviour for long time were experimentally determined and analyzed. The pressure sensor exhibited a good linearity at a relatively high pressure range (100 kPa to 1 MPa) but was not favourable for lower pressure range or used for a long time. The mechanism of the current change under external forces was also explored and was attribute to the leakage current of the microcapacitors in the high-*k* composites.

PUBLICATION LISTS

Referred Journal papers

[1] **J. Li**, W.-Y. Wong, X. Tao, *Nanoscale* **2020**, *12*, 1281.

[2] Z. Zhang, **J. Li**, L. Ma, X. Yang, B. Fei, P. H. M. Leung, X. Tao, *Polymers.* **2020**, *12*, 2735.

[3] L. Ma, Z. Zhang, **J. Li**, X. Yang, B. Fei, P. H. M. Leung, X. Tao, *Macromol. Biosci.* **2019**, *19*, 1800432.

[4] J. Song, B. Yang, W. Zeng, Z. Peng, S. Lin, **J. Li**, X. Tao, *Adv. Mater. Technol.* **2018**, *3*, 1800016.

[5] R. Yin, B. Yang, X. Ding, S. Liu, W. Zeng, **J. Li**, S. Yang, X. Tao, *Adv. Mater. Technol.* **2020**, *5*, 2000341.

ACKNOWLEDGEMENTS

I would like to express my deepest thanks to my supervisor Prof. Xiaoming Tao for her encouragement, support and invaluable suggestions throughout the research project. Prof. Tao is an experienced scientist in textile, flexible electronics and wearable devices and she also serves as an excellent advisor and a generous supporter during my research program. The insightful discussions and professional suggestions from her inspired me a lot. I would also like to show my sincere gratitude to my co-supervisor Prof. Raymond W.-Y. Wong for his kind assistance and suggestions in this project.

Sincere appreciation is given to Prof. Jiyan Dai (Department of Applied Physics) and his Ph.D student Mr. Chiman Wong for their help in the measurement of the dielectric properties. I am also thankful to Mr. Jiangtao Xu and Ms. Jing Yang for their help in sputtering and laser cutting.

I would like to thank my research group members, Prof. Wei Chen, Dr. Wei Zeng, Dr. Bao Yang, Dr. Xi Wang, Dr. Jianliang Gong, Dr. Jian Song, Dr. Rong Yin, Dr. Lisha Zhang, Dr. Ziheng Zhang, Dr. Bo Fong, Dr. Qi Bao, Ms. Ying Li, Ms. Ying Xiong, Ms. Shuping Lin, Ms. Su Liu, Ms. Linlin Ma, Mr. Jin Liu, Mr. Linqi Pan, Mr. Zehua Peng, Ms. Yufei Xiang, Ms. Su Yang, Ms Xujiao Ding, Ms. Ching Lee, Mr. Shirui Liu, Mr. Jingyang Wu, Mr. Heng Luo and Ms. Xingxing Yang for their help and support in my research and life.

In addition, I would like to give special thanks to the scientific officers and staff in the Institute of Textile and Clothing for their technical support and help.

Last but not least, I would also like to thank my family members for their help, support and encouragement during my course of study. Special thanks to my wife Dr. Yurong Liu for her continued support and endless love.

TABLE OF CONTENTS

LIST OF FIGURES

LIST OF TABLES

SYMBOLS

T	Maxwell stress tensor
E	Young's modulus
F	Electroadhesive force
k	Dielectric constant
σ	Conductivity
Φ	Diameter
ε'	Real part of dielectric constant
ε''	Imaginary part of dielectric constant
ε_r	Relative dielectric constant
ε_0	Vacuum dielectric constant
tan δ	Loss tangent
C	Capacitance
G	Flexural rigidity
W	Mass per unit area, g/m2
c	Bending length,mm
Sa	Arithmetical mean height
Sq	Root mean square height
Sz	Maximum height
A	Overlapping area
T	Dielectric thickness

ABBREVIATIONS

DC	Direct current
AC	Alternative current
P(VDF-TrFE-CFE)	Poly (vinylidene-fluoride-trifluoroethylene-chloro- fluoroethylene)
PTFE	Polytetrafluoroethylene
PI	Polyimide
PU	Polyurethane
SEM	The scanning electron microscope
GO	Graphene oxide
J-R effect	The Johnsen-Rahbek effect
DEA	Dielectric elastomer actuator
PE	Polyethylene
PP	Polypropylene
ER	Electrorheological
PCB	Printed circuit board
FEA	Fluidic elastomer actuator
SLJB	Soft layer jamming brake
PMC	Polymer matrix composite
RF	Radio frequency
OFET	Organic filed-effect transistor
PZT	Lead zirconate titanate

BTO	Barium titanate
CCTO	$CaCu_3Ti_4O_{12}$
ZrO_2	Zirconium dioxide
PVDF	Polyvinylidene fluoride
PDMS	Polydimethylsiloxane
PVP	Polyvinylpyrrolidone
ST NF	$SrTiO_3$ nanofiber
BNNS	Boron nitride nanosheet
CuPc	Copper phthalocyanine
CNT	Carbon nanotube
Ag NW	Silver nanowire
HNBR	Hydrogenated nitrile butadiene rubber
PBZ	Polybenzoxazine
MC	Microwave curing
TC	Thermal curing
RGO	Reduced graphene oxide
PDA	Polydopamine
PANI	Polyaniline
HBA	Hyperbranched aromatic polyamide
HTPB	(1-Hexadecyl) triphenylphosphonium bromide
PVA	Poly (vinyl alcohol)
EBA-GMA	Ethylene/n-butyl acrylate/glycidyl methacrylate terpolymer

GA	Graphene aerogel
FLG	Few-layer graphene
SIN	Substitute It Now
FE	Flexible electrode
PVD	Physical vapor deposition
ITO	Indium tin oxide
BOPET	Bi-axially Oriented Polyethylene Terephthalate
SWCNT	Single wall carbon nanotube
CVD	Chemical vapor deposition
R2R	Roll-to-roll
ECG	Electrocardiography
PPy	Polypyrrole
PTh	Polythiophene
PEDOT:PSS	Poly (3,4-ethylenedioxythiophene):polystyrene sulfonate
OECT	Organic electrochemical transistor
OLED	Organic light-emitting diode
TEG	Thermal electric generator
LIG	Laser-induced graphene
SEBS	Styrene ethylene butylene styrene
PAMD	Polymer-assisted metal deposition
LEC	Light-emitting electrochemical cell
IPA	Isopropyl alcohol

THF	Tetrahydrofuran
DMF	N, N-Dimethylformamide
BA	Butyl acetate
ATR-FTIR	Attenuated total reflection Fourier-transform infrared spectroscopy
Pr	Remnant polarization
TENG	Triboelectric nanogenerator
RH	Relative humidity
PVC	Polyvinyl chloride
PRGO	Partially reduced graphene oxide
wt%	Weight percentage

CHAPTER 1 Introduction

1.1 Background

Adhesion is a kind of connection of a particle or surface to another substance.[1] Based on the mechanism of adhesive behavior, adhesion could mainly be divided into chemical and physical adhesion. Chemical adhesion is generally depending on the formation of ionic or covalent bonds[2–4] and is always sticky. Mechanisms for physical adhesion consist of negative air pressure, magnetic force, Van der Waals force and electrostatic attraction. One of the major advantages of physical attachments over chemical adhesion is the reversibility. However, physical connections based on van der Walls force and negative air pressure could not be able to work on rough surfaces and magnetic force-based adhesion is significantly limited by the materials. Electrostatic adhesion which is reversible as well as highly adaptable turns out to be a very promising adhesive method.[5–7] The energy consumption of electroadhesion could be as low as nW and the device structure is generally simple and easy to control.[7,8] Light-weight is also a key feature of the electroadhesive device.[9]

It is well-known that the glass rod will attract small particles when it is rubbed against a fur due to the electrostatic attraction. The first electroadhesive pad used for panel component could be traced back to 1968 for the paper preservation of the flatbed plotter.[10] Electroadhesion is also widely and commercially used as Si wafer chucks

in the semiconductor industry.[11] And current research on electroadhesion is mostly related to the wall-climbing robotics, electroadhesive grippers and clutches.[10,12–14]

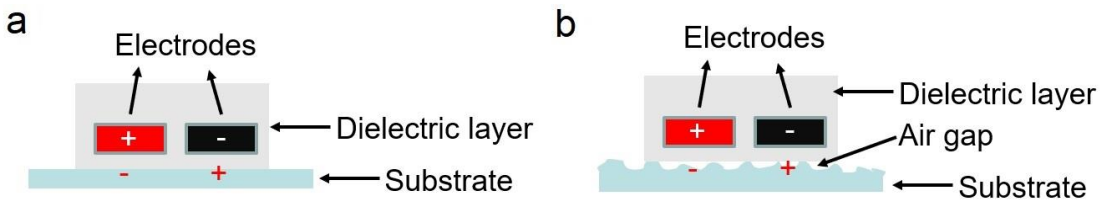

Fig 2.1 The schematic illustration of (a) an ideal and (b) non-ideal electroadhesive pad

The simplest electroadhesive pad which consists of only a thin dielectric layer and an electrode, when an external electric field is applied the opposite charges are generated on the surface of the substrate (the objects to be held), resulted in the electrostatic adhesion of the pad and substrate, as shown in Fig 1.1a. The generated electroadhesive force could be calculated by integrating the Maxwell stress tensor T over the contact area S (Equation 1.1). The electroadhesive force has a positive relationship with the dielectric constant of the dielectric materials, the electric field as well as the active surface area. High dielectric-constant (high-k) materials are thus more desirable in practical applications. However, air gaps always exist due to the imperfect contact between the panel and the substrate (Fig 1.1b), which will dramatically decrease the developed electroadhesive force.[12] One effective solution to this problem is to use soft and flexible electrodes. Apart from the above-mentioned parameters, the electroadhesion will also be influenced by many factors, including the characters of

the substrate (*i.e.* roughness, dielectric properties, thickness), the electrode parameters (*i.e.* electrode space, width, thickness) and the environmental (*i.e.* temperature, humidity).[15]

$$F = \oint_S TdS = \oint_S \frac{\varepsilon}{2}\left(E_y^2 - E_x^2\right)dS \tag{1.1}$$

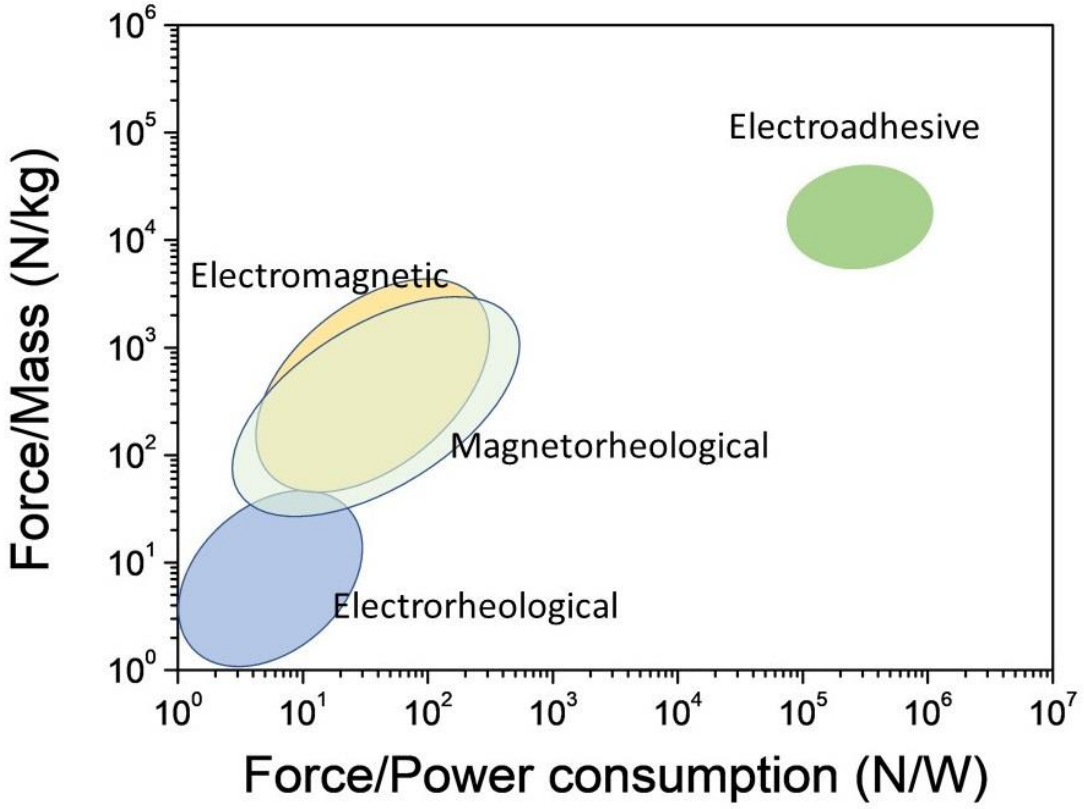

Fig 1.2 Comparison of the current clutch technologies (reproduced form Ref[16])

Electroadhesive clutches have also drawn great research interests during the past decades.[9,14,17,18] As compared with traditional clutch technologies based on

electromagnetic solenoids,[19] magnetorheological fluids[20,21] and electrorheological fluids,[22] electroadhesive clutches have shown advantages such as large holding force, light weight and low power-consumption (Fig 1.2) which are extremely attractive in wearable systems.

1.2 Problem statements

To develop high-performance electroadhesive pads remains a challenge though the mechanism and device structure are simple. There is still a lot of work could be done in both material selection, structure optimization and application exploration and current problems are mainly focused on the following parts:

(1) The first challenge is the high direct current (DC) working voltage which is usually as high as several thousand volts, though the working current of the electroadhesive device is in the range of nA.

(2) The dielectric materials used in electroadhesion generally have relatively low dielectric constant. Most of the current works still use dielectric elastomers with relative dielectric constant lower than 5. Only a few research works adopted the high-*k* inks (ε_r = 35).[9,14] The development and use of dielectric materials with higher dielectric constant are highly desired.

(3) Based on the theoretical models, using soft dielectric materials and flexible electrodes could minimize the air gaps at the interface which will dramatically

increase the induced force as well. Smooth surfaces are preferred and the surface morphology should be evaluated.

(4) Current researches on electroadhesive clutches are all based on symmetric structures, the charge characteristics of the materials themselves and asymmetric structured electroadhesive clutches have not been investigated yet.

(5) Current researches on electroadhesive clutches could only provide holding force, multifunctional clutches and clutches based on multi-mechanism are less studied.

(6) Direct measurement of the engage and release time of the clutches should be proposed.

(7) Developing high-*k* but low loss dielectric materials is also a big challenge.

1.3 Objectives

Based on the research background of electroadhesion, the purpose of this research is to develop high-performance electroadhesive devices with low working voltage, low power consumption and large electroadhesive force.

The specific objectives could be devised as follows:

1. To fabricate flexible electroadhesive clutches with high performance based on high-*k* materials with optimized device structures and parameters;

2. To reduce the working voltage of the electroadhesive clutches and explore the clutch behavior under alternative current (AC) voltages;
3. To fabricate asymmetric structured electroadhesive clutches and investigate the influence of the charge characteristics of the materials on the clutch performance;
4. To develop high dielectric-constant and low dielectric loss polymer matrix composites and investigate their dielectric properties and explore applications;
5. To establish test systems for the direct measurement of the response time;
6. To explore multifunctional and multi-mechanism electroadhesive clutches.

1.4 Methodology

In this section, detailed information about the preparation, characterization and fabrication of the materials and devices are given.

1.4.1 Materials selection

The polymer materials poly (vinylidene-fluoride-trifluoroethylene-chloro-fluoroethylene) (P(VDF-TrFE-CFE)) terpolymer which has the highest dielectric constant (εr ~50 at 1 kHz) among dielectric polymers has been selected as the high-*k* materials and polymer matrix for developing high-*k* polymer composites. The P(VDF-TrFE-CFE) terpolymer is also soft with a Young's modulus of ~ 200-400 MPa.

Thermally reduced graphene oxide is also adopted as conductive fillers due to the easy and even dispersion of graphene oxide into polymer matrix. Polyurethane (PU) with positive surface and polytetrafluoroethylene (PTFE) and polyimide (PI) with negative surfaces are used for the fabrication of asymmetric clutches. Thin metal foil-based electrodes have been used due to the smooth surface and excellent conductivity. Robust conductive fabrics with adhesive layers are also used as the electrodes for the film-based electroadhesive for easy fabrication.

1.4.2 Preparation of the dielectric pads

The dielectric layer based on polymer or polymer composites are fabricated through blade coating on Al foils with different profile rods to produce electroadhesive pads with different thickness. Proper thermal-treatment, such as annealing and thermal reduction are conducted. The commercial film-based (PI and PTFE) are directly adhered on the conductive fabric electrodes.

1.4.3 Materials characterization

General characterization methods include:

1. Fourier-transform infrared spectroscopy (FTIR): To investigate the chemical properties of the dielectric materials through the infrared absorption peaks. FTIR spectra were recorded on Perkin Elmer Spectrum 100 FTIR Spectrometers.

2. Raman spectroscopy: To evaluate the reduction degree of the graphene oxide (GO). The Raman spectrum was recorded on a BaySpec's Nomadic Raman microscope (λ_{exc} = 532 nm).

3. The scanning electron microscope (SEM): To investigate the morphology of the dielectric layer, electrode as well as the samples. SEM images were obtained form Tescan VEGA3 microscope.

4. ZYGO laser interferometric non-contact profile system: To evaluate the surface roughness of the dielectric materials and electrodes.

5. Dielectric constant and dielectric loss measurement: To investigate the dielectric properties including dielectric constant and dielectric loss of the dielectric layers. The dielectric properties were characterized by Agilent 4294A Precigion Impedance Analyzer.

6. Breakdown and electroadhesion: To get the dielectric strength of the dielectric layers for further electrode design. It could also provide high voltage from 0 to 30 kV to trigger the electroadhesion. The experiments were conducted on RK2674A Voltage Withstand Test Instrument.

7. The resistivity of the electrodes: The resistance of the flexible electrodes was measured on ST-2258A four-probe tester.

1.4.4 Performance evaluation

For flexible electrodes, the conductivity, thickness as well as the mechanical properties are the parameters that concerned. For dielectric layers, the thickness, dielectric constant and loss, mechanical properties and surface roughness should be measured and analyzed.

The relationship between the generated electroadhesive force with voltage, dielectric thickness and overlapping area should be investigated. The engage and release time of the clutches should be evaluated as well.

1.5 Research significance

The innovation of this work mainly focuses on:

1. The use of high-*k* polymer materials significantly reduces the working voltage while the generated electroadhesive force increases.
2. The variation of bending stiffness with the DC voltage and the clutch behavior under AC voltage have been evaluated.
3. A novel test system for the direct measurement of the response time has been proposed.
4. Asymmetric structured electroadhesive clutches whose charge characteristics play important roles have also been fabricated and their performance has been evaluated. Apart from the electrostatic adhesion, reversible chemical adhesion based on

hydrogen bonding is also observed in the asymmetric clutches made from PU/PI materials.

5. High-*k* RGO/P(VDF-TrFE-CFE) composites with tunable dielectric properties with different reduction time has been proposed for the first time. Clutch-type pressure sensor has also been developed and illustrated its application potentials.

1.6 Outlines of the thesis

There are six chapters in the report related to the electroadhesive clutches, with their main contents summarized as follows:

Chapter 1 is a brief introduction about the research background, research gaps, research methodology as well as program objectives.

Chapter 2 provides a brief introduction of the electroadhesion, followed by current progress in electroadhesive devices including electroadhesive robots, grippers and clutches. The state-of-the-art progress of high dielectric-constant polymer matrix composites and flexible electrodes have also been reviewed.

In chapter 3, symmetric clutches based on high-*k* P(VDF-TrFE-CFE) terpolymers are developed. The sample preparation, characterization and clutch performance are demonstrated. The relationships between the generated electroadhesive force and applied voltage, dielectric thickness and overlapping area have been investigated. The direct measurement of response times including engage time and release time is also conducted.

Chapter 4 presents the fabrication, characterization and clutch performance of the asymmetric clutches. The relationships between the generated electroadhesive force and applied voltage, dielectric thickness and overlapping area have been investigated. The comparison between the performance of the symmetric and asymmetric clutches is also delivered. Apart from the electrostatic attraction, hydrogen bonding at the interface also contribute to the high clutch performance.

In Chapter 5, high-*k* composites with tunable dielectric properties through *in-situ* thermal reduction of GO in P(VDF-TrFE-CFE) matrix have been developed for the first time. The change of dielectric constant and dielectric loss with the reduction time are investigated. The preliminary study of the clutch-type pressure sensor based on the high-*k* composites has been conducted. The pressure-current relationship under a constant voltage and current-voltage relationship at a constant pressure have been demonstrated. Possible mechanism for the current change under pressure is also proposed.

Conclusions, limitations of the current works and future works are summarized in Chapter 6.

References

[1] M. Vert, Y. Doi, K.-H. Hellwich, M. Hess, P. Hodge, P. Kubisa, M. Rinaudo, F. Schué, *Pure Appl. Chem.* **2012**, *84*, 377.

[2] B. J. Kim, D. X. Oh, S. Kim, J. H. Seo, D. S. Hwang, A. Masic, D. K. Han, H. J. Cha, *Biomacromolecules* **2014**, *15*, 1579.

[3] J. Yang, R. Bai, Z. Suo, *Adv. Mater.* **2018**, *30*, 1800671.

[4] D. Gan, W. Xing, L. Jiang, J. Fang, C. Zhao, F. Ren, L. Fang, K. Wang, X. Lu, *Nat. Commun.* **2019**, *10*, 1487.

[5] G. Gu, J. Zou, R. Zhao, X. Zhao, X. Zhu, *Sci. Robot.* **2018**, *3*, eaat2874.

[6] J. Guo, C. Xiang, J. Rossiter, *Mater. Des.* **2018**, *156*, 586.

[7] J. Germann, B. Schubert, D. Floreano, in *2014 IEEE/RSJ Int. Conf. Intell. Robot. Syst.*, IEEE, **2014**, pp. 3933–3938.

[8] J. Shintake, V. Cacucciolo, D. Floreano, H. Shea, *Adv. Mater.* **2018**, *30*, 1707035.

[9] S. Diller, C. Majidi, S. H. Collins, in *2016 IEEE Int. Conf. Robot. Autom.*, IEEE, **2016**, pp. 682–689.

[10] G. Monkman, *Ind. Robot An Int. J.* **2003**, *30*, 326.

[11] G. A. Wardly, *Rev. Sci. Instrum.* **1973**, *44*, 1506.

[12] R. Liu, R. Chen, H. Shen, R. Zhang, *Int. J. Adv. Robot. Syst.* **2013**, *10*, 36.

[13] J. Kim, G. Lee, R. Heimgartner, D. Arumukhom Revi, N. Karavas, D. Nathanson, I.

Galiana, A. Eckert-Erdheim, P. Murphy, D. Perry, N. Menard, D. K. Choe, P. Malcolm, C. J. Walsh, *Science.* **2019**, *365*, 668.

[14] V. Ramachandran, J. Shintake, D. Floreano, *Adv. Mater. Technol.* **2019**, *4*, 1800313.

[15] J. Guo, M. Tailor, T. Bamber, M. Chamberlain, L. Justham, M. Jackson, *J. Phys. D. Appl. Phys.* **2016**, *49*, 035303.

[16] S. B. Diller, S. H. Collins, C. Majidi, *J. Intell. Mater. Syst. Struct.* **2018**, *29*, 3804.

[17] J.-H. Park, P. R. Stegall, D. P. Roye, S. K. Agrawal, *IEEE Trans. Neural Syst. Rehabil. Eng.* **2018**, *26*, 1026.

[18] R. Hinchet, V. Vechev, H. Shea, O. Hilliges, in *31st Annu. ACM Symp. User Interface Softw. Technol. - UIST '18*, ACM Press, New York, New York, USA, **2018**, pp. 901–912.

[19] E. J. Rouse, L. M. Mooney, H. M. Herr, *Int. J. Rob. Res.* **2014**, *33*, 1611.

[20] T. Kikuchi, K. Otsuki, J. Furusho, H. Abe, J. Noma, M. Naito, N. Lauzier, *Adv. Robot.* **2010**, *24*, 1489.

[21] A. S. Shafer, M. R. Kermani, in *2011 IEEE Int. Conf. Robot. Autom.*, IEEE, **2011**, pp. 4266–4271.

[22] K. Boku, T. Nakamura, *J. Intell. Mater. Syst. Struct.* **2010**, *21*, 1563.

CHAPTER 2 Literature review

2.1 Electroadhesion

2.1.1 Background

Electroadhesion is the electrostatic attraction between the surface of the electroadhesive plate and the substrate which generates opposite charges under an external electric field. Electroadhesive plates are thus able to work on both conductive and nonconductive, smooth and rough surfaces in both air and vacuum circumstance.[1] Electroadhesion could be conducted on both conductive and insulating substrates but the mechanisms are different. On an electrically conductive substrate, the electrostatic induction is the dominant interaction[2] while in an insulating substance, the polarization of the electronic, atomic, molecular and interfacial space charge should be considered, among which the space charge plays a very important role in electroadhesion.[3,4] Electroadhesion to insulating surface has been broadly investigated. Apart from the high adaptivity, electroadhesion also has a simple device structure and are low energy consumption, low cost, fast response as well as light-weight, which makes it easy to be incorporated into robotic or wearable systems.[5,6] It should also be noticed that the induced electroadhesion force will be much lower if air gaps exit between the electroadhesive pad and substrate. Early in the 1960s, the National Aeronautics and Space Administration (NASA) explored the application of electroadhesion in space vehicles.[7] With the rapid development of the semiconductor

industry, electroadhesion was also extensively used as the electrostatic chucks, which are developed for the holding and grasping of the silicon wafers in integrated circuit (IC) fabrication.[8] Due to the soft and non-damaging nature,[9] electroadhesion shows promising applications in handling non-rigid and/or brittle materials such as fabrics and fibers.[10–12] Another emerging application of electroadhesion lies on the perching[13] and wall-climbing robots[1,5,14] due to its lightweight and easy integration with the robot operating systems. Electroadhesion could also been combined with soft grippers and actuators to improve the performance.[15–17] Applications related to haptic systems[18] and suction cups[19] are also reported.

Apart from the single pad based electroadhesive devices, electroadhesion clutches consist of two pieces of electroadhesive pads have been developed as well.[20–23] Interdigital electrodes are widely utilized to improve the electroadhesive performance by taking advantages of the boundaries and a number of research works have focused on the design parameters of the electrodes such as space and the widths.[1,6,24] A lot of electrode patterns have been proposed, examples are shown in Fig 2.1. Those with interdigital geometries such as Fig 2.1a and 2.1b exhibit the largest capacitances under electrical fields while Fig 2.1f with double-electrode shape only shows around 1/7 lower capacitance.[25]

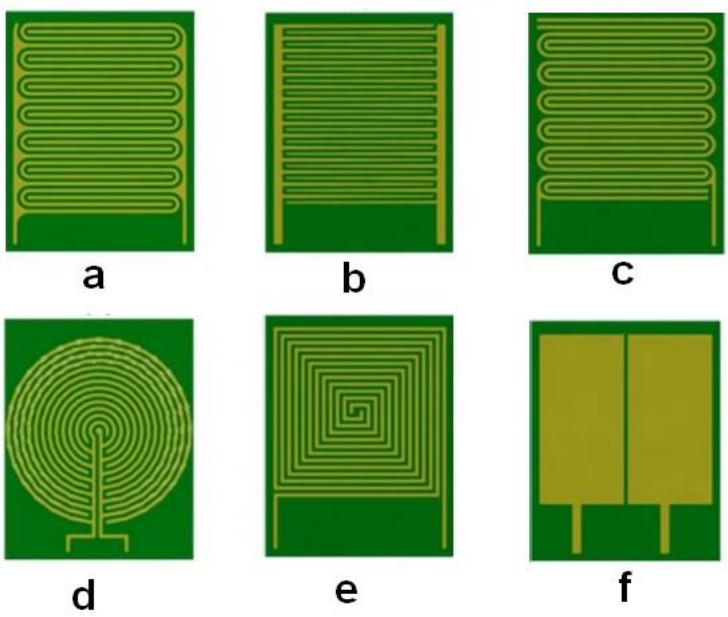

Fig 2.7 Different electrode patterns for electroadhesion[25]

Guo *et al* have summarized more than 30 parameters that would influence the performance of the electroadhesive pads, covering power supply, substrate, dielectric materials, electrode and environmental parameters.[26] Generally, the generated electroadhesive force has a positive relationship with the voltage, the dielectric constant of the dielectric layer and substrate and the surface area while negative to the thickness of the air gap and insulating layers, the electrode width as well as the surface roughness. The generated electroadhesive force is relatively small (~ 0.1 to 1 N/cm^2) as compared with other adhesive methods.[27]

Electroadhesion have been studied for more than one century and several theoretical models have been proposed for the electroadhesion with assumptions that the dielectric layer is rigid and homogeneous, the contact is perfect.[2,26,28] Watanabe and co-workers developed a model based on the Johnsen-Rahbek (J-R) effect in 1993[29] and this model have been widely adopted in electroadhesive chunks[30,31]. The generated electroadhesive force of the chucks increases as a result of charge accumulation at the boundary of the air gaps. However, in the haptic applications such as touchscreen and display the electroadhesive force always decrease with time[32–34], which could not be explained by the J-R model. A leakage model have been proposed[35,36]. The equivalent circuits for the two models are shown in Fig 2.2. Even though the leakage model could explain the force loss which is caused by the leak resistance, the physics behind is still not clear in this model.[37] The induced electroadhesive force is could be calculated by Equation 2.1.

$$F = \frac{\varepsilon}{2}\frac{AV^2}{d^2} \tag{2.1}$$

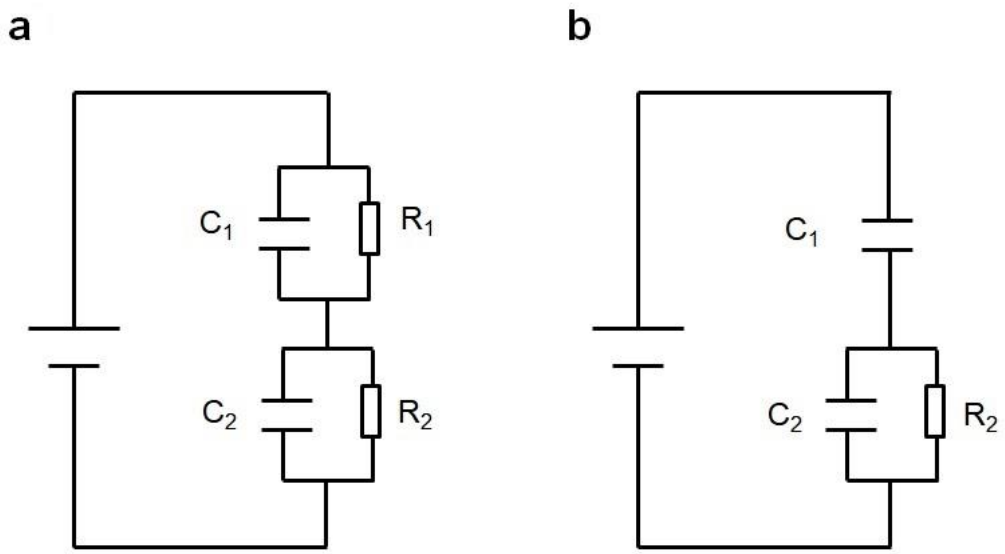

Fig 2.8 Equivalent circuits of a). J-R model[29] and b). leakage model[33]

The J-R model and leakage models only focus the electric behavior of the electroadhesion, the mechanical properties of the electrodes and dielectric materials have not been considered. Nakamura *et al*. have recently developed a model combining both electric and mechanical characteristics of electroadhesion based on the J-R model. The new model could describe the variations in the induced forces.[37] The electro-mechanical model focuses on the electric fields other than voltages in the J-R model and introduces the spring and damper to present the mechanical part, as shown in Fig 2.3. The induced charges on the dielectric-air interface could be either positive or negative, determined by the dielectric constant (ε) and the conductivity (σ) of the dielectric layer and the air gaps. When $\frac{\varepsilon_{dielectric}}{\sigma_{dielectric}} > \frac{\varepsilon_{air}}{\sigma_{air}}$

the charges on the interface are positive, which will lead to an increase in the induced forces and the negative charges will decrease the electroadhesive force.

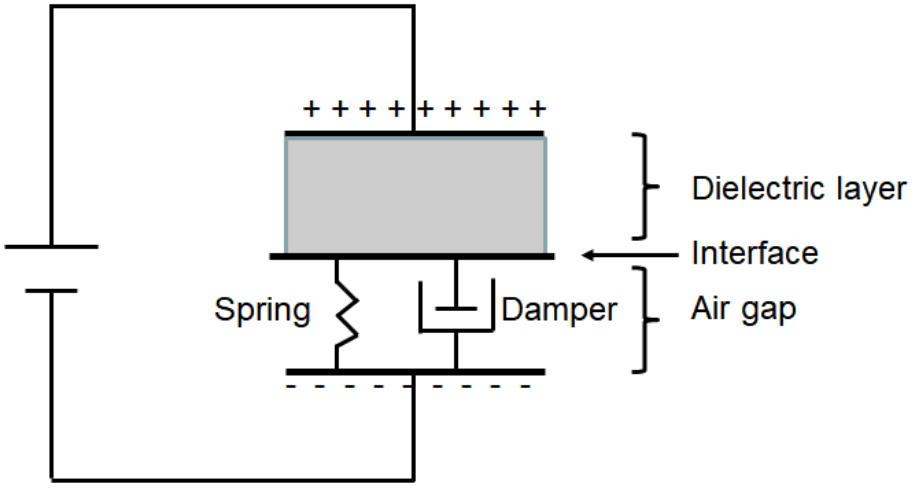

Fig 2.9 The electro-mechanical model of electroadhesion

2.1.2 Electroadhesive applications

2.1.2.1 Electroadhesive robots

NASA also developed the electroadhesive devices for walking of robots on the space vehicles and they had proposed the concept of wall-climbing electroadhesive robots at that time.[7] And the first wall-climbing robot (Fig 2.4a) based on compliant electroadhesion was realized in 2008 by Prahlad and co-workers.[5] The electroadhesion could be triggered by two AAA batteries (with a high voltage

converter) with a power consumption of 0.25 mW to hold a 200 g robot and allow the fast move of the robot (15 cm/s). The generated electroadhesive forces vary from 0.08 to 1.4 N/cm^2 on different surfaces.[5] Another wall-climbing robot with a weight of 700 g could generate a larger force on the wall substrate (1.54 N/cm^2) but the power consumption is as large as 3 W.[1] Disc-shaped electroadhesive footpads have also been developed instead of the rectangular electroadhesive sheet in some wall-climbing robots. Chen proposed a gecko-like wall climbing robot with four footpads (Φ = 1.7 cm) to hold a 400g robot and the moving velocity could reach 2 cm/s under 3 kV.[38] The disc-shaped pads have also been used in a quadrupedal microrobot, which could move slowly under an electric field of 250 V.[39] Two-foot electroadhesive robot implemented with dielectric elastomer actuator (DEA) is also able to move vertically on the wall.[40] Perching and take off of the flying microrobot could also be realized by integrating the electroadhesive pads into the robotics systems.[13] Table 2.1 summarizes the key parameters of some typical electroadhesive robots, mainly including the working voltage, power consumption, electroadhesive stress and dielectric materials.

Polyimide (PI) is the most broadly used dielectric layer in the fabrication of electroadhesive robots due to its relatively high dielectric strength of 150 kV/mm and relatively high dielectric constant (ε_r) of 3.5 as compared with other commercially available polymers such as polyethylene (PE) and polypropylene (PP), whose dielectric constant are only 2.2 and dielectric breakdown strength lower than 25 kV /

mm. Mylar film is a kind of polyester film with a dielectric constant of 3.7 and Ecoflex is a kind of rubber with a dielectric constant of 2.8. The electroadhesive force is significantly influenced by the dielectric layer, driving voltage and the properties of the substrate, further and comprehensive study of the device parameters on the performance of the electroadhesion are still demanded.

Table 2.1 Key parameters of the electroadhesive robots

	Self-weight / g	Size / cm^2	Adhesion voltage / kV	Power consumption	Moving velocity / cm/s	Electroadhesion stress / N/cm^2	Dielectric material	Reference
1	200	240	3	0.25 mW	15	1.4 (steel)	-	[5]
2	700	13	3	3 W	0.02	1.54 (wall)	PI	[1]
3	400	9	3	-	2	0.36 (glass)	PI	[38]
4	94	4.74	0.6	-	3.53	1.41 (Al broad)	-	[41]
5	0.1	1.7	1	7 μW	-	-	PI	[13]
6	100	50	4.5	-	0.01	0.40 (glass)	Mylar film	[42]
7	3.3	4	2	-	-	0.375 (cellulose)	Ecoflex	[43]
8	10	0.16	5	-	6.34	2.17 (wood)	PI	[40]
9	1.48	3.14	0.25	-	0.12	0.2 (conductive)	PI	[39]

2.1.2.2 Electroadhesive grippers

Electroadhesion incorporated with other external deforming systems such as dielectric elastomer actuators (DEAs) are very attractive for the development of soft grippers, especially in handling the delicate and fragile objects with irregular shapes.[44] Carbon fiber-based electroadhesive gripper was already developed in the 1990s to hold fibrous materials.[11] The first electroadhesive microgripper integrated with a piezoelectric actuator was demonstrated by Monkman in 2003 for handling the delicate spherical microlens.[16] Electrorheological (ER) fluids have also been associated with electroadhesion and the fluids could lead to better shape adaptivity.[28] The Grabit Inc. has demonstrated an electroadhesive soft gripper with flexible printed circuit boards (PCBs), which could grasp paper boxes, metal cans, plastic bags as well as fruits with the assistance of electromagnetic motors (Fig 2.4c).[45] Fluidic elastomer actuators (FEAs) are also combined with electroadhesion to pick globular objects (Fig 2.4d).[46] Dielectric elastomer actuators with intrinsic electroadhesion (Fig 2.4e) has been developed which could lift objectives 100-time heavier than itself.[15] A smart shape-adaptive electroadhesion-DEA gripper with the ability to sense the internal and external deformations by combining the Maxwell force and the electrostatic attraction was proposed by Guo and co-workers.[47] Robotic material handling system based on adaptive electroadhesion has also been established by the same group.[9] They have also reported the hybrid of pneumatic/electroadhesive[17] and magnetoadhesive/electroadhesive[48] grippers recently, aiming at improving the

performance of the adhesion in the delicate and complex-shaped substances as well as broaden the potential applications of electroadhesion.

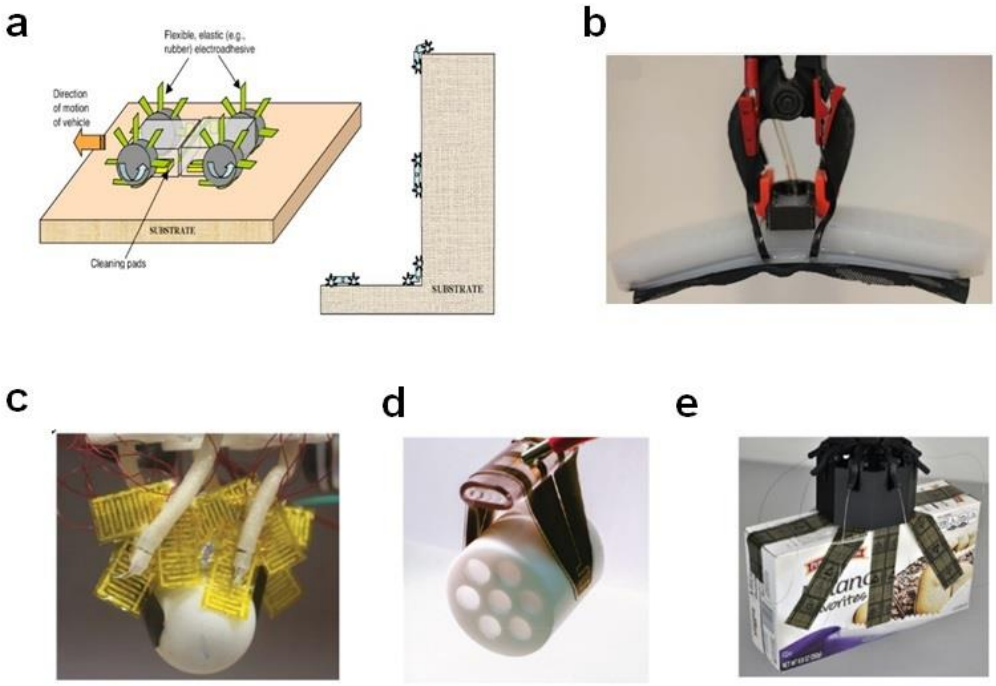

Fig 2.10 Demonstration of (a) electroadhesion wall-climbing robot[5]; electroadhesion integrated with (b) soft pneumatic actuator[17];(c) PCBs and electromagnetic motors[45]; (d) FEAs[46]; (e) DEAs[15]

2.1.2.3 Electroadhesive clutches

Clutches have been widely used in robotics[49] and actuators[50–52] to enable versatile performance as well as improve power efficiency. Clutches could also adjust the stiffness to control mechanical performance in haptics applications.[53,54] Traditional

clutches based on electromagnetic solenoids[55] or magnetorheological fluids[56,57] are very bulky and heavy due to the use of solenoids. The power consumption could be as high as several hundred watts. The mass and size could be narrowed down by using electrorheological clutches, however, the driving voltage is much higher and the force generated also decreases.[58] Passive clutches are difficult to control though they could work without power supply.[59] Choi's group reported a soft layer jamming brake (SLJB) which could generate large force at low energy consumption, but the slow response time and the need for a compressor will greatly limit its application.[60] Electroadhesive clutches with good controllability, fast response, low power consumption and light weight are thus talented in fabricating high-quality clutches.[21]

Early in the 1950s, Fitch reported an electrostatic clutch with conductive carbon filled rubber-based plastic, which could work at only 150 V while the current was as high as 30 mA.[20] However, little progress had been made in the electroadhesive clutches though high-performance electroadhesive pads have already been achieved and the reported clutches usually has a slow on/off time and large force hysteresis.[61] This is mainly owing to the relatively low dielectric constant of the dielectric elastomers and the structure design. In 2016, Diller *et al.* developed the electroadhesive clutch with a high-*k* ink (Luxprint, Dupont, ε_r = 35) and multi-layer structure, the resulted clutch exhibit very fast response time in the microsecond range and each clutch could generate about 100 N force under a 0.6 mW power consumption.[22] The clutch is wearable and could act as an exoskeleton. They have also investigated the influence

factors to the maximum holding force and the results show that the force increase with the increase of the voltage and contact area, and the decrease of the electrode thickness.[21] It is also interesting that the holding force increases with the increase of the dielectric thickness and reaches a peak at around 60 μm and then comes down due to the effect of the back plate.[21] Floreano and co-workers developed a fabric-based wearable electroadhesive clutch with the same high-*k* material and lighter weight, the generated force is lower than Diller's work mainly due to the air gaps in the fabric electrode.[23] It could work under power consumption as low as 0.9 mW and generate a shear stress of 3.5 kPa. The induced force also shows a good linear relationship with the number of the clutch layer.[23] The typical clutch structures used in wearable devices are demonstrated in Fig 2.5.

Though the electroadhesive clutches have shown huge advantages and great potentials, there are still some issues to be addressed. Firstly and most importantly is the development of proper high-*k* materials with high dielectric properties, electrical stability as well as mechanical properties. And the edges of the electrodes are easy to break down due to the arc discharge and this requires better structure designs and careful materials selection. The force hysteresis under large loads should also be considered. Recently, Kim *et al.* have proposed a novel kind of electroadhesive junction based on a pair of opposite-charged ionoelastomers with a driving-voltage as low as 1 V and could give a shear stress of 5 kPa.[62] The ionic double layer in the molecular scale is the mechanism for the low driving-voltage which is different from

the mechanism of the abovementioned dielectric polymer based electroadhesive clutches. This work provides a novel material system for the low voltage electroadhesion though the polyanion and polycation are inherent adhesive without external voltages.

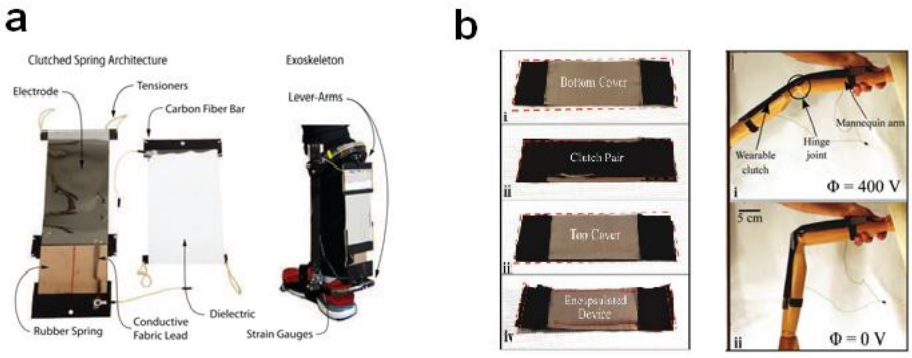

Fig 2.11 Clutch structures and demonstrations for (a). exoskeleton actuation[22] and (b). a wearable clutch that constrains the rotation of the joint.[23]

2.1.2.4 Others

Electroadhesion has also found applications in surface haptic systems in which human fingers act as one plate and represent one of the leading technologies over the past decades. Early in 1923, Johnsen and Rahbek had demonstrated the electroadhesion phenomenon between human fingers and a metal surface and they had also established the J-R model.[63] Later in 1953, Mallinckrodt and co-workers reported the electrical induced friction when a dry finger touch on an insulating varnish coated aluminium plate under an alternating electrical field.[64] When the finger moved gently on the

insulating surface, periodically electrostatic attraction will be induced, causing drag and release of the fingers and produce a resiny sensations. Following works have proved that the frequency, wave profile and amplitude of the input voltage will significantly influence the generated electroadhesive forces and thus could result in a rich set of haptic effects.[65–67]

Lee and co-workers have recently developed ionic spiderwebs based on electroadhesion of silicone rubber encapsulated ionic conductive organogels, which could allow electrostatic capturing, sensing of approaching objectives.[68] The biomimetic electroadhesive webs could also be self-cleaning by simply changing the frequency of working voltages.[68] This work has expanded the application of electroadhesion to multifunctional soft robotics and also indicate the ionic gels could also be used in electroadhesion based on the migration of ions other than induced electrostatic charges in dielectric materials.

2.2 High-*k* polymer matrix composites

Dielectric materials are a kind of materials which could be polarized under an external field and their energy band gaps are higher than 3 eV.[69] High-*k* materials refer to the materials with high relative dielectric constants higher than silicon dioxide which is 3.9.[70] The dielectric constant is a complex, the real part (ε') reflect the relative dielectric constant and the imaginary part (ε'') is corresponding to the dielectric

dissipation which is described as loss tangent (tan δ = ε''/ ε') in most cases. There are five polarizations in dielectric polymers, namely electronic polarization, atomic (or vibrational) polarization, ionic polarization, dipolar (or orientation) polarization and interfacial (or space charge) polarization.[71] The relative intensity and frequency range of the five polarizations are shown in Fig 2.6a[71] and the schematic illustration of the polarizations are demonstrated in Fig 2.6b.[72] As shown in Fig 2.6a, the interfacial polarization, which originates from the charges accumulated at the fill/polymer interface, is the dominant polarization especially in the low frequency range (<1000 Hz), though the caused dissipation is also large. Increasing the interfacial polarization is the most widely used strategy to prepare high-*k* polymer matrix composites (PMCs). Dipolar, ionic and electronic polarizations come from the reorientation of dipoles, ions and electrons respectively and atomic polarization arises from the vibrations of chemical bonds under electric fields.

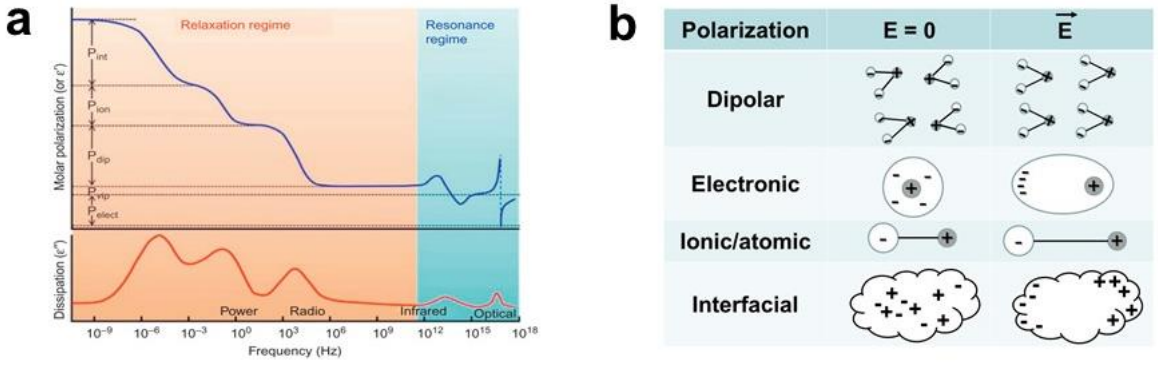

Fig 2.12 (a). Five polarizations in dielectric polymers[71] and (b). schematic illustration of the five polarizations.[72]

Flexible high-*k* systems are also desirable in a wide range of applications including actuators[73–75], radio frequency (RF) and microwave applications[70,76,77], memory[78], organic filed-effect transistors (OFETs)[79] and energy storage[77,80,81]. As mentioned in the last section, developing high dielectric-constant dielectric materials is also very important to fabricate high-performance electroadhesive clutches. Inorganic high-*k* materials, such as lead zirconate titanate (PZT)[82,83] and Barium titanate (BTO)[84], have been extensively investigated due to their high dielectric constant, low dielectric loss and high dielectric strength. However, high-*k* ceramics are inherently brittle and stiff, which greatly hinder their applications in flexible devices and wearable electronics.[81,85] Dielectric polymers have many advantages such as high flexibility, dielectric strength, versatile processing approaches and tuneable properties, but most of the polymeric materials have relative dielectric constant lower than 5.[70,86] There are several strategies to increase the dielectric constant of the polymers, mainly including introducing polar side groups into the polymers, doping with high-*k* materials and conductive fillers.[77,87–89] And here we will discuss the polymer matrix composites with both high dielectric constant and flexibility, which represents one of the most common design strategies to obtain flexible high-k systems.[70,90,91]

2.2.1 High-*k* dielectrics/polymer composites

High-*k* ceramics such as PZT[82,83] $CaCu_3Ti_4O_{12}$ (CCTO)[90], and $BaTiO_3$[84] are broadly used as the fillers and dielectric constants of the resultant composites could

increase more than one order of magnitude with the doping ratio higher than 50 vol%. However, the high contents of the stiff ceramics will always lead to weak mechanical strength and low dielectric break-down strength, due to the aggregation of the nanoparticles (NPs).[90,92] Polymer-grafted nanoparticles could suppress the aggregation to a certain extent and the resultant composites exhibit higher dielectric constant and dielectric strength while the dielectric loss is reduced.[89] The size of the nanoparticles has also shown significant influence on the dielectric constant. Experimental results show that composites with small size BTO nanoparticles have higher permittivity at room temperature and the enhancement is result from the interfacial and dipolar polarization.[93]

50% loaded Zirconium dioxide (ZrO_2)/PI nanocomposites have also been developed for organic thin film transistors (OTFTs) with a dielectric constant of 8.3 (@ 10K Hz).[94] $MgCaTiO_2$ reinforced PDMS composites with 25% doping ratio exhibit a dielectric constant of 12.1 and a dielectric loss of 0.021 at 20G Hz and thus could be potentially used in radio-frequency (RF) devices and antennas.[95]

Compared with the 0D nanoparticles/polymer composites, 1D nanofillers/polymer composites have received widespread attention due to their large dipole moments and high dielectric strength.[88,96] Core–shell structured SiC/SiO_2 whisker/polyvinylidene fluoride (PVDF) (25 vol%) composite exhibits a permittivity of 1280 while its dielectric loss is only 0.42.[97] Similar strategies have been widely adopted to prepare

high-*k* but low loss dielectric PMCs by taking advantages of interfacial polarization.[98–101] The insulating layers could effectively prevent the migration of charge carriers and is beneficial to the well-dispersion of the nanofillers.[97,102] 1D BTO nanowire/PVDF composite shows a 3-time higher dielectric constant as compared with 0D BTO nanoparticle system with the same doping ratio, which results from the stronger interfacial polarization in 1D nanowire/polymer composites and the high aspect ratio of 1D nanowires.[103] Polyvinylpyrrolidone (PVP) modified $SrTiO_3$ nanofibers (ST NFs) have also been used as 1D nanofillers to increase the permittivity of PVDF by solution casting.[104]

Zhu and co-workers have doped the same amount (only 5 wt%) 0D TiO_2 nanoparticle, 1D TiO_2 nanowire and 2D TiO_2 nanosheet into the same polymer matrix, interestingly, the dielectric constant, discharged energy densities and dielectric strength of 2D-TiO_2/PVDF are much superior than the others.[105] And this is ascribed to the special geometric morphology and homogeneous electric field distribution.[105] Li's group crosslinked boron nitride nanosheets (BNNSs) to the polymer chains and the composite features a stable dielectric properties over a wide range of frequency and temperature.[106]

Luo *et al* developed a 3D BTO network/PVDF composites with relative dielectric constant of 200 at 30 vol% and 34.5 at 16 vol% and this work has also proved that the 3D interconnected network could facilitate the polarization of BTO in the

composite.[107] Apart from the inorganic high-*k* ceramics, some organic high-*k* fillers have also been developed. Semiconductive copper phthalocyanine (CuPc) oligomer with a relative dielectric constant larger than 10000 has also been widely used as a high-*k* filler.[108]

Doping with high-*k* dielectrics has been proved to be a promising design strategy to prepare PMSs with good dielectric properties, however, the mechanical strength of the polymer matrixes will be greatly destroyed due to the high loading of the brittle ceramic fillers.

2.2.2 Conductive fillers/polymer composites

Another doping strategy is to add a small number of conductive fillers, such as metal nanoparticles[109,110], carbon nanotubes (CNT)[111,112] and graphene[113,114]. Unlike the dielectric ceramic/polymer composites, high-*k* PMCs could be obtained at low doping concentration (generally lower than 5%) of conductive fillers and the mechanical properties of the polymer substrates will not be significantly influenced. The addition of conductive fillers could induce several orders of magnitudes increasement in dielectric constant[115], which is extremely attractive in PMCs. However, the large dielectric loss (tanδ) as well as leakage current near the percolation threshold are the critical disadvantages that will limit the application.[91,116] The formation of numerous microcapactiors are generally used mechanism for conductive nanomaterials filled

high-*k* PMCs, where the conductive fillers act as electrodes and are separated with the dielectric polymers,[117,118] as shown in Fig 2.7.

Metal particles including silver,[98,109,119] zinc,[110] copper,[110] aluminium,[120] nickel[121] and gold[116] have been reported to be adopted as conductive fillers to enhance the dielectric properties of PMCs. Interfacial polarization is the dominant factor for the huge increase in dielectric constant, especially at low frequency range. In order to minimize the dielectric loss, the metal particles are generally decorated with thin insulating layers. Silver particles are widely investigated as conductive fillers and various shell layer including carbonaceous shells,[98] polylactic acid[119] and graphene oxide[122] could be decorated on the surface of silver to reduce the dielectric loss and improve the dispersity in polymer matrixes. Apart from the silver nanoparticles, silver nanowires (Ag NWs)/PVDF giant dielectric composites have also been developed at a low loading (1.8 vol%) of Ag NWs.[123] A high dielectric constant of 80,000 was obtained at 1 kHz due to the exitance of microcapacitors and strong interfacial polarization, however, the loss tangent was also as high as 44.[123] Other than organic coating, dielectric metal oxides could also act as insulating shells. Core-shell metal-semiconductor structured Zn/ZnO,[110,124] Al/Al_2O_3[120] and Cu/SiO_2[125] nanoparticles have been developed as conductive fillers.

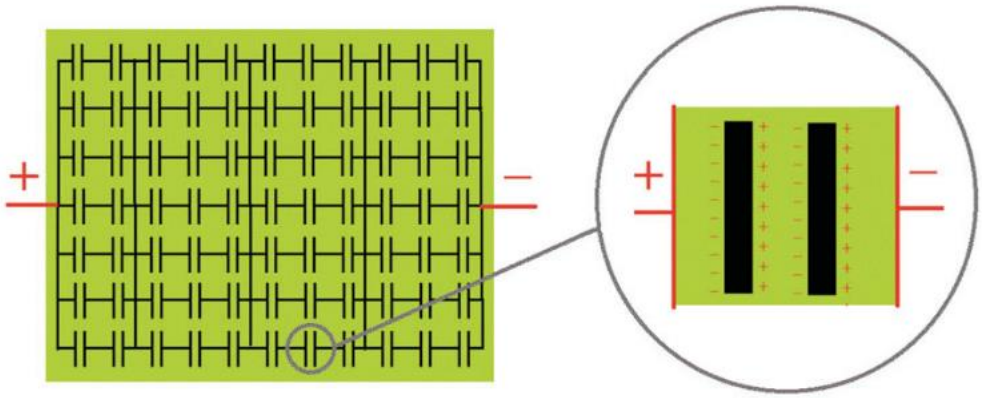

Fig 2.7 Schematic illustration of microcapacitors in ideal dielectric composites.[118]

Carbon-based conductive fillers, typically carbon black,[126] carbon nanotubes (CNTs),[127,128] graphene[129,130] and graphite[131,132] have drawn much research attention recent year, among which the 1D CNTs and 2D graphene represent the 2 main categories. The first CNT/PVDF dielectric composites was reported by Dang's group with a permittivity of 300 and tanδ of 0.4 at only 1.61 vol%.[133] A series of research works based on CNT and other polymer matrixes, including epoxy,[134] polyethylene (PE),[135] natural rubber[136] and hydrogenated nitrile butadiene rubber (HNBR)[127] have been reported afterwards. The resultant PMCs with higher polarity of polymer matrix always exhibit larger dielectric constant, which results from the stronger interfacial polarization.[127] However, CNTs tend to be aggregated and entangled during the fabrication process due to the strong intermolecular interactions.[137,138] To get a uniform dispersion of the nanomaterials and prevent the

formation of the conductive networks remain huge challenges in developing carbon-based high-*k* PMCs. [87] Fortunately, the rich oxygen-containing end groups on CNTs could allow further chemical crosslinking and surface modification which could effectively address the above-mentioned problems.

CNTs could be directly linked to the polymer side chains through chemical bonds.[136] CNTs with carboxylic and ester groups have also been developed and both of their PVDF composites show superior dielectric properties over the pristine one.[139] The carboxylic functionalized CNT/PVDF composite perform best with a dielectric constant of 3600 at 3.8 vol% loading. Carboxylic functionalized CNTs could also modified with CuPc through π-π stacking to form core-shell structures and dielectric constant of the resultant PVDF PMCs was significantly improved.[128] Benzoxazine functionalized CNTs could be evenly dispersed into polybenzoxazine (PBZ) matrix through one-step in-situ polymerization and was used in printed circuit board (PCB).[138] In addition, the processing method will has an effect on the dielectric performance. Chang *et al* developed CNT/epoxy composite through both microwave curing (MC) and thermal curing (TC) and the results show that the dielectric constant of the PMCs prepared via microwave curing was 2.5-time higher than the thermal curing one.[134] Interestingly the dielectric loss of MC-CNT based PMC was 20-time lower than the TC-CNT/epoxy composite due to the well-controlled dispersion and spatial distribution of CNT.[134] Melt-mixing could also be used to prepare homogeneous CNT/PVDF composites with a certain degree of ordered orientation of

CNT.[140] The orientation of CNT in the polymer matrix is also benefit to the high dielectric constant.[141] Increasing the viscosity of the polymer solution turn out to be an effective method as well, as demonstrated in CNT/PI[142] and CNT/rubber[143] systems.

Graphene with excellent electrical and mechanical properties has also drawn extensive research interests since its first discovery in 2004.[144,145] The unique 2D structure, high electrical conductivity and rich reactive properties of graphene makes it a promising conductive filler to fabricate high-*k* PMCs. Previous research has demonstrated the aggregation of graphene nanoplates in the polymer matrix due to the high surface free energy.[146] Since graphene oxide (GO) could be well dispersed into polymer matrix such as PVDF, in situ reduction of GO is a promising method to prepare graphene (or reduced graphene oxide, RGO)/PVDF nanocomposites.[147–149] This strategy could effectively hinder the aggregation of graphene nanosheets and the reduction of GO is generally realized by thermal treatment.[148] Zhang and co-workers also reported that graphene could facilitate formation of β-phase PVDF which features superior dielectric property than other phases.[150] Core-shell structured graphene is widely adopted to increase the dielectric constant and reduce dielectric loss as well. Polydopamine (PDA),[130] polyaniline (PANI),[151] hyperbranched aromatic polyamide (HBA),[152] (1-hexadecyl) triphenylphosphonium bromide (HTPB),[130] poly(vinyl alcohol) (PVA),[153] tannic-Fe complexes (TA-Fe),[78] Ethylene/n-butyl acrylate/glycidyl methacrylate terpolymer (EBA-GMA)[154] and even silver

nanoparticles[109] could be introduced as coating layers on graphene. Modification on the atom level (*i.e.* chlorinated RGO) also gives a 7-time increase in dielectric constant while the dielectric loss remain unchanged at 10 Hz as compared with pristine RGO-based composites.[155] Light-weight graphene aerogel (GA)/PVA composite was also developed with high dielectric and low loss, due to the uniform dispersion and ordered alignment of graphene.[156] Sandwich-structured few layer graphene (FLG)/PVDF composites has a dielectric constant higher than 100000.[129]

However, the use of nanoparticles may be detrimental to the human health due to the size effect[157] and CNT have been added to the 'Substitute It Now' (SIN) list recently.[158] Graphene seems to be a good candidate as the conductive filler at current stage and the 2D-structure of graphene are also favourable since the formation of microcapacitors will effectively increase the dielectric constant of the PMCs.[149,153,159]

2.2.3 Other polymer composites

Ternary composites combined with both conductive fillers and high-*k* ceramics have also been developed and the dielectric properties are generally superior to the binary ones.[70,160] Nan's group reported the first Ni/$BaTiO_3$/PVDF ternary PMC with a relative dielectric constant of 800.[161] Polyvinylidene fluoride (PVDF)-based ternary PMCs have been widely investigated and Young's modulus (E) is relatively high due to the inherent high E of PVDF (~2 GPa).[91,162] All organic CuPC/PANI/PU ternary

PMC was also developed for potential application in DEA.[163] Ning *et al.* have developed an organic conductive filler consists of gelatin and glycerol (GG) with dielectric constant as high as 41000 and elastic modulus lower than 1.5MPa and they have developed GG/TPU[164] and GG/CNC[165] systems with ε_r = 629 and 930 at 100 HZ and could be used as DEAs under very low electrical fields, though the tanδ are quite large. CNT/BTP/Polymer hybrid composites have also been developed which exhibit excellent dielectric and mechanic properties.[166] CNT/graphene hybrid TPU[167] and cyanoethyl pullulan polymer (CEP)[168] were also investigated with enhanced dielectric performance.

Chemical modification of the dielectric polymers, such as copolymerization,[169,170] grafting[74,171,172] and the addition of plasticizers[173,174] could also enlarge the dielectric constant in a certain degree due to the increase in the molecular polarity.

Ambrosio *et al* developed ZnO/PVA composite recently and the dielectric constant could be as high as 2000 at 1 kHz and the high dielectric constant was originated from the strong intermolecular interactions between -OH groups and ZnO nanoparticles.[175] The dipolar polarization turns out to be the dominant reason for the huge increasement, which is different from the interfacial polarization from most high-*k* systems.

Table 2.2 summarizes the dielectric and mechanical properties of some typical high-*k* PMCs reported in the literature. Developing high-*k* PMCs with the low dielectric loss, low working voltage and suitable mechanical properties remains a big challenge and is of great significance.

Table 2.2 Dielectric and mechanical properties of some high-*k* PMCs

No.	Materials	ε_r	Y / MPa	Loss tanδ	E / kV/mm	Ref
1	GG/TPU (50%)	629[a]	2.8	8.7[a]	0.5	[164]
2	GG/CNC (5%)	930[a]	2.1	2.3[a]	0.3	[165]
3	DAN/TPU (30%)	8[b]	7.1	0.04[b]	20	[174]
4	PDA-GO/rubber (0.25 g / L)	500[a] 200[b]	3.6	1.5[a] 1.3[b]	2	[176]
5	Easter-Grafted SBS (81%)	12.2[b]	0.34	0.07[b]	15.7	[171]
6	CNT-Graphene/TPU (3 vol %)	162[b]	7.8	0.8[b]	7.5	[167]
7	rGO/PEG/TPU (1.5% / 30%)	71[b]	0.9	2[b]	5	[177]
8	CNT/rubber (2 vol %)	574[b]	-	0.4[b]	-	[127]
9	SiC-SiO_2 /PVDF	2230[a] 1280[b]	1.9G	0.86[a] 0.42[b]	-	[97]
10	FLG/PVDF	4500[b]	-	2.83[b]	-	[129]

11	Acrylate copolymer	5.67[b]	2..59	0.02[b]	10	[169]
12	BT/ Slide-ring polymer (10%)	~10[b]	0.056	<0.1[b]	12	[73]
13	PHT/PDMS (1%)	~9.5[b]	0.02	-	8	[178]
14	PDA-Al_2O_3/rubber (30%)	11.5[b]	2.59	0.02	-	[179]
15	MG-grafted SBS (98.5%)	11.4[b]	2.87	0.009[b]	25	[74]
16	CuPc/P(VDF-TrFE) 40%	425[c]	0.6G	0.7[c]	13	[108]
17	PVA/ZnO	11468[d]	-	-	-	[175]
18	PVA/Graphene areogel	5720[b]	-	< 0.1[b]	-	[156]
	PEG 10%	6.8[b]	4.9	0.26[b]	5	
19	PU/plasticizer PMG30%	7.9[b]	2.2	0.22[b]	5	[173]
	TPP 10%	5.2[b]	2.3	0.09[b]	5	

[a]: measured at 100 HZ [b]: measured at 1000 HZ [c]: measured at 1 HZ [d]: measured at 500 HZ

2.3 Flexible electrodes

Flexible electrodes (FEs) have drawn an increasing research interest due to the rapid development of wearable electronics and flexible devices recent years.[180–183] A flexible electrode generally consists of a thin conductive layer and a flexible substrate, and sometimes an adhesive layer is introduced between the two layers for better connection.[184] Traditional electrodes are generally based on metals, which are highly conductive and the manufacturing technology are well-established, including electroplating,[185,186] electroless plating[187,188] and physical vapor deposition

(PVD).[189–191] Metal-based nanomaterials (*i.e.* Ag NPs, Ag NWs and Cu NWs) which could enable spin/spray coating[192,193] or even advanced printing technology (*i.e.* screen printing, inkjet printing and 3D printing)[194–196] to prepare designed patterns have shown emerging research interest recent years. FEs based on carbon materials have also been widely investigated, due to their light weight, high conductivity, intrinsic flexibility and easy manufacturing process.[197–199] Conductive polymers have also been developed for flexible electrodes due to their tunable chemical structures and inherent flexibility.

In this section, flexible electrodes based on the flexible film and textile substrates are introduced, mainly focus on the materials selection and manufacturing technologies.

2.3.1 Film-based electrodes

Early in 1970s, flexible electrodes based on Ag/polyester films have been developed[200] and later on PDMS[201,202], PI[203–205] and other polymers have been used as substrates for flexible electrodes as well. The most famous trade names for PET, PI and PDMS films are Mylar, Kapton and Ecoflex respectively. Thin film-based flexible electrodes play very important roles in the emerging flexible devices and wearable electronics.[206–209]

2.3.1.1 Polyester-based flexible electrodes

Indium tin oxide (ITO)/PET films are one of the most widely used flexible electrodes and are commercially available due to their low sheet resistance (<10 Ω sq^{-1}) and broadband transmittance.[210–212] However, the lack of indium, the high cost of manufacturing process and the inherent brittle of ITO have greatly limited their application.[213–215] Current research works on FEs mainly focus on metals, carbon materials and conductive polymers.[215]

Al/BOPET (Bi-axially Oriented Polyethylene Terephthalate) film prepared through magnetron sputtering was widely used in lightweight exoskeleton device[22] and electroadhesive clutch.[21] Al/Mylar flexible electrodes were also widely adopted in electroadhesion due to the easy shape deformation, which could minimize the air gaps and improve the performance.[216] Ni/Mylar flexible electrodes were used in wall-climbing robots where the thin Mylar film also act as dielectric materials.[42] Flexible OFET was proposed based on thermal evaporated Ag/Mylar electrodes in 2012.[217] Au/PET films could also be used for *in vivo* drug delivery systems.[218]

Apart from the thin metal layer, metal-based nanowires, nanofibers and nanogrids have also been widely used especially in transparent electrodes.[219,220] Cui's group reported large-scale fabrication of Ag NWs/PET transparent flexible electrodes by blade coating which is comparable with ITO in both electrical conductivity and diffusive

transmittance in 2010.[221] Their group also developed a novel strategy to develop highly conductive stretchable electrodes based on template synthesis of metal nanotrough network with superior mechanical and optoelectronic properties in 2013.[222] This method could allow various metals (*i.e*, Au, Ag, Cu, Al, Pt and Ni) thermal evaporated or electron-beam evaporated on different substrates including rigid glass slide and flexible PET, paper and textile. Ag NWs/PET has also been developed as transparent electrode for flexible OLED.[223]

Single wall carbon nanotubes (SWCNTs)/Mylar electrode has been developed for dielectric elastomer actuator through electrode transfer.[224] Though CNTs have shown excellent electrical conductivity and electron mobility,[225] the safety concern may limited their applications in wearable electronic.[226] As compared with the 1D CNT, the 2D graphene seems to be more promising conductive materials due to its high electrical conductivity and intrinsic flexibility.[227,228] Graphene-based flexible electrodes are mainly prepared through chemical vapor deposition (CVD) or reduction of graphene oxide on flexible substrates.[229,230] The thickness and properties of the graphene could be well-controlled in CVD process and even single-layer graphene could be successfully synthesized.[231–233] However, the high equipment, material and energy costs generated by CVD and the relatively small sizes (centimeter scale) have greatly limited its application.[233] Solution-based RGO has shown superior advantages such as low cost, large-scale processability, ease of surface modification and tunable functions.[230,234,235] The existence of the residual oxygen-containing functional groups

on RGO will reduce the electrical conductivity, as compared with the CVD-graphene.[236] A roll-to-roll (R2R) method for RGO/PET based transparent electrodes was proposed by Zhi and co-workers through spray coating of $SnCl_2$/ethanol on GO/PET films.[237] Electrochemically exfoliated graphene was also reported to be vacuum filtered and then transferred to PET substrates and the resultant electrodes could be used for OFET.[238] Graphene/PET flexible electrodes transferred from Cu foil was developed for long-term dynamic monitoring of electrocardiography (ECG) signals.[239]

Apart from the metal-based and carbon-based materials, conductive polymers with large π-conjugation are also promising candidates for FEs due to their high conductivity, inherent flexibility, ease of synthesis, low cost and solution processability.[240–242] Polyaniline (PANI), polypyrrole (PPy), polythiophene (PTh) and their derivatives are the most widely investigated conductive polymers. PANI and PPy exhibit good redox properties and are generally used in electrochemical applications, such as electrochromic devices[243–245] and electrochemical plasmonic switching.[246] PTh and its derivatives, typically the commercial available poly(3,4-ethylenedioxythiophene):polystyrene sulfonate (PEDOT:PSS) are relatively less active in redox reaction and are thus fascinating as electrode materials,[247] though there are also some examples of electrochromic windows based on PTh.[248–250] The electrical conductivity of pristine PEDOT:PSS is generally lower than 10 S/cm,[251] secondary doping of polar dopants such as glycerol,[252] ethylene glycol,[251] diethylene

glycol,[253] dimethyl sulfoxide (DMSO),[254] ionic liquid,[255] and strong acid[255,256] could increase the electrical conductivity two to three orders. Bao's group reported methanol-doped PEDOT:PSS electrodes prepared by solution shearing on PET substrate, the electrode exhibit a conductivity up to 4600 S/cm and transmission higher than 97% which remains the best electrical conductivity up to now.[257] The aqueous PEDOT:PSS could allow various fabrication technologies, including spin coating, blade coating, screen printing, inkjet printing and 3D printing.[247,258]

Due to the high transmittance in visible light, PEDOT:PSS is attractive in optoelectronic devices. Flexible organic solar cells based on PEDOT:PSS/PET electrodes with power conversion efficiency over 10% was developed through an all-solution-processed method.[259] Flexible perovskite solar cells was also reported based on a spin-coated PEDOT:PSS/PET films.[260] PEDOT:PSS is also widely used in flexible organic electrochemical transistors (OECTs) for saliva testing[261] and ECG recording.[262]

Stretchable organic light-emitting diodes (OLEDs) based on spin-coated PEDOT:PSS/Mylar electrodes was reported by White and co-workers in 2013.[263] Dip coating has also reported to prepare PEDOT:PSS/PET electrodes for fiber-shaped OLEDs.[264]

2.3.1.2 PI-based flexible electrodes

PI is also a broadly used substrate for FEs due to their excellent thermal stability, chemical inertness and superior mechanical strength.[205] PI-based flexible interdigital electrodes and printed circuit boards (PCBs) have already been commercialized. Transparent ITO/colorless PI electrodes which could enable the following thermal treatment processing for flexible perovskite solar cells was reported.[265] CNT/PI and Ag NW/PI electrodes have been proved to be more robust against bending as compared with ITO-based flexible electrodes.[205] Ag/PI electrodes was developed for flexible thermal electric generator (TEG).[266] Au/PI electrode array was developed for intracortical implants and PI could act as reactive interfaces for bioactive species.[267] Intra-neural implants based on stainless steel wires/PI electrodes was also reported and the PI-based electrodes exhibited good biocompatibility and reliability during the long-term monitoring.[268] Copper-clad PI interdigital electrodes were also widely used in electroadhesive pads and robots.[13,269] Graphene/PI electrodes were also demonstrated for rechargeable batteries[270–272] and EEG signal monitoring.[271] Graphene/PEDOT/PI electrodes with enhanced electrical conductivity were proposed for transparent microsupercapacitors.[273] Laser-induced graphene (LIG) could also be directly formed from PI by CO_2 laser was firstly proposed by Tour's group[274] and has turned out to be promising and facile method to prepare flexible electrodes with designed patterns.[273,275] Lu and co-worker prepared large-size flexible electrodes based on CNTs and a synthetic PI derivative as cathode for lithium ion batteries and the CNT network could be directly pressed on the substrate.[204] Wu's group presented an

electro-thermally driven actuators based on gap-coated graphite nanoplates/PI films.[276] A wearable sweat glucose sensor fabricated on multilayer Au/RGO/AuPtNP/PI electrode was proposed as well.[277]

2.3.1.3 PDMS-based flexible electrodes

In most cases, polyester and PI substrates could only make the devices flexible, and stretchable electrodes are generally based on elastomers, such as PDMS,[218,278] styrene ethylene butylene styrene (SEBS)[255,279] and polyurethane(PU).[280,281] Early in 2006, Huck *et al* have proposed a polymer-assisted metal deposition (PAMD) method of Cu on PDMS[282] and buckled Cu layer was introduced to increase the stretchability of the electrode.[283] PAMD could allow metal deposit on fiber, film and porous substrates through ink-jet printing, screen printing, nanolithography and electroless deposition.[182,284] The resistance change under stretch will also be significantly reduced by rolling the Au/PDMS films into fiber shape.[285] Core-shell structured Au-Ag nanowires-embedded stretchable PDMS electrode for wearable electrochromic supercapacitor was also reported recently.[286] Ko *et al* proposed a filtration-based method to prepare Ag nanowire percolation network in 2012, which could be easily transferred to other substrates, such as PDMS to obtain stretchable electrodes.[287] Ag NWs/PDMS conductors for human motion detection was developed by simple drop casting.[288] Stretchable Ag NWs/PDMS conductors for capacitive strain sensors with electrical conductivity higher than 8000 S/cm were developed by substrate transfer.[289]

Fan and coworkers reported a transfer method to prepare large-size PEDOT:PSS/PDMS electrodes and this strategy could effectively avoid the substrate damage caused by post-treatment.[290] Wrinkled PEDOT:PSS/PDMS conductors prepared by blade coating were used in stretchable and wearable triboelectric nanogenerator (TENG).[291] Carbon black/PDMS electrodes for low driving-voltage electroadhesive pads was also reported by Chen *et al*.[292] Buckled[293] and aligned CNTs[294] was dry spun on pre-stretched PDMS thin film to prepare flexible electrodes for stretchable supercapacitors. 3D interconnected CNT/Ecoflex stretchable electrodes for static and dynamic human motion sensing was also reported.[295]

2.3.1.4 Paper-based flexible electrodes

Apart from the polymeric thin film based flexible electrodes, paper-based electrodes have also attracted considerable research interests in the past several years due to their low-cost, bendable, disposable and renewable features.[296–298] Papers are generally made by pressing of randomly interconnected fibers and thus exhibit some unique characteristics as compared with polymeric films, including large surface area, outstanding tear resistance and firm bonding with coating layers.[296,299]

In 2007, Whitesides and coworkers firstly demonstrated a portable lab-on-paper platform for glucose and protein detection with patterned chromatography paper.[300] This work provides a simple yet effective method to the development of paper-based

flexible electronics, especially for electronic circuits,[301–303] energy harvesting and convention,[304–306] sensors,[299,307,308] microfluidics[309–311] and biomedical applications.[297,298,312]

Paper-based resistive strain sensor and capacitive proximity sensor could be fabricated by inkjet printing of nano silver inks and could be able to easily integrated with fluidic elastomer actuators (FEAs).[313] Copper tape/paper electrodes for interfacial connection of modular components based on electroadhsion was demonstrated recently by Guo *et al*, where papers also act as functional layers.[314] Physical vapor deposition (PVD) was a broadly used approach for manufacturing metal/paper electrodes.[305] Al foil could also be used as conductive materials in paper-based TENG.[315] Thin-film Cu and Al could also be directly used as conductive layer in paper-based batteries and transistors.[316] Inkjet printing of commercial Ag NP inks was also adopted in fabricating paper electrodes for OTFT.[317] Ag NWs were able to be spray coated on paper as cathode for light-emitting electrochemical cell (LEC). Filtration of Au NP through paper could form conductive networks which was used as working electrodes for microfluidic paper-based analytical devices (μ-PADs) and screen-printed carbon/paper films could act as counter electrodes.[318] Dipping the paper into chloroform solution of Au NWs is also a facile method to fabricate flexible paper electrodes.[319]

Vacuum filtration of graphene suspension could also directly deposit graphene on paper substrate to prepare freestanding bendable electrodes for flexible supercapacitors[320] and sodium ion batteries.[321] Stencil-printed graphene/paper electrode for foldable Organic thin-film transistors was also reported.[322] Graphite/paper electrodes could even be drawn by pencils for adaptive tactile sensor,[323] TENG[304] and supercapacitors.[324] Flexible electrodes could also be fabricated by simply soaking the air-laid papers into CNT aqueous suspension and even when through-holes were made on paper as breathable electronics, the paper-based supercapacitor still exhibited good mechanical strength.[325] Similar strategy was adopted in preparing CNT/paper electrode foldable lithium ion batteries.[326] Xu's group demonstrated the first example of CNT/paper bipolar electrodes(BPEs) for the detection of a cancer biomarker through screen printing of CNT inks.[327] Inkjet printing could also be used in the fabrication of CNT/Paper electrodes.[328] Meyer Rod coating of CNT on transparent paper substrates for OFET was also reported.[329] Drop casting of carbon inks on papers was also reported for 3D μ-PADs.[330] PEDOT could be deposited on paper through oxidative chemical vapor deposition (oCVD)[331] or interfacial polymerization of ethylenedioxythiophene (EDOT).[306,332]

2.3.1.5 Others

Printable Ag NP/fluorine rubber electrodes with electrical conductivity of 935 S/cm at 400% tensile strain (> 4000 S/cm at 0% strain) for sensor networks has been

demonstrated by Someya and co-worker.[333] Ag/NWs could also be dip-coated on twined cotton/PU fibers for stretchable electric circuits.[302] Electron beam deposited Cu on polysulfone substrate which exhibited programmable rigidity triggered by redox reaction was also demonstrated for stretchable electronics.[334]

2.3.2 Textile-based electrodes

Smart textiles which could enable sensing, communicating, data processing, actuating and energy harvesting have shown promising applications in wearable electronics.[183,335–337] Textile-based electrode (or conductive textile) as an essential component play very important roles in smart textiles. Apart from the general strategies used in fabricating film-based electrodes, textile technologies such as weaving, knitting or embroidery could also incorporate the conductive fibers/yarns into conductive textiles.[338–340]

Wearable antennas based on metal-plated textiles that enable wireless sensing, locating and communicating are necessary elements in interactive textile systems.[341] Plasma-coated Ag/PET yarn embroidered electrode[338] and screen-printed Ag paste/woven fabric (made of Lycra, cotton and polyester fiber)[342] for long-term monitoring of ECG were also reported. Inkjet printing could also be used as non-contact method to create Ag NP/fabric electrodes.[343] In-situ formation of Ag nanoparticle networks on the surface of SBS rubber fiber[344] and Kevlar fiber (a kind of aramid fiber)[345] could

produce highly conductive fibers and the high conductivity could be maintained even under large deformations. Stainless steel fabric was also reported to be used as negative electrode for lithium ion batteries.[346] Stretchable electrical circuits based on dip-coated Ag NWs/twining cotton/PU yarns were proposed.[302] Stretchable knitted fabric electrodes prepared by electroless plating of Cu was developed recently, which exhibited a sheet resistance as low as 2.0 Ω·sq at 500% strain.[188]

RGO/cotton fabric electrodes for wearable ECG were fabricated by dip-coating and in-situ reduction.[347] Carbon loaded rubber was used as conductive ink for breathable fabric electrode array by screen printing.[348] Stretchable RGO fibers based on core-shell structured PU/PET fibers by dip coating of GO followed by in situ reduction was demonstrated for wearable sensors[349] and electrothermal chromic devices.[350] Graphene fibers for wearable heater was also reported in a similar manner with bar coating.[351] CVD was also widely adopted in producing graphene woven farbics.[352,353] CNT/TPE fibers prepared through coaxial wet spinning for wearable strain sensors were reported.[354] Dip coating was also used in making CNT-based fiber electrodes.[355,356]

Polypyrrole (PPy) could be deposited on cotton fabrics through electrochemical polymerization and the resultant textile electrodes could be utilized as counter electrodes for DSSC.[357] Vapour phase polymerization of PEDOT on PET fabrics with application in ECG sensor was reported.[358] Inkjet and screen printing of PEDOT:PSS

were also conducted on knitted fabrics for long-term health monitoring.[359] PEDOT:PSS composite electrodes could be fabricated through drop casting for textile actuators.[360,361] Stencil printing could also deposit PEDOT"PSS onto nonwoven PET fabrics.[362]

2.4 Summary

A brief introduction of electroadhesion, high-*k* polymer matrix composites and flexible electrodes have been delivered. The materials, preparation methods and key characteristics have been summarized. Electroadhesive clutches which have advantages of light-weight, fast-response, low power-consumption, low working current and easy fabrication have shown promising potentials in robotics and wearable systems. Though the electroadhesion has been investigated for several decades, limited progress has been made and some problems still need to be addressed. Current problems mainly lie in the following aspects:

(1) The working voltage of the electroadhesive clutches is still as high as several hundred volts, which may cause safety problems for wearable applications;

(2) The performance of the electroadhesive clutch especially the generated shear stress should be improved at a relatively low driving-voltage (best performance reported in dielectric electroadhesive clutches: 23.8 kPa at 320 V[21]);

(3) The material systems for both dielectric layer and flexible electrodes are less investigated, developing novel high-*k* dielectric materials with high dielectric constant but low dielectric loss is also significant;

(4) Current researches on electroadhesive clutches are all focused on symmetric architectures comprising of two same electroadhesive pads, asymmetric structured electroadhesive clutches have not been investigated and the charge characteristics of the materials have not been considered.

Based on the theoretical models and current research works on electroadhesion, soft electroadhesive pads and high-*k* dielectric layers are two key points to obtain high-performance electroadhesive devices. So future works will mainly focus on developing more flexible electrodes and dielectric materials and novel high-*k* systems should be developed as the dielectric layers. Intelligent structure design and smart material selection will be made to obtain electroadhesive clutches with large force and low driving voltage.

References

[1] R. Liu, R. Chen, H. Shen, R. Zhang, *Int. J. Adv. Robot. Syst.* **2013**, *10*, 36.

[2] J. Mao, L. Qin, Y. Wang, J. Liu, L. Xue, in *2014 IEEE Int. Conf. Mechatronics Autom.*, IEEE, **2014**, pp. 987–992.

[3] A. R. Von Hippel, *Dielectrics and Waves*, Artech House, **1995**.

[4] D. Ruffatto, A. Parness, M. Spenko, *J. R. Soc. Interface* **2014**, *11*, 20131089.

[5] H. Prahlad, R. Pelrine, S. Stanford, J. Marlow, R. Kornbluh, in *2008 IEEE Int. Conf. Robot. Autom.*, IEEE, **2008**, pp. 3028–3033.

[6] C. Cao, X. Sun, Y. Fang, Q.-H. Qin, A. Yu, X.-Q. Feng, *Mater. Des.* **2016**, *89*, 485.

[7] R. P. Krape, C. C. S. Division, L. R. Center, *Applications Study of Electroadhesive Devices*, National Aeronautics And Space Administration; For Sale By The Clearinghouse For Federal Scientific And Technical Information, Springfield, Va., **1968**.

[8] G. A. Wardly, *Rev. Sci. Instrum.* **1973**, *44*, 1506.

[9] J. Guo, T. Bamber, Y. Zhao, M. Chamberlain, L. Justham, M. Jackson, *IEEE Robot. Autom. Lett.* **2017**, *2*, 538.

[10] G. J. Monkman, P. M. Taylor, G. J. Farnworth, *Int. J. Cloth. Sci. Technol.* **1989**, *1*, 14.

[11] G. J. Monkman, *Int. J. Rob. Res.* **1995**, *14*, 144.

[12] Z. Zhang, J. A. Chestney, M. Sarhadi, *Proc. Inst. Mech. Eng. Part B J. Eng. Manuf.* **2001**, *215*, 21.

[13] M. A. Graule, P. Chirarattananon, S. B. Fuller, N. T. Jafferis, K. Y. Ma, M. Spenko, R. Kornbluh, R. J. Wood, *Science* **2016**, *352*, 978.

[14] A. Yamamoto, T. Nakashima, T. Higuchi, in *2007 Int. Symp. Micro-NanoMechatronics Hum. Sci.*, IEEE, **2007**, pp. 389–394.

[15] J. Shintake, S. Rosset, B. Schubert, D. Floreano, H. Shea, *Adv. Mater.* **2016**, *28*, 231.

[16] G. Monkman, *Ind. Robot An Int. J.* **2003**, *30*, 326.

[17] J. Guo, K. Elgeneidy, C. Xiang, N. Lohse, L. Justham, J. Rossiter, *Smart Mater. Struct.* **2018**, *27*, 055006.

[18] O. Sirin, M. Ayyildiz, B. N. J. Persson, C. Basdogan, *Soft Matter* **2019**, *15*, 1758.

[19] Y. Okuno, H. Shigemune, Y. Kuwajima, S. Maeda, *Adv. Mater. Technol.* **2019**, *4*, 1800304.

[20] C. J. Fitch, *IBM J. Res. Dev.* **1957**, *1*, 49.

[21] S. B. Diller, S. H. Collins, C. Majidi, *J. Intell. Mater. Syst. Struct.* **2018**, *29*, 3804.

[22] S. Diller, C. Majidi, S. H. Collins, in *2016 IEEE Int. Conf. Robot. Autom.*, IEEE, **2016**, pp. 682–689.

[23] V. Ramachandran, J. Shintake, D. Floreano, *Adv. Mater. Technol.* **2019**, *4*, 1800313.

[24] J. Guo, T. Bamber, M. Chamberlain, L. Justham, M. Jackson, *J. Phys. D. Appl. Phys.*

2016, *49*, 415304.

[25] M. Jackson, L. Justham, J. Guo, T. Bamber, T. Hovell, M. Chamberlain, *IFAC-PapersOnLine* **2016**, *49*, 309.

[26] J. Guo, M. Tailor, T. Bamber, M. Chamberlain, L. Justham, M. Jackson, *J. Phys. D. Appl. Phys.* **2016**, *49*, 035303.

[27] J. L. Guo, L. Justham, M. Jackson, R. Parkin, *Key Eng. Mater.* **2015**, *649*, 22.

[28] G. J. Monkman, *Robotica* **1992**, *10*, 183.

[29] T. Watanabe, T. Kitabayashi, C. Nakayama, *Jpn. J. Appl. Phys.* **1993**, *32*, 864.

[30] S. Kanno, K. Kato, K. Yoshioka, R. Nishio, T. Tsubone, *J. Vac. Sci. Technol. B Microelectron. Nanom. Struct.* **2006**, *24*, 216.

[31] S. Kanno, T. Usui, *J. Vac. Sci. Technol. B Microelectron. Nanom. Struct.* **2003**, *21*, 2371.

[32] T. Nakamura, A. Yamamoto, in *2013 World Haptics Conf.*, IEEE, **2013**, pp. 37–42.

[33] F. Giraud, M. Amberg, B. Lemaire-Semail, in *2013 World Haptics Conf.*, IEEE, **2013**, pp. 199–203.

[34] A. Yamamoto, S. Nagasawa, H. Yamamoto, T. Higuchi, *IEEE Trans. Vis. Comput. Graph.* **2006**, *12*, 168.

[35] D. J. Meyer, M. A. Peshkin, J. E. Colgate, in *2013 World Haptics Conf.*, IEEE, **2013**, pp. 43–48.

[36] M. Auvray, C. Duriez, *Haptics: Neuroscience, Devices, Modeling, and Applications*, Springer Berlin Heidelberg, Berlin, Heidelberg, **2014**.

[37] T. Nakamura, A. Yamamoto, *ROBOMECH J.* **2017**, *4*, 18.

[38] R. Chen, *IEEE Potentials* **2015**, *34*, 15.

[39] S. D. de Rivaz, B. Goldberg, N. Doshi, K. Jayaram, J. Zhou, R. J. Wood, *Sci. Robot.* **2018**, *3*, eaau3038.

[40] G. Gu, J. Zou, R. Zhao, X. Zhao, X. Zhu, *Sci. Robot.* **2018**, *3*, eaat2874.

[41] H. Wang, A. Yamamoto, T. Higuchi, *Int. J. Adv. Robot. Syst.* **2014**, *11*, 191.

[42] W. J. Tong, Cheng Siong Chin, Wei Peng Lin, in *2014 9th IEEE Conf. Ind. Electron. Appl.*, IEEE, **2014**, pp. 473–477.

[43] J. Germann, B. Schubert, D. Floreano, in *2014 IEEE/RSJ Int. Conf. Intell. Robot. Syst.*, IEEE, **2014**, pp. 3933–3938.

[44] J. Shintake, V. Cacucciolo, D. Floreano, H. Shea, *Adv. Mater.* **2018**, *30*, 1707035.

[45] "Grabit electroadhesion robotic each pick gripper - boxes, bags, cans, bare goods," can be found under https://www.youtube.com/watch?v=0DgORq2bbTI, **n.d.**

[46] H. R. X. Liang, Y. Sun, H. Wang, R. C. H. Yeow, S. L. Kukreja, N. Thakor, in *IEEE RAS EMBS Int. Conf. Biomed. Robot. Bio-Mechatronics, IEEE, Piscataway, NJ, USA*, **2016**, pp. 401–406.

[47] J. Guo, C. Xiang, J. Rossiter, *Mater. Des.* **2018**, *156*, 586.

[48] J. Guo, C. Xiang, P. Zanini, J. Rossiter, *IEEE Robot. Autom. Lett.* **2019**, *4*, 2364.

[49] M. Plooij, G. Mathijssen, P. Cherelle, D. Lefeber, B. Vanderborght, *IEEE Robot. Autom. Mag.* **2015**, *22*, 106.

[50] W. J. Wu, P. C. Lin, *IEEE/ASME Int. Conf. Adv. Intell. Mechatronics, AIM* **2017**, 1173.

[51] A. Girard, H. H. Asada, in *2016 IEEE Int. Conf. Robot. Autom.*, IEEE, **2016**, pp. 4572–4577.

[52] M. Plooij, W. Wolfslag, M. Wisse, *IEEE/ASME Trans. Mechatronics* **2017**, *22*, 739.

[53] C. Rossa, J. Lozada, A. Micaelli, *IEEE Trans. Haptics* **2014**, *7*, 442.

[54] M. I. Awad, D. Gan, A. Az-Zu'Bi, J. Thattamparambil, C. Stefanini, J. Dias, L. Seneviratne, *2016 IEEE Int. Conf. Robot. Biomimetics, ROBIO 2016* **2016**, 1808.

[55] E. J. Rouse, L. M. Mooney, H. M. Herr, *Int. J. Rob. Res.* **2014**, *33*, 1611.

[56] T. Kikuchi, K. Otsuki, J. Furusho, H. Abe, J. Noma, M. Naito, N. Lauzier, *Adv. Robot.* **2010**, *24*, 1489.

[57] A. S. Shafer, M. R. Kermani, in *2011 IEEE Int. Conf. Robot. Autom.*, IEEE, **2011**, pp. 4266–4271.

[58] K. Boku, T. Nakamura, *J. Intell. Mater. Syst. Struct.* **2010**, *21*, 1563.

[59] S. H. Collins, M. B. Wiggin, G. S. Sawicki, *Nature* **2015**, *522*, 212.

[60] I. Choi, N. Corson, L. Peiros, E. W. Hawkes, S. Keller, S. Follmer, *IEEE Robot.*

Autom. Lett. **2018**, *3*, 450.

[61] D. M. Aukes, B. Heyneman, J. Ulmen, H. Stuart, M. R. Cutkosky, S. Kim, P. Garcia, A. Edsinger, *Int. J. Rob. Res.* **2014**, *33*, 721.

[62] H. J. Kim, L. Paquin, C. W. Barney, S. So, B. Chen, Z. Suo, A. J. Crosby, R. C. Hayward, *Adv. Mater.* **2020**, *32*, 2000600.

[63] A. Johnsen, K. Rahbek, *J. Inst. Electr. Eng.* **1923**, *61*, 713.

[64] E. Mallinckrodt, A. L. Hughes, W. Sleator, *Science* **1953**, *118*, 277.

[65] S.-C. Kim, A. Israr, I. Poupyrev, in *Proc. 26th Annu. ACM Symp. User Interface Softw. Technol. - UIST '13*, ACM Press, New York, New York, USA, **2013**, pp. 531–538.

[66] Y. Vardar, B. Guclu, C. Basdogan, *IEEE Trans. Haptics* **2017**, *10*, 488.

[67] D. Wijekoon, M. E. Cecchinato, E. Hoggan, J. Linjama, in *Haptics Perception, Devices, Mobility, Commun. EuroHaptics*, Springer, Berlin, Heidelberg, **2012**, pp. 613–624.

[68] Y. Lee, W. J. Song, Y. Jung, H. Yoo, M.-Y. Kim, H. Kim, J. Sun, *Sci. Robot.* **2020**, *5*, eaaz5405.

[69] G. C. Psarras, in *Dielectr. Polym. Mater. High-Density Energy Storage*, Elsevier, **2018**, pp. 11–57.

[70] Z. Dang, J. Yuan, J. Zha, T. Zhou, S.-T. Li, G.-H. Hu, *Prog. Mater. Sci.* **2012**, *57*, 660.

[71] W. Xia, J. Lu, S. Tan, J. Liu, Z. Zhang, in *Dielectr. Polym. Mater. High-Density*

Energy Storage, Elsevier, **2018**, pp. 103–163.

[72] R. Raihan, F. Rabbi, V. Vadlamudi, K. Reifsnider, *Mater. Sci. Appl.* **2015**, *06*, 1033.

[73] D. Yang, F. Ge, M. Tian, N. Ning, L. Zhang, C. Zhao, K. Ito, T. Nishi, H. Wang, Y. Luan, *J. Mater. Chem. A* **2015**, *3*, 9468.

[74] C. Ellingford, R. Zhang, A. M. Wemyss, C. Bowen, T. McNally, Ł. Figiel, C. Wan, *ACS Appl. Mater. Interfaces* **2018**, *10*, 38438.

[75] M. Molberg, D. Crespy, P. Rupper, F. Nüesch, J.-A. E. Månson, C. Löwe, D. M. Opris, *Adv. Funct. Mater.* **2010**, *20*, 3280.

[76] R. Czarny, T. Q. V. Hoang, B. Loiseaux, G. Bellomonte, R. Lebourgeois, A. Leuliet, L. Qassym, C. Galindo, J. M. Heintz, N. Penin, L. Fourier, C. Elissalde, J. F. Silvain, T. Fournier, C. Jegou, P. Pouliguen, in *2018 IEEE Conf. Antenna Meas. Appl. CAMA 2018*, IEEE, **2018**, pp. 1–4.

[77] B. Wang, W. Huang, L. Chi, M. Al-Hashimi, T. J. Marks, A. Facchetti, *Chem. Rev.* **2018**, *118*, 5690.

[78] P. Ding, Y. Yang, Y. Wang, C. Liu, J. Yin, Y. Xia, A. Li, Z. Liu, *Appl. Phys. Lett.* **2019**, *114*, 053506.

[79] Y. Wang, X. Huang, T. Li, L. Li, X. Guo, P. Jiang, *Chem. Mater.* **2019**, *31*, 2212.

[80] L. Yao, D. Wang, P. Hu, B.-Z. Han, Z.-M. Dang, *Adv. Mater. Interfaces* **2016**, *3*, 1600016.

[81] L. Yang, X. Kong, F. Li, H. Hao, Z. Cheng, H. Liu, J.-F. Li, S. Zhang, *Prog. Mater.*

Sci. **2019**, *102*, 72.

[82] A. K. Zak, W. C. Gan, W. H. A. Majid, M. Darroudi, T. S. Velayutham, *Ceram. Int.* **2011**, *37*, 1653.

[83] L. Dong, C. Xiong, H. Quan, G. Zhao, *Scr. Mater.* **2006**, *55*, 835.

[84] G. Zhang, D. Brannum, D. Dong, L. Tang, E. Allahyarov, S. Tang, K. Kodweis, J. K. Lee, L. Zhu, *Chem. Mater.* **2016**, *28*, 4646.

[85] A. Rahmanudin, D. J. Tate, R. Marcial-Hernandez, N. Bull, S. K. Garlapati, A. Zamhuri, R. U. Khan, S. Faraji, S. R. Gollu, K. C. Persaud, M. L. Turner, *Adv. Electron. Mater.* **2020**, *6*, 1901127.

[86] W. Hu, Z. Ren, J. Li, E. Askounis, Z. Xie, Q. Pei, *Adv. Funct. Mater.* **2015**, *25*, 4827.

[87] Z.-M. Dang, M.-S. Zheng, J.-W. Zha, *Small* **2016**, *12*, 1688.

[88] H. Zhang, M. A. Marwat, B. Xie, M. Ashtar, K. Liu, Y. Zhu, L. Zhang, P. Fan, C. Samart, Z. Ye, *ACS Appl. Mater. Interfaces* **2020**, *12*, 1.

[89] Y. Feng, P. Liang, B. Tang, Y. Wang, J. Liu, L. Shui, H. Li, M. Tian, L. Zhang, G. Zhou, *Nano Energy* **2019**, *64*, 103985.

[90] M. Arbatti, X. Shan, Z.-Y. Cheng, *Adv. Mater.* **2007**, *19*, 1369.

[91] D. Wang, T. Zhou, J.-W. Zha, J. Zhao, C.-Y. Shi, Z.-M. Dang, *J. Mater. Chem. A* **2013**, *1*, 6162.

[92] Y. Bai, Z. Y. Cheng, V. Bharti, H. S. Xu, Q. M. Zhang, *Appl. Phys. Lett.* **2000**, *76*, 3804.

[93] B.-H. Fan, J.-W. Zha, D. Wang, J. Zhao, Z.-M. Dang, *Appl. Phys. Lett.* **2012**, *100*, 012903.

[94] Y.-Y. Yu, C.-T. Chiu, C.-C. Chueh, *Asian J. Org. Chem.* **2018**, *7*, 2263.

[95] J. Castro, E. Rojas, T. Weller, J. Wang, in *2015 IEEE 16th Annu. Wirel. Microw. Technol. Conf.*, IEEE, **2015**, pp. 1–5.

[96] X. Huang, B. Sun, Y. Zhu, S. Li, P. Jiang, *Prog. Mater. Sci.* **2019**, *100*, 187.

[97] J. Bi, Y. Gu, Z. Zhang, S. Wang, M. Li, Z. Zhang, *Mater. Des.* **2016**, *89*, 933.

[98] Y. Shen, Y. H. Lin, C.-W. Nan, *Adv. Funct. Mater.* **2007**, *17*, 2405.

[99] Y. Feng, W. L. Li, J. P. Wang, J. H. Yin, W. D. Fei, *J. Mater. Chem. A* **2015**, *3*, 20313.

[100] Q. G. Chi, L. Gao, X. Wang, Y. Chen, J. F. Dong, Y. Cui, Q. Q. Lei, *AIP Adv.* **2015**, *5*, 117103.

[101] K. Yang, X. Huang, Y. Huang, L. Xie, P. Jiang, *Chem. Mater.* **2013**, *25*, 2327.

[102] G. Jian, M. Liu, C. Yan, F. Wu, B. Song, K. S. Moon, C. P. Wong, *Nano Energy* **2019**, *58*, 419.

[103] Y. Feng, W. L. Li, Y. F. Hou, Y. Yu, W. P. Cao, T. D. Zhang, W. D. Fei, *J. Mater. Chem. C* **2015**, *3*, 1250.

[104] S. Liu, J. Zhai, *J. Mater. Chem. A* **2015**, *3*, 1511.

[105] Y. Zhu, H. Yao, P. Jiang, J. Wu, X. Zhu, X. Huang, *J. Phys. Chem. C* **2018**, *122*, 18282.

[106] Q. Li, L. Chen, M. R. Gadinski, S. Zhang, G. Zhang, H. U. Li, E. Iagodkine, A. Haque, L.-Q. Chen, T. N. Jackson, Q. Wang, *Nature* **2015**, *523*, 576.

[107] S. Luo, Y. Shen, S. Yu, Y. Wan, W.-H. Liao, R. Sun, C.-P. Wong, *Energy Environ. Sci.* **2017**, *10*, 137.

[108] Q. M. Zhang, H. Li, M. Poh, F. Xia, Z.-Y. Cheng, H. Xu, C. Huang, *Nature* **2002**, *419*, 284.

[109] X.-Z. Tang, X. Li, Z. Cao, J. Yang, H. Wang, X. Pu, Z.-Z. Yu, *Carbon* **2013**, *59*, 93.

[110] Y. Zhang, Y. Wang, Y. Deng, M. Li, J. Bai, *ACS Appl. Mater. Interfaces* **2012**, *4*, 65.

[111] Z. Zeng, H. Jin, M. Chen, W. Li, L. Zhou, Z. Zhang, *Adv. Funct. Mater.* **2016**, *26*, 303.

[112] Y. Chen, H.-B. Zhang, Y. Yang, M. Wang, A. Cao, Z.-Z. Yu, *Adv. Funct. Mater.* **2016**, *26*, 447.

[113] Y. Chen, Y. Wang, H.-B. Zhang, X. Li, C.-X. Gui, Z.-Z. Yu, *Carbon* **2015**, *82*, 67.

[114] S. Wu, R. B. Ladani, J. Zhang, K. Ghorbani, X. Zhang, A. P. Mouritz, A. J. Kinloch, C. H. Wang, *ACS Appl. Mater. Interfaces* **2016**, *8*, 24853.

[115] F. He, S. Lau, H. L. Chan, J. Fan, *Adv. Mater.* **2009**, *21*, 710.

[116] M. Gökçen, T. Tunç, *Int. J. Appl. Ceram. Technol.* **2013**, *10*, E64.

[117] M. H. Al-Saleh, *Nanotechnology* **2019**, *30*, 062001.

[118] N. Yousefi, X. Sun, X. Lin, X. Shen, J. Jia, B. Zhang, B. Tang, M. Chan, J.-K. Kim,

Adv. Mater. **2014**, *26*, 5480.

[119] T. Lertprapaporn, H. Manuspiya, A. Laobuthee, *Mater. Today Proc.* **2018**, *5*, 9326.

[120] Z. Wang, W. Zhou, L. Dong, X. Sui, J. Zuo, H. Cai, X. Liu, Q. Chen, J. Cai, *J. Alloys Compd.* **2016**, *689*, 342.

[121] Z. Wang, W. Zhou, L. Dong, X. Sui, H. Cai, J. Zuo, Q. Chen, *J. Alloys Compd.* **2016**, *682*, 738.

[122] S. Moharana, R. N. Mahaling, *Chem. Phys. Lett.* **2017**, *680*, 31.

[123] X. Liang, T. Zhao, Y. Hu, R. Sun, *J. Nanoparticle Res.* **2014**, *16*, 2578.

[124] W. Zhou, Z. Wang, L. Dong, X. Sui, Q. Chen, *Compos. Part A Appl. Sci. Manuf.* **2015**, *79*, 183.

[125] W. Zhou, L. Xu, L. Jiang, J. Peng, Y. Gong, X. Liu, H. Cai, G. Wang, Q. Chen, *J. Alloys Compd.* **2017**, *710*, 47.

[126] J. Zhu, J. Shen, S. Guo, H.-J. Sue, *Carbon* **2015**, *84*, 355.

[127] H. Sun, H. Zhang, S. Liu, N. Ning, L. Zhang, M. Tian, Y. Wang, *Compos. Sci. Technol.* **2018**, *154*, 145.

[128] Y. Zhang, D. Xu, W. Xu, W. Wei, S. Guan, Z. Jiang, *Compos. Sci. Technol.* **2014**, *104*, 89.

[129] L. Chu, Q. Xue, J. Sun, F. Xia, W. Xing, D. Xia, M. Dong, *Compos. Sci. Technol.* **2013**, *86*, 70.

[130] Y. Li, M. Fan, K. Wu, F. Yu, S. Chai, F. Chen, Q. Fu, *Compos. Part A Appl. Sci. Manuf.* **2015**, *73*, 85.

[131] C. Min, D. Yu, J. Cao, G. Wang, L. Feng, *Carbon* **2013**, *55*, 116.

[132] M. Shi, W. Yang, Y. Zhang, J. Tan, L. Cheng, Z. Jiao, X. Zhen, *J. Appl. Polym. Sci.* **2019**, *136*, 48131.

[133] L. Wang, Z.-M. Dang, *Appl. Phys. Lett.* **2005**, *87*, 042903.

[134] J. Chang, G. Liang, A. Gu, S. Cai, L. Yuan, *Carbon* **2012**, *50*, 689.

[135] B. Wang, G. Liang, Y. Jiao, A. Gu, L. Liu, L. Yuan, W. Zhang, *Carbon* **2013**, *54*, 224.

[136] N. Ning, D. Cheng, J. Yang, L. Liu, M. Tian, Y. Wu, W. Wang, L. Zhang, Y. Lu, *Compos. Sci. Technol.* **2017**, *142*, 214.

[137] R. Simoes, J. Silva, R. Vaia, V. Sencadas, P. Costa, J. Gomes, S. Lanceros-Méndez, *Nanotechnology* **2009**, *20*, 035703.

[138] M. Selvi, M. Rangaraj Vengatesan, P. Prabunathan, J. Kun Song, M. Alagar, *Appl. Phys. Lett.* **2013**, *103*, 2011.

[139] Q. LI, Q. XUE, L. HAO, X. GAO, Q. ZHENG, *Compos. Sci. Technol.* **2008**, *68*, 2290.

[140] J.-K. Yuan, S.-H. Yao, Z.-M. Dang, A. Sylvestre, M. Genestoux, J. Bai, *J. Phys. Chem. C* **2011**, *115*, 5515.

[141] S.-H. Yao, J.-K. Yuan, T. Zhou, Z.-M. Dang, J. Bai, *J. Phys. Chem. C* **2011**, *115*, 20011.

[142] B. ZHU, S. XIE, Z. XU, Y. XU, *Compos. Sci. Technol.* **2006**, *66*, 548.

[143] A. Das, K. W. Stöckelhuber, R. Jurk, M. Saphiannikova, J. Fritzsche, H. Lorenz, M. Klüppel, G. Heinrich, *Polymer (Guildf).* **2008**, *49*, 5276.

[144] A. K. Geim, *Science* **2009**, *324*, 1530.

[145] A. K. Geim, K. S. Novoselov, *Nat. Mater.* **2007**, *6*, 183.

[146] J. Wang, X. Wang, C. Xu, M. Zhang, X. Shang, *Polym. Int.* **2011**, *60*, 816.

[147] X.-J. Zhang, G.-S. Wang, W.-Q. Cao, Y.-Z. Wei, M.-S. Cao, L. Guo, *RSC Adv.* **2014**, *4*, 19594.

[148] H. Tang, G. J. Ehlert, Y. Lin, H. A. Sodano, *Nano Lett.* **2012**, *12*, 84.

[149] J. Shang, Y. Zhang, L. Yu, B. Shen, F. Lv, P. K. Chu, *Mater. Chem. Phys.* **2012**, *134*, 867.

[150] Y. Zhang, S. Jiang, M. Fan, Y. Zeng, Y. Yu, J. He, *J. Mater. Sci. Mater. Electron.* **2013**, *24*, 927.

[151] J. Shang, Y. Zhang, L. Yu, X. Luan, B. Shen, Z. Zhang, F. Lv, P. K. Chu, *J. Mater. Chem. A* **2013**, *1*, 884.

[152] C. Wu, X. Huang, G. Wang, X. Wu, K. Yang, S. Li, P. Jiang, *J. Mater. Chem.* **2012**, *22*, 7010.

[153] D. Wang, Y. Bao, J. W. Zha, J. Zhao, Z. M. Dang, G. H. Hu, *ACS Appl. Mater. Interfaces* **2012**, *4*, 6273.

[154] Y. Fu, L. Liu, J. Zhang, *ACS Appl. Mater. Interfaces* **2014**, *6*, 14069.

[155] J.-Y. Kim, W. H. Lee, J. W. Suk, J. R. Potts, H. Chou, I. N. Kholmanov, R. D. Piner, J. Lee, D. Akinwande, R. S. Ruoff, *Adv. Mater.* **2013**, *25*, 2308.

[156] Z. Wang, N. M. Han, Y. Wu, X. Liu, X. Shen, Q. Zheng, J.-K. Kim, *Carbon* **2017**, *123*, 385.

[157] A. Nel, *Science* **2006**, *311*, 622.

[158] J. C. Release, **2020**, *15*, 627.

[159] J. Shang, Y. Zhang, L. Yu, B. Shen, F. Lv, P. K. Chu, *Mater. Chem. Phys.* **2012**, *134*, 867.

[160] C.-W. Nan, Y. Shen, J. Ma, *Annu. Rev. Mater. Res.* **2010**, *40*, 131.

[161] Z.-M. Dang, Y. Shen, C.-W. Nan, *Appl. Phys. Lett.* **2002**, *81*, 4814.

[162] Y. C. Li, S. C. Tjong, R. K. Y. Li, *Express Polym. Lett.* **2011**, *5*, 526.

[163] C. Huang, Q. M. Zhang, G. DeBotton, K. Bhattacharya, *Appl. Phys. Lett.* **2004**, *84*, 4391.

[164] M. Tian, Y. Yao, S. Liu, D. Yang, L. Zhang, T. Nishi, N. Ning, *J. Mater. Chem. A* **2015**, *3*, 1483.

[165] N. Ning, Z. Wang, Y. Yao, L. Zhang, M. Tian, *Carbohydr. Polym.* **2015**, *130*, 262.

[166] D. Zhao, L. Yuan, G. Liang, A. Gu, *Compos. Part B Eng.* **2019**, *173*, 107030.

[167] S. Liu, H. Sun, N. Ning, L. Zhang, M. Tian, W. Zhu, T. W. Chan, *Compos. Sci.*

Technol. **2016**, *125*, 30.

[168] J.-Y. Kim, T. Kim, J. W. Suk, H. Chou, J.-H. Jang, J. H. Lee, I. N. Kholmanov, D. Akinwande, R. S. Ruoff, *Small* **2014**, *10*, 3405.

[169] Y. Zhao, J.-W. Zha, L.-J. Yin, Z.-S. Gao, Y.-Q. Wen, Z.-M. Dang, *Polymer* **2018**, *137*, 269.

[170] Y. Zhao, J.-W. Zha, L.-J. Yin, S.-T. Li, Y.-Q. Wen, Z.-M. Dang, *Polymer* **2018**, *149*, 39.

[171] H. Sun, C. Jiang, N. Ning, L. Zhang, M. Tian, S. Yuan, *Polym. Chem.* **2016**, *7*, 4072.

[172] M. Tian, H. Yan, H. Sun, L. Zhang, N. Ning, *RSC Adv.* **2016**, *6*, 96190.

[173] C. Renard, D. Wang, Y. Yang, S. Xiong, C.-Y. Shi, Z.-M. Dang, *J. Appl. Polym. Sci.* **2017**, *134*, 45123.

[174] N. Ning, B. Yan, S. Liu, Y. Yao, L. Zhang, T. W. Chan, T. Nishi, M. Tian, *Smart Mater. Struct.* **2015**, *24*, 032002.

[175] R. Torrealba, M. Mota, H. Vazquez, R. Ambrosio, J. Flores, I. Vivaldo, M. Moreno, K. de la Torre, A. Carrillo, *Polymers* **2018**, *10*, 1370.

[176] N. Ning, Q. Ma, S. Liu, M. Tian, L. Zhang, T. Nishi, *ACS Appl. Mater. Interfaces* **2015**, *7*, 10755.

[177] N. Ning, S. Li, H. Sun, Y. Wang, S. Liu, Y. Yao, B. Yan, L. Zhang, M. Tian, *Compos. Sci. Technol.* **2017**, *142*, 311.

[178] F. Carpi, G. Gallone, F. Galantini, D. De Rossi, *Adv. Funct. Mater.* **2008**, *18*, 235.

[179] M. Ruan, D. Yang, W. Guo, L. Zhang, S. Li, Y. Shang, Y. Wu, M. Zhang, H. Wang, *Appl. Surf. Sci.* **2018**, *439*, 186.

[180] W. Zeng, L. Shu, Q. Li, S. Chen, F. Wang, X.-M. Tao, *Adv. Mater.* **2014**, *26*, 5310.

[181] X. Tao, *Acc. Chem. Res.* **2019**, *52*, 307.

[182] P. Li, Y. Zhang, Z. Zheng, *Adv. Mater.* **2019**, *31*, 1902987.

[183] J. Shi, S. Liu, L. Zhang, B. Yang, L. Shu, Y. Yang, M. Ren, Y. Wang, J. Chen, W. Chen, Y. Chai, X. Tao, *Adv. Mater.* **2020**, *32*, 1901958.

[184] C. Wang, G. G. Wallace, *Electrochim. Acta* **2015**, *175*, 87.

[185] X. Wang, W. Zeng, L. Hong, W. Xu, H. Yang, F. Wang, H. Duan, M. Tang, H. Jiang, *Nat. Energy* **2018**, *3*, 227.

[186] J. Park, J. Eom, H. Kwon, *Electrochim. Acta* **2010**, *55*, 1825.

[187] S.-Y. Min, Y. Lee, S. H. Kim, C. Park, T.-W. Lee, *ACS Nano* **2017**, *11*, 3681.

[188] X. Lin, M. Wu, L. Zhang, D. Wang, *ACS Appl. Electron. Mater.* **2019**, *1*, 397.

[189] G. Mauer, R. Vaßen, *Adv. Eng. Mater.* **2020**, *22*, 1900988.

[190] Y. J. Jo, T. F. Zhang, M. J. Son, K. H. Kim, *Appl. Surf. Sci.* **2018**, *433*, 1184.

[191] J. Zhao, Z. Liu, Q. Shen, B. Wang, Q. Wang, *Materials* **2018**, *11*, 1281.

[192] V. Scardaci, R. Coull, P. E. Lyons, D. Rickard, J. N. Coleman, *Small* **2011**, *7*, 2621.

[193] H. Kang, Y. Kim, S. Cheon, G. Yi, J. H. Cho, *ACS Appl. Mater. Interfaces* **2017**, *9*, 30779.

[194] C. Yang, H. Zhang, Y. Liu, Z. Yu, X. Wei, Y. Hu, *Adv. Sci.* **2018**, *5*, 1801070.

[195] M. KARAKAWA, T. TOKUNO, M. NOGI, Y. ASO, K. SUGANUMA, *Electrochemistry* **2017**, *85*, 245.

[196] X. Li, Y. Wang, C. Yin, Z. Yin, *J. Mater. Chem. C* **2020**, *8*, 849.

[197] C. Wang, K. Xia, H. Wang, X. Liang, Z. Yin, Y. Zhang, *Adv. Mater.* **2019**, *31*, 1801072.

[198] Y. Cheng, S. Lu, H. Zhang, C. V. Varanasi, J. Liu, *Nano Lett.* **2012**, *12*, 4206.

[199] N. Karim, S. Afroj, A. Malandraki, S. Butterworth, C. Beach, M. Rigout, K. S. Novoselov, A. J. Casson, S. G. Yeates, *J. Mater. Chem. C* **2017**, *5*, 11640.

[200] V. L. D. S. N. Button, in *Princ. Meas. Transduct. Biomed. Var.*, **2015**, pp. 25–76.

[201] J.-Y. Baek, J.-H. An, J.-M. Choi, K.-S. Park, S.-H. Lee, *Sensors Actuators A Phys.* **2008**, *143*, 423.

[202] M. Ochoa, P. Wei, A. J. Wolley, K. J. Otto, B. Ziaie, *Biomed. Microdevices* **2013**, *15*, 437.

[203] D.-H. Baek, J. Moon, Y. Y. Choi, M. Lee, J. H. Choi, J. J. Pak, S.-H. Lee, *Microsyst. Technol.* **2011**, *17*, 7.

[204] H. Wu, Q. Meng, Q. Yang, M. Zhang, K. Lu, Z. Wei, *Adv. Mater.* **2015**, *27*, 6504.

[205] C.-Y. Lin, D.-H. Kuo, W.-C. Chen, M.-W. Ma, G.-S. Liou, *Org. Electron.* **2012**, *13*, 2469.

[206] D. Chen, K. Jiang, T. Huang, G. Shen, *Adv. Mater.* **2020**, *32*, 1901806.

[207] C. Yu, J. An, Q. Chen, J. Zhou, W. Huang, Y. Kim, G. Sun, *Small Methods* **2020**, *4*, 1900824.

[208] J. S. Chae, S. K. Park, K. C. Roh, H. S. Park, *Energy Storage Mater.* **2020**, *24*, 113.

[209] Y. Zhang, S. Ng, X. Lu, Z. Zheng, *Chem. Rev.* **2020**, *120*, 2049.

[210] K. Choi, J. Jeong, J. Kang, D.-G. Kim, J. K. Kim, S. Na, D.-Y. Kim, S.-S. Kim, H. Kim, *Sol. Energy Mater. Sol. Cells* **2009**, *93*, 1248.

[211] Q. Qin, R. Zhang, *Electrochim. Acta* **2013**, *89*, 726.

[212] U. Betz, M. Kharrazi Olsson, J. Marthy, M. F. Escolá, F. Atamny, *Surf. Coatings Technol.* **2006**, *200*, 5751.

[213] D. S. Hecht, L. Hu, G. Irvin, *Adv. Mater.* **2011**, *23*, 1482.

[214] W. Guo, Z. Xu, F. Zhang, S. Xie, H. Xu, X. Y. Liu, *Adv. Funct. Mater.* **2016**, *26*, 8854.

[215] Y. Bi, Y. Liu, X. Zhang, D. Yin, W. Wang, J. Feng, H. Sun, *Adv. Opt. Mater.* **2019**, *7*, 1800778.

[216] M. Ritter, D. Barnhart, in *2017 IEEE Aerosp. Conf.*, IEEE, **2017**, pp. 1–8.

[217] H. T. Yi, M. M. Payne, J. E. Anthony, V. Podzorov, *Nat. Commun.* **2012**, *3*, 1259.

[218] J. Jeong, J. G. McCall, G. Shin, Y. Zhang, R. Al-Hasani, M. Kim, S. Li, J. Y. Sim, K.-I. Jang, Y. Shi, D. Y. Hong, Y. Liu, G. P. Schmitz, L. Xia, Z. He, P. Gamble, W.

Z. Ray, Y. Huang, M. R. Bruchas, J. A. Rogers, *Cell* **2015**, *162*, 662.

[219] J. Lee, S. T. Connor, Y. Cui, P. Peumans, *Nano Lett.* **2008**, *8*, 689.

[220] L. Hu, H. Wu, Y. Cui, *MRS Bull.* **2011**, *36*, 760.

[221] L. Hu, H. S. Kim, J.-Y. Lee, P. Peumans, Y. Cui, *ACS Nano* **2010**, *4*, 2955.

[222] H. Wu, D. Kong, Z. Ruan, P.-C. Hsu, S. Wang, Z. Yu, T. J. Carney, L. Hu, S. Fan, Y. Cui, *Nat. Nanotechnol.* **2013**, *8*, 421.

[223] J. Lee, K. An, P. Won, Y. Ka, H. Hwang, H. Moon, Y. Kwon, S. Hong, C. Kim, C. Lee, S. H. Ko, *Nanoscale* **2017**, *9*, 1978.

[224] M. Duduta, R. J. Wood, D. R. Clarke, *Adv. Mater.* **2016**, *28*, 8058.

[225] D. Zhang, K. Ryu, X. Liu, E. Polikarpov, J. Ly, M. E. Tompson, C. Zhou, *Nano Lett.* **2006**, *6*, 1880.

[226] Y. Liu, Y. Zhao, B. Sun, C. Chen, *Acc. Chem. Res.* **2013**, *46*, 702.

[227] Y.-F. Li, J. Feng, F.-X. Dong, R. Ding, Z.-Y. Zhang, X.-L. Zhang, Y. Chen, Y.-G. Bi, H.-B. Sun, *Nanoscale* **2017**, *9*, 19353.

[228] D. S. Hecht, L. Hu, G. Irvin, *Adv. Mater.* **2011**, *23*, 1482.

[229] D.-D. Han, Y. Zhang, Y. Liu, Y. Liu, H. Jiang, B. Han, X.-Y. Fu, H. Ding, H.-L. Xu, H.-B. Sun, *Adv. Funct. Mater.* **2015**, *25*, 4548.

[230] R. Garg, S. Elmas, T. Nann, M. R. Andersson, *Adv. Energy Mater.* **2017**, *7*, 1601393.

[231] Y. Hao, L. Wang, Y. Liu, H. Chen, X. Wang, C. Tan, S. Nie, J. W. Suk, T. Jiang, T.

Liang, J. Xiao, W. Ye, C. R. Dean, B. I. Yakobson, K. F. McCarty, P. Kim, J. Hone, L. Colombo, R. S. Ruoff, *Nat. Nanotechnol.* **2016**, *11*, 426.

[232] J.-H. Lee, E. K. Lee, W.-J. Joo, Y. Jang, B.-S. Kim, J. Y. Lim, S.-H. Choi, S. J. Ahn, J. R. Ahn, M.-H. Park, C.-W. Yang, B. L. Choi, S.-W. Hwang, D. Whang, *Science (80-.).* **2014**, *344*, 286.

[233] X. Li, L. Colombo, R. S. Ruoff, *Adv. Mater.* **2016**, *28*, 6247.

[234] D. C. Marcano, D. V. Kosynkin, J. M. Berlin, A. Sinitskii, Z. Sun, A. S. Slesarev, L. B. Alemany, W. Lu, J. M. Tour, *ACS Nano* **2018**, *12*, 2078.

[235] W. Zeng, X.-M. Tao, S. Lin, C. Lee, D. Shi, K. Lam, B. Huang, Q. Wang, Y. Zhao, *Nano Energy* **2018**, *54*, 163.

[236] Q. Jiangying, G. Feng, Z. Quan, W. Zhiyu, H. Han, L. Beibei, W. Wubo, W. Xuzhen, Q. Jieshan, *Nanoscale* **2013**, *5*, 2999.

[237] J. Ning, L. Hao, M. Jin, X. Qiu, Y. Shen, J. Liang, X. Zhang, B. Wang, X. Li, L. Zhi, *Adv. Mater.* **2017**, *29*, 1605028.

[238] K. Parvez, R. Li, S. R. Puniredd, Y. Hernandez, F. Hinkel, S. Wang, X. Feng, K. Müllen, *ACS Nano* **2013**, *7*, 3598.

[239] C. Lou, R. Li, Z. Li, T. Liang, Z. Wei, M. Run, X. Yan, X. Liu, *Sensors* **2016**, *16*, 1833.

[240] C. Zhao, X. Jia, K. Shu, C. Yu, G. G. Wallace, C. Wang, *J. Mater. Chem. A* **2020**, *8*, 4677.

[241] S. Cho, J. S. Lee, H. Joo, *Polymers* **2019**, *11*, 1965.

[242] X. Fan, W. Nie, H. Tsai, N. Wang, H. Huang, Y. Cheng, R. Wen, L. Ma, F. Yan, Y. Xia, *Adv. Sci.* **2019**, *6*, 1900813.

[243] S. Zhang, G. Sun, Y. He, R. Fu, Y. Gu, S. Chen, *ACS Appl. Mater. Interfaces* **2017**, *9*, 16426.

[244] J. Wei, S. Xiong, Y. Bai, P. Jia, J. Ma, X. Lu, *Sol. Energy Mater. Sol. Cells* **2012**, *99*, 141.

[245] S. Ahmad, S. Sen Gursoy, S. Kazim, A. Uygun, *Sol. Energy Mater. Sol. Cells* **2012**, *99*, 95.

[246] W. Lu, N. Jiang, J. Wang, *Adv. Mater.* **2017**, *29*, 1604862.

[247] L. Hu, J. Song, X. Yin, Z. Su, Z. Li, *Polymers* **2020**, *12*, 145.

[248] H. Li, L. McRae, A. Y. Elezzabi, *ACS Appl. Mater. Interfaces* **2018**, *10*, 10520.

[249] A. W. Lang, Y. Li, M. De Keersmaecker, D. E. Shen, A. M. Österholm, L. Berglund, J. R. Reynolds, *ChemSusChem* **2018**, *11*, 854.

[250] C.-G. Wu, M.-I. Lu, S.-J. Chang, C.-S. Wei, *Adv. Funct. Mater.* **2007**, *17*, 1063.

[251] Y. H. Kim, C. Sachse, M. L. Machala, C. May, L. Müller-Meskamp, K. Leo, *Adv. Funct. Mater.* **2011**, *21*, 1076.

[252] F. Zhang, M. Johansson, M. R. Andersson, J. C. Hummelen, O. Inganäs, *Adv. Mater.* **2002**, *14*, 662.

[253] X. Crispin, F. L. E. Jakobsson, A. Crispin, P. C. M. Grim, P. Andersson, A. Volodin, C. Van Haesendonck, M. Van Der Auweraer, W. R. Salaneck, M. Berggren, *Chem. Mater.* **2006**, *18*, 4354.

[254] J. Ouyang, C.-W. Chu, F.-C. Chen, Q. Xu, Y. Yang, *Adv. Funct. Mater.* **2005**, *15*, 203.

[255] Y. Wang, C. Zhu, R. Pfattner, H. Yan, L. Jin, S. Chen, F. Molina-Lopez, F. Lissel, J. Liu, N. I. Rabiah, Z. Chen, J. W. Chung, C. Linder, M. F. Toney, B. Murmann, Z. Bao, *Sci. Adv.* **2017**, *3*, e1602076.

[256] X. Fan, B. Xu, S. Liu, C. Cui, J. Wang, F. Yan, *ACS Appl. Mater. Interfaces* **2016**, *8*, 14029.

[257] B. J. Worfolk, S. C. Andrews, S. Park, J. Reinspach, N. Liu, M. F. Toney, S. C. B. Mannsfeld, Z. Bao, *Proc. Natl. Acad. Sci.* **2015**, *112*, 14138.

[258] H. Yuk, B. Lu, S. Lin, K. Qu, J. Xu, J. Luo, X. Zhao, *Nat. Commun.* **2020**, *11*, 1604.

[259] W. Song, X. Fan, B. Xu, F. Yan, H. Cui, Q. Wei, R. Peng, L. Hong, J. Huang, Z. Ge, *Adv. Mater.* **2018**, *30*, 1800075.

[260] M. Kaltenbrunner, G. Adam, E. D. Głowacki, M. Drack, R. Schwödiauer, L. Leonat, D. H. Apaydin, H. Groiss, M. C. Scharber, M. S. White, N. S. Sariciftci, S. Bauer, *Nat. Mater.* **2015**, *14*, 1032.

[261] C. Liao, C. Mak, M. Zhang, H. L. W. Chan, F. Yan, *Adv. Mater.* **2015**, *27*, 676.

[262] A. Campana, T. Cramer, D. T. Simon, M. Berggren, F. Biscarini, *Adv. Mater.* **2014**, *26*, 3874.

[263] M. S. White, M. Kaltenbrunner, E. D. Głowacki, K. Gutnichenko, G. Kettlgruber, I. Graz, S. Aazou, C. Ulbricht, D. A. M. Egbe, M. C. Miron, Z. Major, M. C. Scharber, T. Sekitani, T. Someya, S. Bauer, N. S. Sariciftci, *Nat. Photonics* **2013**, *7*, 811.

[264] S. Kwon, W. Kim, H. Kim, S. Choi, B.-C. Park, S.-H. Kang, K. C. Choi, *Adv. Electron. Mater.* **2015**, *1*, 1500103.

[265] J.-I. Park, J. H. Heo, S.-H. Park, K. Il Hong, H. G. Jeong, S. H. Im, H.-K. Kim, *J. Power Sources* **2017**, *341*, 340.

[266] H. Song, K. Cai, *Energy* **2017**, *125*, 519.

[267] P. J. Rousche, D. S. Pellinen, D. P. Pivin, J. C. Williams, R. J. Vetter, D. R. Kipke, *IEEE Trans. Biomed. Eng.* **2001**, *48*, 361.

[268] S. Wurth, M. Capogrosso, S. Raspopovic, J. Gandar, G. Federici, N. Kinany, A. Cutrone, A. Piersigilli, N. Pavlova, R. Guiet, G. Taverni, J. Rigosa, P. Shkorbatova, X. Navarro, Q. Barraud, G. Courtine, S. Micera, *Biomaterials* **2017**, *122*, 114.

[269] K. Choi, Y. Chan Kim, H. Sun, S.-H. Kim, J. W. Yoo, I.-K. Park, P.-C. Lee, H. J. Choi, H. R. Choi, T. Kim, J. Suhr, Y. K. Lee, J.-D. Nam, *ACS Omega* **2019**, *4*, 7994.

[270] Z. Song, T. Xu, M. L. Gordin, Y.-B. Jiang, I.-T. Bae, Q. Xiao, H. Zhan, J. Liu, D. Wang, *Nano Lett.* **2012**, *12*, 2205.

[271] D.-H. Baek, J. Moon, Y. Y. Choi, M. Lee, J. H. Choi, J. J. Pak, S.-H. Lee, *Microsyst. Technol.* **2011**, *17*, 7.

[272] M. Tang, H. Li, E. Wang, C. Wang, *Chinese Chem. Lett.* **2018**, *29*, 232.

[273] W. Song, J. Zhu, B. Gan, S. Zhao, H. Wang, C. Li, J. Wang, *Small* **2018**, *14*, 1702249.

[274] J. Lin, Z. Peng, Y. Liu, F. Ruiz-Zepeda, R. Ye, E. L. G. Samuel, M. J. Yacaman, B. I. Yakobson, J. M. Tour, *Nat. Commun.* **2014**, *5*, 5714.

[275] S. P. Singh, Y. Li, J. Zhang, J. M. Tour, C. J. Arnusch, *ACS Nano* **2018**, *12*, 289.

[276] Y. Wang, K. Li, X. Li, H. Cui, G. Liu, H. Xu, X. Wu, W. Yao, B. Zhong, X. Huang, H. Wang, T. Wu, *Carbon* **2019**, *152*, 873.

[277] X. Xuan, H. S. Yoon, J. Y. Park, *Biosens. Bioelectron.* **2018**, *109*, 75.

[278] S. Zhang, E. Hubis, G. Tomasello, G. Soliveri, P. Kumar, F. Cicoira, *Chem. Mater.* **2017**, *29*, 3126.

[279] Y. Li, H. Shimizu, *Macromolecules* **2009**, *42*, 2587.

[280] J. Xiong, M.-F. Lin, J. Wang, S. L. Gaw, K. Parida, P. S. Lee, *Adv. Energy Mater.* **2017**, *7*, 1701243.

[281] B.-Y. Hwang, S.-H. Choi, K.-W. Lee, J.-Y. Kim, *Compos. Part B Eng.* **2018**, *151*, 1.

[282] O. Azzaroni, Z. Zheng, Z. Yang, W. T. S. Huck, *Langmuir* **2006**, *22*, 6730.

[283] X. Wang, H. Hu, Y. Shen, X. Zhou, Z. Zheng, *Adv. Mater.* **2011**, *23*, 3090.

[284] Y. Yu, C. Yan, Z. Zheng, *Adv. Mater.* **2014**, *26*, 5508.

[285] B. Zhang, J. Lei, D. Qi, Z. Liu, Y. Wang, G. Xiao, J. Wu, W. Zhang, F. Huo, X. Chen, *Adv. Funct. Mater.* **2018**, *28*, 1801683.

[286] T. G. Yun, M. Park, D.-H. Kim, D. Kim, J. Y. Cheong, J. G. Bae, S. M. Han, I.-D.

Kim, *ACS Nano* **2019**, *13*, 3141.

[287] P. Lee, J. Lee, H. Lee, J. Yeo, S. Hong, K. H. Nam, D. Lee, S. S. Lee, S. H. Ko, *Adv. Mater.* **2012**, *24*, 3326.

[288] M. Amjadi, A. Pichitpajongkit, S. Lee, S. Ryu, I. Park, *ACS Nano* **2014**, *8*, 5154.

[289] F. Xu, Y. Zhu, *Adv. Mater.* **2012**, *24*, 5117.

[290] X. Fan, B. Xu, N. Wang, J. Wang, S. Liu, H. Wang, F. Yan, *Adv. Electron. Mater.* **2017**, *3*, 1600471.

[291] Z. Wen, Y. Yang, N. Sun, G. Li, Y. Liu, C. Chen, J. Shi, L. Xie, H. Jiang, D. Bao, Q. Zhuo, X. Sun, *Adv. Funct. Mater.* **2018**, *28*, 1803684.

[292] A. S. Chen, S. Bergbreiter, *Smart Mater. Struct.* **2017**, *26*, 025028.

[293] Z. Niu, H. Dong, B. Zhu, J. Li, H. H. Hng, W. Zhou, X. Chen, S. Xie, *Adv. Mater.* **2013**, *25*, 1058.

[294] X. Chen, H. Lin, P. Chen, G. Guan, J. Deng, H. Peng, *Adv. Mater.* **2014**, *26*, 4444.

[295] U.-H. Shin, D.-W. Jeong, S.-M. Park, S.-H. Kim, H. W. Lee, J.-M. Kim, *Carbon* **2014**, *80*, 396.

[296] Y. Zhang, L. Zhang, K. Cui, S. Ge, X. Cheng, M. Yan, J. Yu, H. Liu, *Adv. Mater.* **2018**, *30*, 1801588.

[297] M. Li, J. Tian, M. Al-Tamimi, W. Shen, *Angew. Chemie Int. Ed.* **2012**, *51*, 5497.

[298] S. Wang, T. Chinnasamy, M. A. Lifson, F. Inci, U. Demirci, *Trends Biotechnol.* **2016**,

34, 909.

[299] H. Golmohammadi, E. Morales-Narváez, T. Naghdi, A. Merkoçi, *Chem. Mater.* **2017**, *29*, 5426.

[300] A. W. Martinez, S. T. Phillips, M. J. Butte, G. M. Whitesides, *Angew. Chemie Int. Ed.* **2007**, *46*, 1318.

[301] W. J. Hyun, O. O. Park, B. D. Chin, *Adv. Mater.* **2013**, *25*, 4729.

[302] Y. Cheng, R. Wang, J. Sun, L. Gao, *ACS Nano* **2015**, *9*, 3887.

[303] H. Chen, J. Cogswell, C. Anagnostopoulos, M. Faghri, *Lab Chip* **2012**, *12*, 2909.

[304] X. S. Zhang, M. Su, J. Brugger, B. Kim, *Nano Energy* **2017**, *33*, 393.

[305] A. Ahmed, Z. Saadatnia, I. Hassan, Y. Zi, Y. Xi, X. He, J. Zu, Z. L. Wang, *Adv. Energy Mater.* **2017**, *7*, 1601705.

[306] B. Anothumakkool, I. Agrawal, S. N. Bhange, R. Soni, O. Game, S. B. Ogale, S. Kurungot, *ACS Appl. Mater. Interfaces* **2016**, *8*, 553.

[307] K. E. Boehle, J. Gilliand, C. R. Wheeldon, A. Holder, J. A. Adkins, B. J. Geiss, E. P. Ryan, C. S. Henry, *Angew. Chemie Int. Ed.* **2017**, *56*, 6886.

[308] C. Cheng, C. Zhang, X. Gao, Z. Zhuang, C. Du, W. Chen, *Anal. Chem.* **2018**, *90*, 1983.

[309] D. M. Cate, J. A. Adkins, J. Mettakoonpitak, C. S. Henry, *Anal. Chem.* **2015**, *87*, 19.

[310] M. M. Gong, D. Sinton, *Chem. Rev.* **2017**, *117*, 8447.

[311] R. B. Channon, M. P. Nguyen, A. G. Scorzelli, E. M. Henry, J. Volckens, D. S. Dandy,

C. S. Henry, *Lab Chip* **2018**, *18*, 793.

[312] M. Sakar, H. R. Chandan, R. Shwetharani, in *Graphene-Based Electrochem. Sensors Biomol.*, Elsevier, **2019**, pp. 297–320.

[313] T. H. Yang, J. Shintake, R. Kanno, C. R. Kao, J. Mizuno, *Adv. Intell. Syst.* **2020**, 2000025.

[314] J. Guo, C. Xiang, J. Rossiter, *Smart Mater. Struct.* **2019**, *28*, 105012.

[315] Y. Feng, Y. Zheng, Z. U. Rahman, D. Wang, F. Zhou, W. Liu, *J. Mater. Chem. A* **2016**, *4*, 18022.

[316] I. Ferreira, B. Brás, J. I. Martins, N. Correia, P. Barquinha, E. Fortunato, R. Martins, *Electrochim. Acta* **2011**, *56*, 1099.

[317] G. Grau, R. Kitsomboonloha, S. L. Swisher, H. Kang, V. Subramanian, *Adv. Funct. Mater.* **2014**, *24*, 5067.

[318] L. Ge, S. Wang, J. Yu, N. Li, S. Ge, M. Yan, *Adv. Funct. Mater.* **2013**, *23*, 3115.

[319] S. Gong, W. Schwalb, Y. Wang, Y. Chen, Y. Tang, J. Si, B. Shirinzadeh, W. Cheng, *Nat. Commun.* **2014**, *5*, 3132.

[320] D.-W. Wang, F. Li, J. Zhao, W. Ren, Z.-G. Chen, J. Tan, Z.-S. Wu, I. Gentle, G. Q. Lu, H.-M. Cheng, *ACS Nano* **2009**, *3*, 1745.

[321] L. David, R. Bhandavat, G. Singh, *ACS Nano* **2014**, *8*, 1759.

[322] W. J. Hyun, E. B. Secor, G. A. Rojas, M. C. Hersam, L. F. Francis, C. D. Frisbie, *Adv. Mater.* **2015**, *27*, 7058.

[323] Q. Hua, H. Liu, J. Zhao, D. Peng, X. Yang, L. Gu, C. Pan, *Adv. Electron. Mater.* **2016**, *2*, 1600093.

[324] Y. Yu, J. Zhang, *J. Mater. Chem. A* **2017**, *5*, 4719.

[325] L. Dong, C. Xu, Y. Li, Z. Pan, G. Liang, E. Zhou, F. Kang, Q.-H. Yang, *Adv. Mater.* **2016**, *28*, 9313.

[326] Q. Cheng, Z. Song, T. Ma, B. B. Smith, R. Tang, H. Yu, H. Jiang, C. K. Chan, *Nano Lett.* **2013**, *13*, 4969.

[327] Q.-M. Feng, J.-B. Pan, H.-R. Zhang, J.-J. Xu, H.-Y. Chen, *Chem. Commun.* **2014**, *50*, 10949.

[328] K.-H. Choi, J. Yoo, C. K. Lee, S.-Y. Lee, *Energy Environ. Sci.* **2016**, *9*, 2812.

[329] J. Huang, H. Zhu, Y. Chen, C. Preston, K. Rohrbach, J. Cumings, L. Hu, *ACS Nano* **2013**, *7*, 2106.

[330] J. Ding, B. Li, L. Chen, W. Qin, *Angew. Chemie Int. Ed.* **2016**, *55*, 13033.

[331] M. C. Barr, J. A. Rowehl, R. R. Lunt, J. Xu, A. Wang, C. M. Boyce, S. G. Im, V. Bulović, K. K. Gleason, *Adv. Mater.* **2011**, *23*, 3500.

[332] B. Anothumakkool, R. Soni, S. N. Bhange, S. Kurungot, *Energy Environ. Sci.* **2015**, *8*, 1339.

[333] N. Matsuhisa, D. Inoue, P. Zalar, H. Jin, Y. Matsuba, A. Itoh, T. Yokota, D. Hashizume, T. Someya, *Nat. Mater.* **2017**, *16*, 834.

[334] Y. Cao, G. Zhang, Y. Zhang, M. Yue, Y. Chen, S. Cai, T. Xie, X. Feng, *Adv. Funct.*

Mater. **2018**, *28*, 1804604.

[335] A. Lymberis, D. D. R. Eds, *Smart Textiles*, John Wiley & Sons, Inc., Hoboken, NJ, USA, **2018**.

[336] W. Weng, P. Chen, S. He, X. Sun, H. Peng, *Angew. Chemie Int. Ed.* **2016**, *55*, 6140.

[337] F. Haghdoost, V. Mottaghitalab, A. K. Haghi, *Sens. Rev.* **2015**, *35*, 20.

[338] M. Weder, D. Hegemann, M. Amberg, M. Hess, L. Boesel, R. Abächerli, V. Meyer, R. Rossi, *Sensors* **2015**, *15*, 1750.

[339] G. Acar, O. Ozturk, A. J. Golparvar, T. A. Elboshra, K. Böhringer, M. K. Yapici, *Electronics* **2019**, *8*, 479.

[340] S. Takamatsu, T. Lonjaret, D. Crisp, J.-M. Badier, G. G. Malliaras, E. Ismailova, *Sci. Rep.* **2015**, *5*, 15003.

[341] H. Rogier, in *Handb. Smart Text.*, Springer Singapore, Singapore, **2015**, pp. 1–21.

[342] G. Paul, R. Torah, S. Beeby, J. Tudor, *Sensors Actuators A Phys.* **2015**, *221*, 60.

[343] S. M. Bidoki, J. Nouri, A. A. Heidari, *J. Micromechanics Microengineering* **2010**, *20*, 055023.

[344] M. Park, J. Im, M. Shin, Y. Min, J. Park, H. Cho, S. Park, M.-B. Shim, S. Jeon, D.-Y. Chung, J. Bae, J. Park, U. Jeong, K. Kim, *Nat. Nanotechnol.* **2012**, *7*, 803.

[345] J. Lee, H. Kwon, J. Seo, S. Shin, J. H. Koo, C. Pang, S. Son, J. H. Kim, Y. H. Jang, D. E. Kim, T. Lee, *Adv. Mater.* **2015**, *27*, 2433.

[346] H. S. Hwang, J. B. Lee, J. Jung, S. Lee, J. H. Ryu, S. M. Oh, *J. Power Sources* **2016**, *330*, 204.

[347] S. M. Saleh, S. M. Jusob, F. K. C. Harun, L. Yuliati, D. H. B. Wicaksono, *IEEE Sens. J.* **2020**, *1748*, 1.

[348] K. Yang, C. Freeman, R. Torah, S. Beeby, J. Tudor, *Sensors Actuators A Phys.* **2014**, *213*, 108.

[349] Y. Cheng, R. Wang, J. Sun, L. Gao, *Adv. Mater.* **2015**, *27*, 7365.

[350] Q. Li, K. Li, H. Fan, C. Hou, Y. Li, Q. Zhang, H. Wang, *J. Mater. Chem. C* **2017**, *5*, 11448.

[351] R. Wang, Z. Xu, J. Zhuang, Z. Liu, L. Peng, Z. Li, Y. Liu, W. Gao, C. Gao, *Adv. Electron. Mater.* **2017**, *3*, 1600425.

[352] X. Zang, Q. Chen, P. Li, Y. He, X. Li, M. Zhu, X. Li, K. Wang, M. Zhong, D. Wu, H. Zhu, *Small* **2014**, *10*, 2583.

[353] X. Lee, T. Yang, X. Li, R. Zhang, M. Zhu, H. Zhang, D. Xie, J. Wei, M. Zhong, K. Wang, D. Wu, Z. Li, H. Zhu, *Appl. Phys. Lett.* **2013**, *102*, 1.

[354] J. Zhou, X. Xu, Y. Xin, G. Lubineau, *Adv. Funct. Mater.* **2018**, *28*, 1705591.

[355] S. Jiang, H. Zhang, S. Song, Y. Ma, J. Li, G. H. Lee, Q. Han, J. Liu, *ACS Nano* **2015**, *9*, 10252.

[356] Y. Li, B. Zhou, G. Zheng, X. Liu, T. Li, C. Yan, C. Cheng, K. Dai, C. Liu, C. Shen, Z. Guo, *J. Mater. Chem. C* **2018**, *6*, 2258.

[357] Q. Xu, M. Li, P. Yan, C. Wei, L. Fang, W. Wei, H. Bao, J. Xu, W. Xu, *Org. Electron.* **2016**, *29*, 107.

[358] I. G. Trindade, F. Martins, P. Baptista, *Synth. Met.* **2015**, *210*, 179.

[359] S. Takamatsu, T. Lonjaret, D. Crisp, J.-M. Badier, G. G. Malliaras, E. Ismailova, *Sci. Rep.* **2015**, *5*, 15003.

[360] D. Wang, C. Lu, J. Zhao, S. Han, M. Wu, W. Chen, *RSC Adv.* **2017**, *7*, 31264.

[361] Y. Wu, Y. Yang, C. Li, Y. Li, W. Chen, *Front. Bioeng. Biotechnol.* **2020**, *8*, 1.

[362] Y. Guo, M. T. Otley, M. Li, X. Zhang, S. K. Sinha, G. M. Treich, G. A. Sotzing, *ACS Appl. Mater. Interfaces* **2016**, *8*, 26998.

Chapter 3 Symmetric-structured electroadhesive clutches based on high-*k* P(VDF-TrFE-CFE) and flexible electrodes

3.1 Introduction

Electroadhesive clutch as a novel kind of high performance and low power consumption clutch technology have found potential applications in haptic feedback systems and exoskeletons.[1–3] Current electroadhesive clutches could exhibit a best performance of ~24 kPa shear force under a driving voltage of 320 volts with high-*k* inks (Luxprint) as the dielectric layer.[4] However, the relatively high working voltage (> 300 V) will lead to unwanted space charge and arc discharge, which are detrimental to the clutch performance and may cause safety problems.[1,4] Since doping of high-*k* ceramics or conductive fillers will always result in low breakdown voltages of the polymer composites, high-*k* polymers seem to be good candidates for the high performance electroadhesive clutches. To the best of our knowledge, poly (vinylidene fluoride-trifluoroethylene-chloro-fluoroethylene (P(VDF-TrFE-CFE)) terpolymer exhibits the highest dielectric constant (ε_r ~50 at 1 kHz) among dielectric polymers and have found promising applications in electro-active actuators, microfluidic devices, energy storage and haptic systems.[5–8] The low dielectric loss and high breakdown voltage[6,7,9] of the pure polymer material are also favourable for the clutch performance. As discussed in Chapter 2, the theoretical electroadhesive force increases linearly with the dielectric

constant and flexible electrodes could minimize the air gaps between the two electroadhesive pads to improve the performance of the clutches.

In this chapter, symmetric-structured electroadhesive clutches (see Fig 3.1) based on high-*k* P(VDF-TrFE-CFE) terpolymers and flexible Al/PVC or conductive fabric electrodes have been fabricated through blade coating. The surface morphologies, chemical and mechanical properties of the dielectric layers and electrodes will be firstly investigated. Then the performance of the clutches, including the relationship between the dielectric thickness, overlapping area, working voltage and the generated electrostatic shear force will be investigated. A novel method will also be proposed for the direct determination of the engage time and release time of the clutches. The flexural rigidity changes under different voltages have also been demonstrated for potential application in stiffness regulation. The possibility of the adhesion under AC square-wave voltage has also been proved.

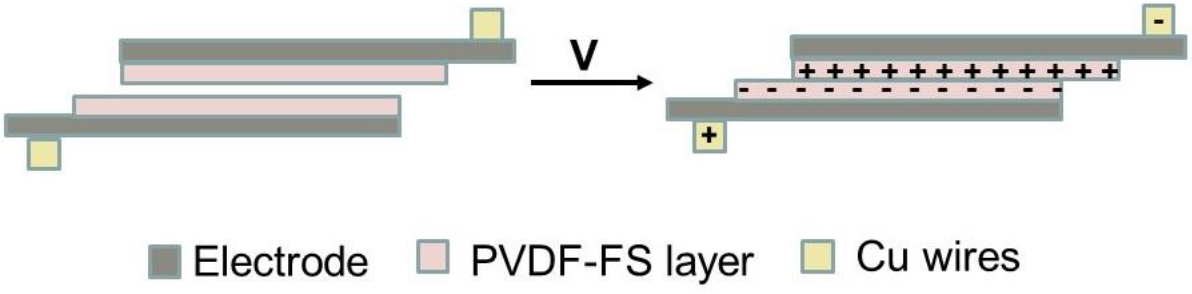

Fig 3.1 Schematic illustration of the symmetric electroadhesive clutch and its working mechanism

3.2 Experimental section

3.2.1 Materials selection

PVDF-TrFE-CFE has the highest dielectric constant among pure polymer materials and it exhibits a relatively low modulus of 200-400 MPa which is softer than other commonly used dielectric polymers such as PI and polyacrylic.[10,11] Thin metal foils and conductive fabrics are widely used flexible electrodes with advantages of low-cost, excellent electric conductivity and good mechanical strength.[12–14]

The P(VDF-TrFE-CFE) terpolymers (PIEZOTECH ® RT-FS) (PVDF-FS) were purchased form Arkema (French) and were used without any purification. The molar ratio of the VDF, TrFE and CFE was 64.8%, 27.4% and 7.8% respectively. PVC tape (Scotch, 65 μm), conductive fabric (3M, 30 μm) and Al foil (Glad, 15 μm) were used directly. Silver paste (sigma) was diluted with small amount of isopropyl alcohol (IPA) to adjust the viscosity before screen printing. Solvents including acetone, ethanol, tetrahydrofuran (THF), N, N-Dimethylformamide (DMF) and butyl acetate (BA) were purchased from TCI chemicals.

3.2.1.1 General procedures for the sample preparation

Blade coating was conducted on a *k* control coater. The PVDF-FS terpolymer was firstly dissolved in butyl acetate or DMF with a concentration of 0.1 g/mL under ultrasonic.

Dielectric layers with different thicknesses were directly blade coated on Al foils by different profile bars. The resultant films were dried at 65 ^{o}C for 3 hours and then annealed at 120 ^{o}C overnight under vacuum to remove the residue solvents and improve the crystallinity degree of the polymers.[9,15] For non-annealing samples, the films were dried at 65 ^{o}C overnight. Then the PVC tape was attached on the backside to protect the Al layers and improve the mechanical strength of the pads. The blade coating was conducted on both sides of the conductive fabric substrates which is fixed on a PTFE plate to fill the interspace caused by the textile texture. The annealing procedure was same as the Al/PVC based samples.

3.2.2 Materials characterization

The chemical properties and crystallinity of the PVDF-FS were characterized by attenuated total reflection Fourier-transform infrared spectroscopy (ATR-FTIR) and X-Ray diffraction (XRD). The dielectric properties including the dielectric constant and loss tangent at different frequencies were recorded by the impedance analyzer. FTIR spectrum was measured on a Perkin spectrum 100 FTIR. XRD data were collected on a Rigaku SmartLab 9kW at 293 K. The Keysight E4980A precision impedance analyzer was used to analysis the dielectric properties. The surface roughness of the dielectric layer and electrode was measured on a ZYGO laser interferometric non-contact profile system with sample size of 4 cm^2. Scanning electron microscope (SEM) images were taken on a JEOL

Model JSM-6490. The resistivity of the electrode was measured on a ST-2258A four-probe tester.

3.2.2.1 Procedures for the dielectric measurement

The dielectric films were cut into small pieces with size of ~ 2 cm^2 and both sides of the films were coated with silver paste as the electrodes through screen printing. The capacitance and dielectric loss at different frequency were recorded by impedance analyzer and the relative dielectric constant was calculated by Equation (3-1), where C is the measured capacitance, d is the thickness, A is the effective area of the samples and ε_0 is the vacuum dielectric constant which is 8.85 x 10^{-12} F/m.

$$\varepsilon_r = \frac{C \cdot d}{A \cdot \varepsilon_0} \quad \textbf{(3-1)}$$

3.2.3 Device performance evaluation

The mechanical properties and the performance of the clutches including the generated shear force and response time were measured on a Instron 5944. The high voltage direct voltage was provided by the RK2674A voltage withstand test instrument. The voltage-current (V-I) curves were recorded on a Keithley 2400 with constant voltage output. The flexural rigidity measurement was conducted on a Shirley stiffness tester based on stiffness test Standard ASTM D1388-08 (2002).

3.2.3.1 Procedures for the generated shear force measurement

The schematic illustration of the test system is shown in Fig 3.2. The direct-current (DC) voltage was provided by a RK2674A high-voltage power source. When the two electroadhesive pads were engaged under the external electrical field, the load cell start to move with a constant speed of 40 N/min. The maximum shear force was recorded as the maximum load before the slip of the two electroadhesive pads. Between each test, the dielectric layers were wiped with ethanol and rested for around 5 mins to exclude the possible residue charges at the interface of the clutch.[16] Meanwhile, the pad was connected to the Instron machine which could also help to neutralize the charges. No electrostatic attraction of the pads was observed before the next load of voltages. For the measurement of electroadhesive force under AC voltages, the test system is the same as Fig 3.2 except the power supplier is a Keithley 2400. Each point was measured five times to obtain the average value and standard deviation (STD).

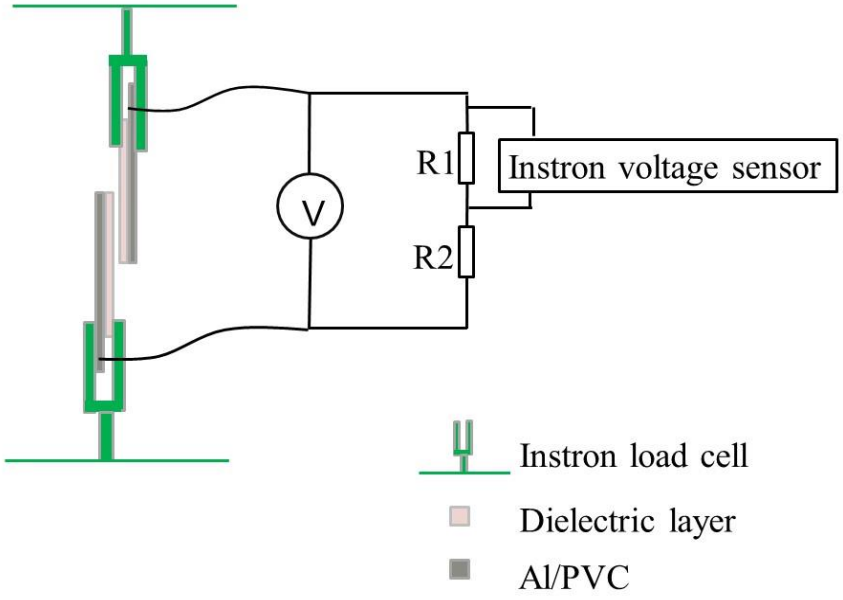

Fig 3.2 Schematic illustration of the test system

3.2.3.2 Procedures for the response time measurement

The reported measurement methods for response time of the clutch include capacitor charging/discharging[1] and baseline force-displacement,[2] which are indirect methods. Herein, a direct measurement of the response time was proposed. The circuit design was shown in Fig 3.2. Since the measuring range of the voltage sensor is limited to 10 volts, a voltage division circuit was designed accordingly, where the resistance values of R1 and R2 were 100 kΩ and 10 MΩ respectively. Through the simple parallel circuit, the force sensor and voltage sensor were integrated into the Instron machine and the force and voltage signals could be synchronously measured.

To measure the time needed for the engagement of the clutch, the upper fixture moved with a velocity of 2 mm/min, after a few seconds the voltage was turned on to activate the clutch. The time needed from the switch of voltage to the generation of the shear force is defined as the engage time. For the measurement of release time, the clutch was firstly engaged and a load of half maximum shear force was given. Then the voltage was turned off and the time between the power outage and the separation of the two pads (the point that shear force starts to decrease) is defined as the release time.

3.2.3.3 Procedures for the stiffness measurement

According to the ASTM standard, the sample used for the stiffness test is 1 inch (wide) x 20 cm (length). The photo and testing mechanism of the stiffness tester was shown in Fig 3.3. The flexural rigidity (G) could be calculated by Equation (3-2), where W is the mass per unit area (g/m^2) and c is the bending length (mm).

$$G = 1.421 \times 10^{-5} \times W \times c^3 \quad \textbf{(3-2)}$$

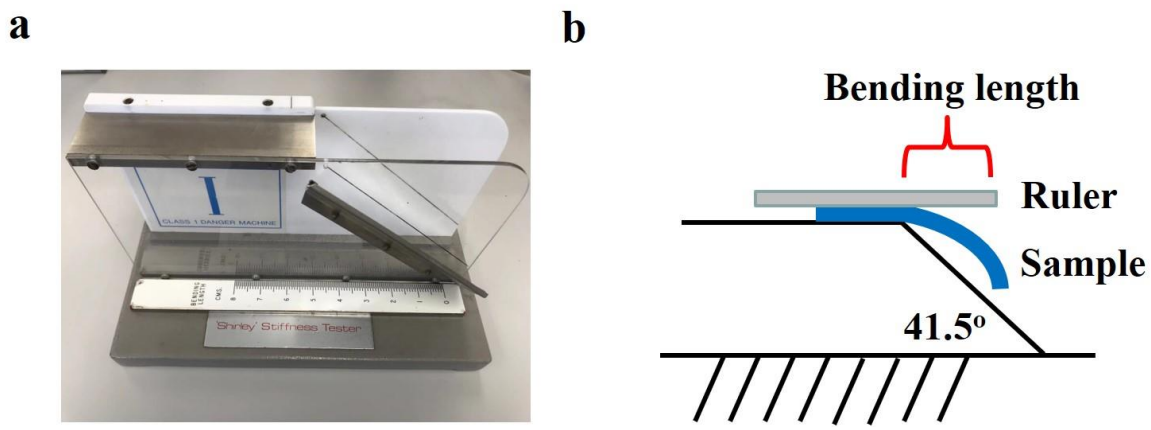

Fig 3.3 (a). Photograph of the Shirley stiffness tester and (b) schematic illustration of the stiffness test

3.3 Results and discussion

3.3.1 Electrode properties

The resistivity of the Al/PVC and conductive fabric was measured to be 0.30 ± 0.04 and 11.76 ± 1.72 $\Omega \cdot cm \cdot sq^{-1}$ with the total thickness of 80 μm and 30 μm. Both electrodes show excellent electrical conductivities and the fabric electrode exhibit stronger tensile stress than the film electrode. The typical strain-stress and strain-load relationships of the two electrodes were shown in Fig 3.4. The maximum load of the Al/PVC film is higher than 130 N, which is much higher than the fabric electrode (~ 64 N) due to its larger thickness. The mechanical and electrical properties of the electrodes were summarized in Table 3.1. The surface roughness of the electrodes was also investigated (Fig 3.7) and will be discussed together with the dielectric layer.

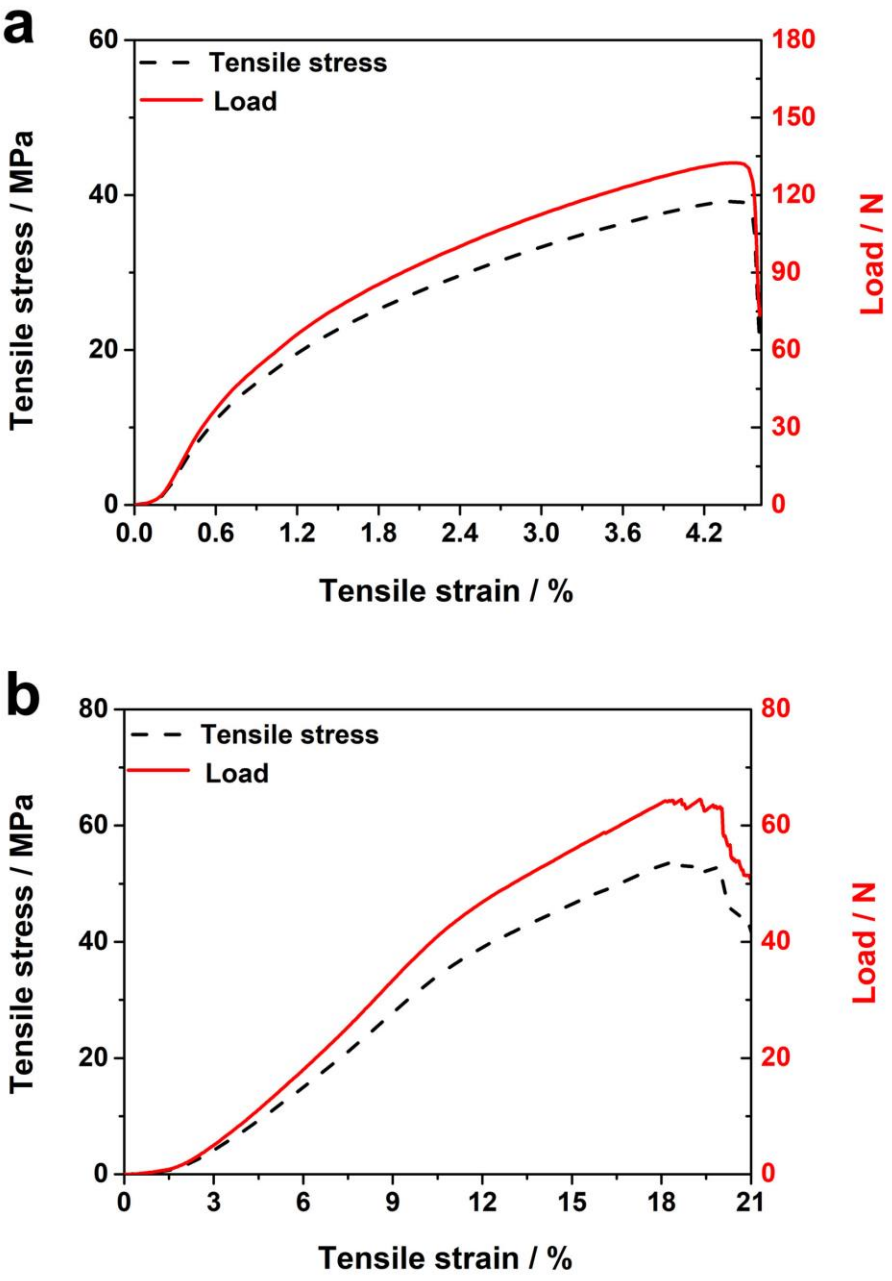

Fig 3.4 Typical strain-stress curves of the (a) Al/PVC and (b) conductive fabric electrodes

Table 3.1 Mechanical and electrical properties of the electrodes

	Resistivity / $\Omega \cdot cm \cdot sq^{-1}$	Tensile stress / MPa	Maximum Load / N	Y / MPa
Al/PVC	0.30 ± 0.04	39.13 ± 4.03	133.76 ± 11.14	1024.33 ± 73.65
Conductive fabric	11.76 ± 1.72	53.42 ± 1.27	64.11 ± 1.52	441.92 ± 9.76

3.3.2 Dielectric properties

The dielectric constant and dielectric loss of the PVDF-FS before and after annealing as a function of frequency have been evaluated by the impedance analyser and the results are shown in Fig 3.5. The relative dielectric constant (ε_r) decreases while the dielectric loss (tan δ) increases when moves to higher frequencies and this tendency is quite typical in polar polymers.[17,18] Both samples show relatively low dielectric loss at low frequency range (< 10^4 Hz) which arises from the dipolar polarization and the high loss at high frequency area should be ascribed to the electronic polarization.[19–21] The annealed (A) sample exhibits a huge increase (34 % at 1 kHz) in dielectric constant as compared with the non-annealed (NA) one. The reason should be ascribed to the increase of the crystallinity degree after annealing,[15] which could be further confirmed by the XRD spectra (see Fig 3.6a). The improved orientation of the polymer chains will result in higher dielectric constant and the dense packed structure contributes to the lower loss.[22]

The slight blue-shift of the 2θ degree of the annealed polymer results from the residue lattice stress during the annealing process.[23]

The FTIR spectra of the PVDF-FS terpolymers were also recorded in Fig 3.6b. Symmetric stretching of the all-trans (β phase) -CF_2 and -CH_2 vibration could be observed at 846 cm^{-1} and 1398 cm^{-1} respectively. The annealed samples exhibits a stronger peak at 770 cm^{-1}, which should be ascribed to the γ phase.[24–26] The corresponding XRD and dielectric data are summarized in Table 3.2. Since annealing turns out to be quite an effective method to improve the dielectric performance of the PVDF-FS films, namely increase the dielectric constant and decrease dielectric loss simultaneously at low frequency, this process is carried out for all samples used in the fabrication of the electroadhesive clutches.

Table 3.2 Dielectric properties and XRD data of annealed(A) and non-annealed (NA) PVDF-FS films

	100 Hz		1000 Hz		XRD data	
	ε_r	tan δ	ε_r	tan δ	2θ/ degree	Intensity
PVDF-FS (A)	48.2	0.048	44.7	0.073	18.08	6452
PVDF-FS (NA)	36.6	0.060	33.3	0.080	18.14	4769

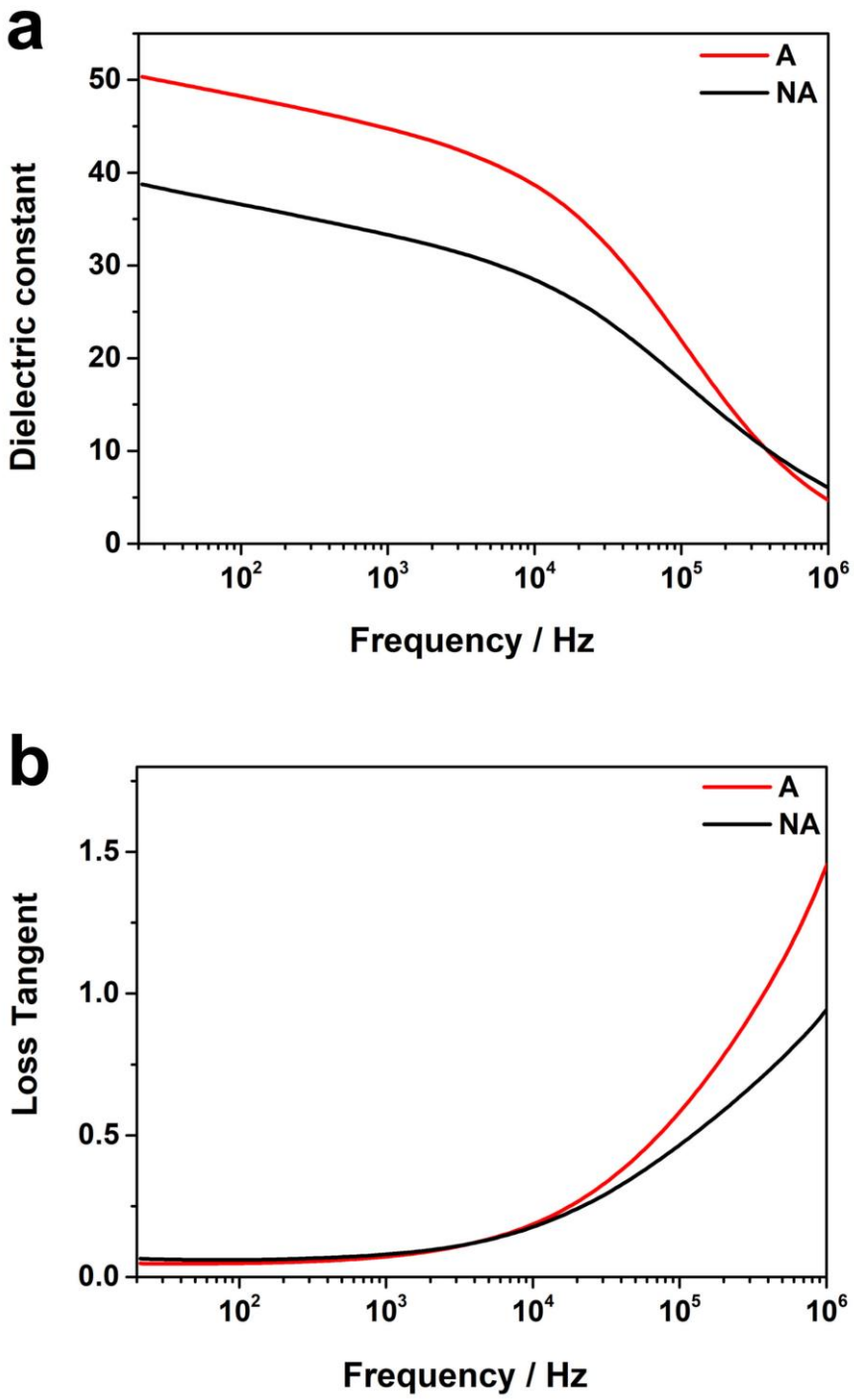

Fig 3.5 Frequency dependent relative dielectric constant and loss tangent of the annealed (A) and non-annealed (NA) PVDF-FS

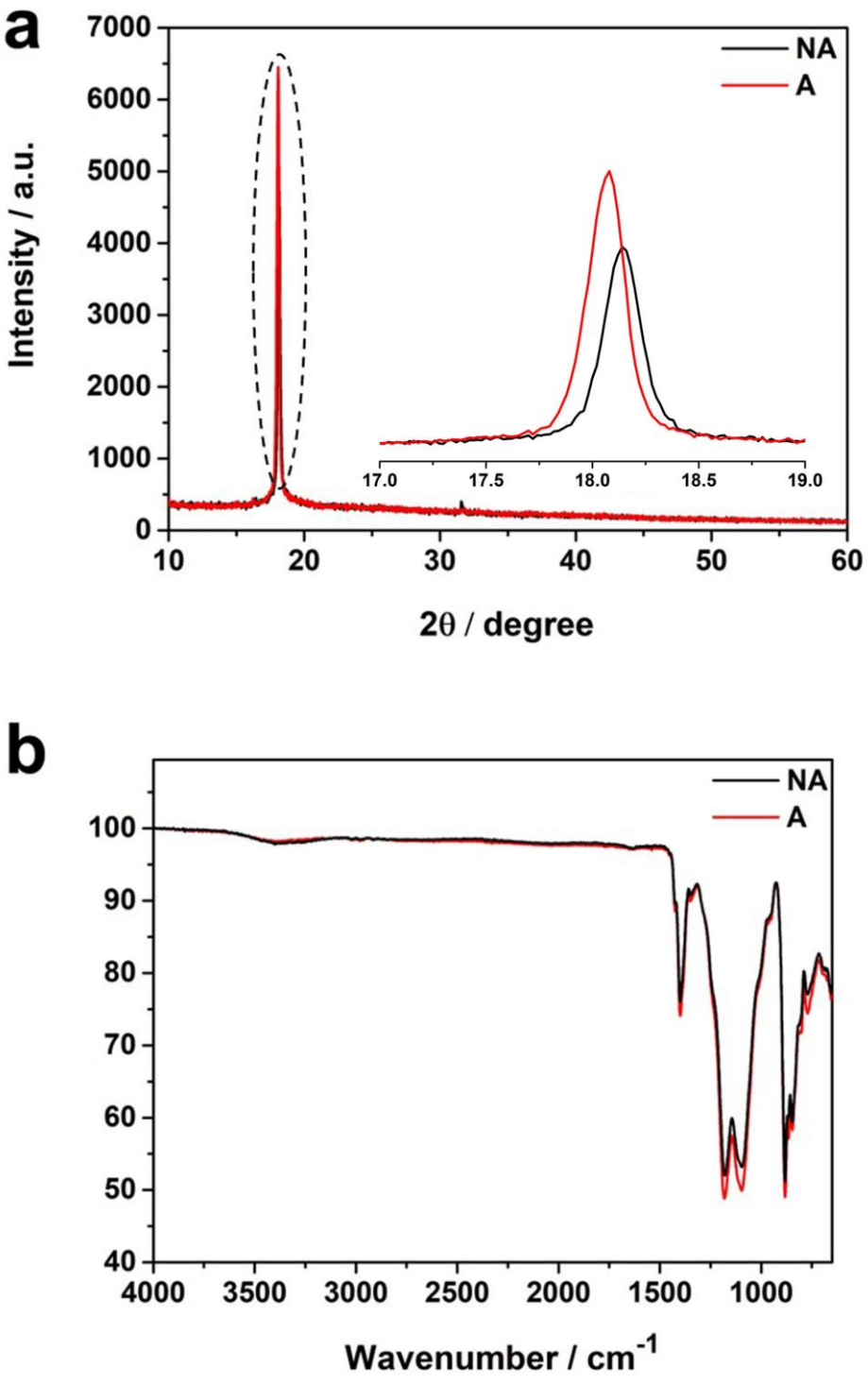

Fig 3.6 (a) XRD patterns and (b) FTIR spectra of annealed(A) and non-annealed (NA) PVDF-FS films

3.3.3 Surface morphology

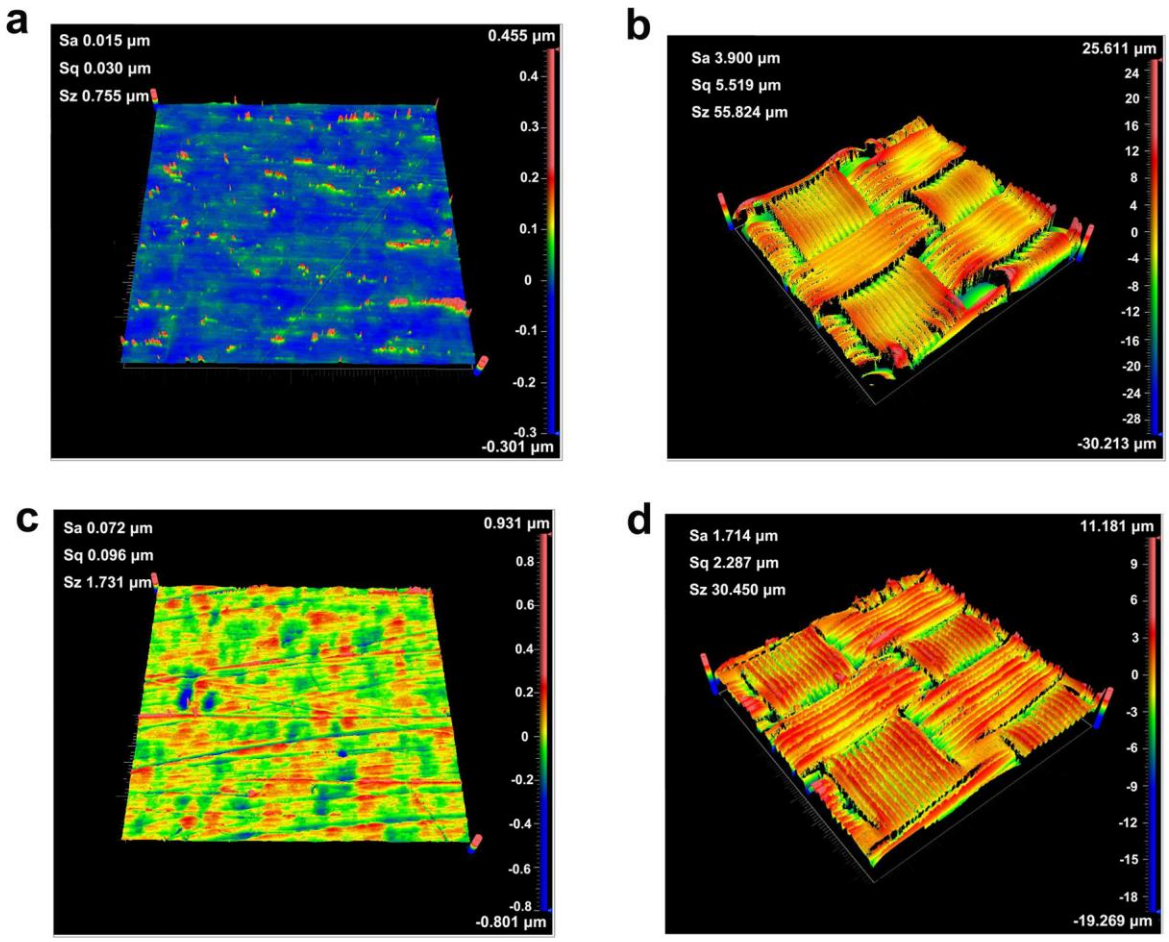

Fig 3.7 Surface roughness of the (a) Al/PVC electrode; (b) Conductive fabric electrode; (c) PVDF-FS layer on Al/PVC and (d) PVDF-FS layer on conductive fabric.

The surface morphologies of the electrodes and dielectric layers were characterized by the surface roughness. Sa, Sq and Sz refer to the arithmetical mean height, root mean square height and maximum height of the samples. The average roughness of the Al/PVC and conductive fabric was measured to be 15 nm and 3.9 µm respectively. After the blade

coating of dielectric layers, the roughness of film-based pad increased to 72 nm while the fabric-based pad decreased to 1.71 μm, as shown in Fig 3.7. Both Al foil and the coating on Al/PVC exhibit very smooth surface morphologies, which is favourable to improve the shear force of the clutches. The PVDF-FS polymers could fill into the blank space of the textile structures to reduce the roughness, though the surface roughness is still in the micrometer level. The large roughness should be the main reason for the poor performance of the fabric electrode-based electroadhesive clutches.

More detailed information was given by the SEM images (see Fig 3.8). No holes or wrinkles could be observed from the film electrode-based samples. The protrusions observed from the right of Fig 3.7a should be attributed to the crystallization of the PVDF-FS.[27,28] The friction coefficient of the PVDF-FS on Al/PVC is measured to be 0.40. The fabric electrode was also well-coated with the dielectric polymers as demonstrated in Fig 3.7b. However, the space between weft and warp yarns of the fabrics, and the space between the adjacent fibers still exist. The hollow space will form a large amount of air gaps at the interface of the clutch, which will significantly decrease the generated electroadhesive forces. The friction coefficient of the PVDF-FS on conductive fabric is measured to be 0.30.

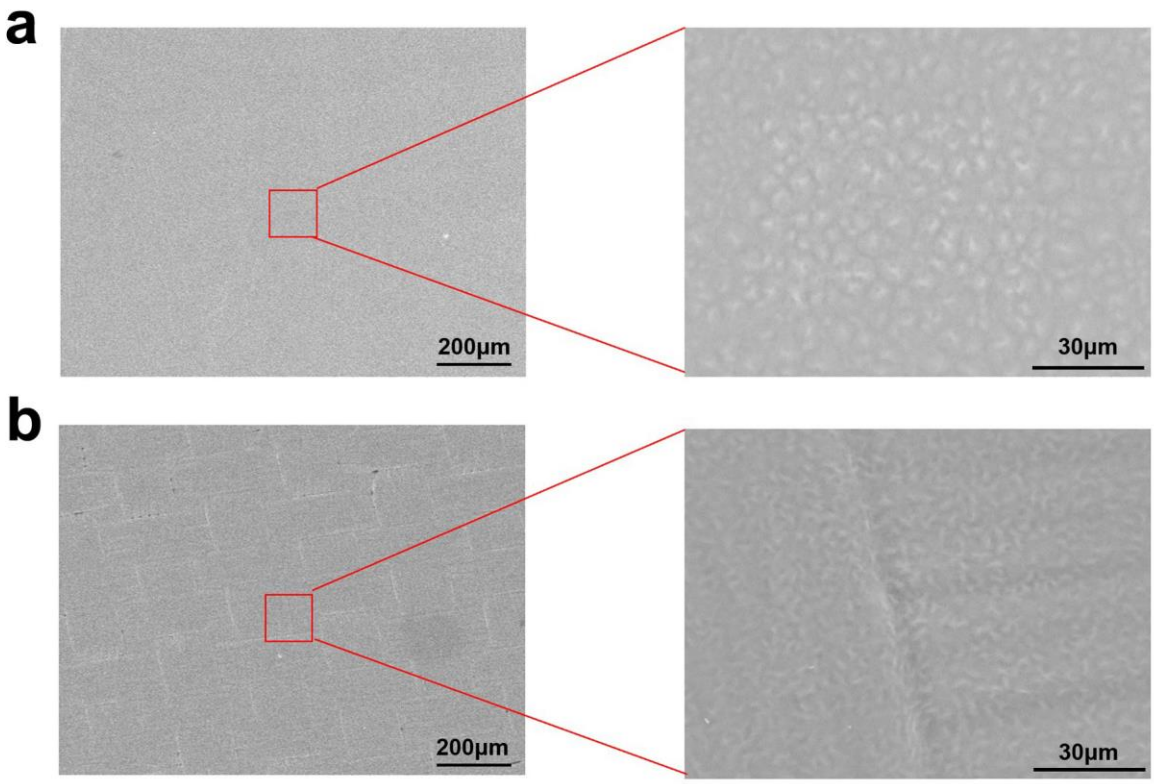

Fig 3.8 SEM images of the (a) PVDF-FS layer on Al/PVC, left (x 200), right (x 2000) and (b) PVDF-FS layer on conductive fabric, left (x 200), right (x 2000).

3.3.4 Clutch performance

Two kinds of clutches with different flexible electrodes, namely Al/PVC and conductive fabric have been fabricated and the performance of the clutches have been evaluated. However, preliminary research shows that the fabric-based clutch could only produce electroadhesive force lower than 0.5 N (see Fig 3.9) though it could also response at a

relatively low working voltage (140 V). The overlapping area is 4 cm^2 and the total dielectric thickness is ~10 μm. The poor performance should be ascribed to the large surface roughness[4,29,30] caused by the textile texture. Thefabric-based electroadhesive pads could only draw together but could not provide large shear force. Therefore, fabric electrodes should not be good candidates for preparing electroadhesive clutches with large holding force. In this section, we mainly investigate and discuss the performance of the film electrode-based clutch.

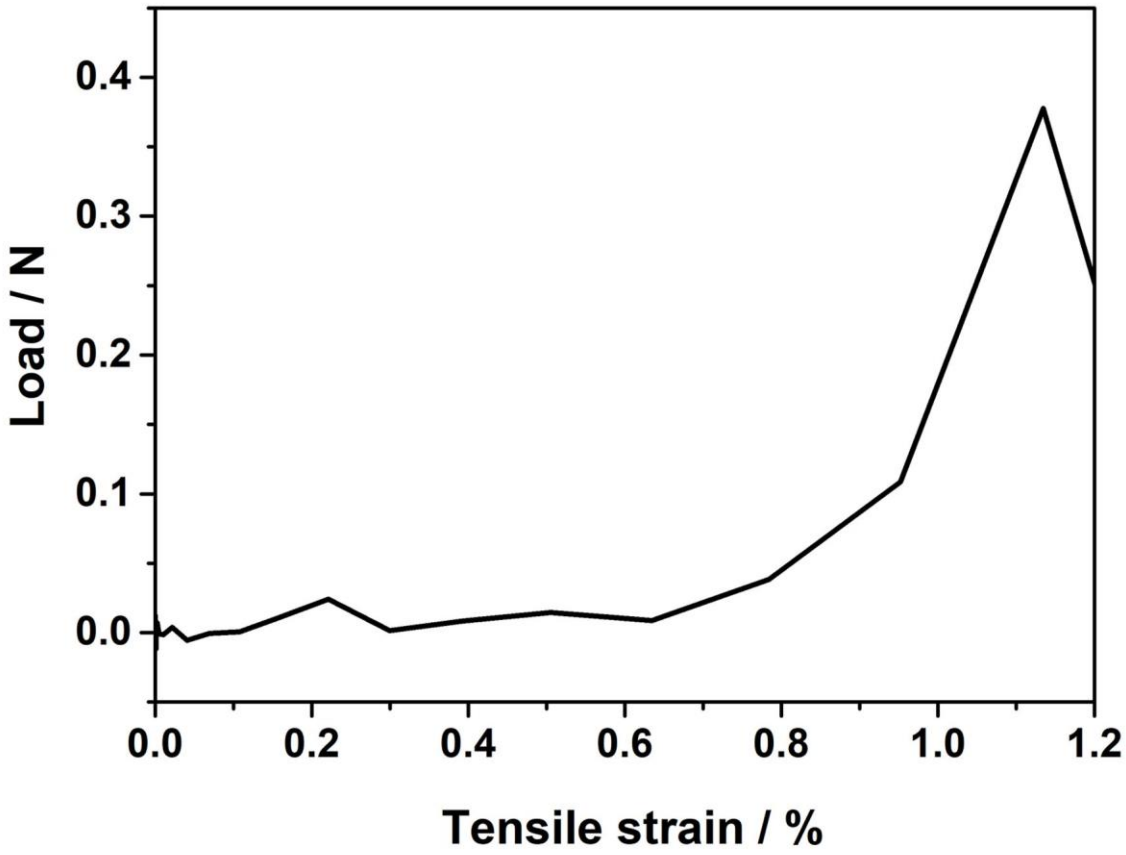

Fig 3.9 Performance of the fabric electrode-based clutch

As demonstrated in Equation (2-1)[1,2] (**Chapter 2**), for a certain dielectric material, the generated shear force (F) is related to the overlapping area (A), dielectric thickness (t) and working voltage (V). In this part, the A-F, t-F, V-F relationships as well as the engage and release times of the electroadhesive clutches will be systematically investigated. The working voltage of the clutches could be significantly decreased to ~100 V with the use of high-*k* PVDF-FS polymers, implying that increase the dielectric constant of the dielectric layer is quite effective in lowering down the driving-voltage of the electroadhesive clutch. And during the tests, no arc discharge or electrical spark was observed, which should be attributed to the high dielectric break-down strength of the polymer and the relatively low working voltage.

3.3.4.1 V-F relationship

The effect of working voltage on the generated shear force was firstly investigated with a constant overlapping area of 6 cm^2 and a dielectric thickness of 17.7 ± 2.6 μm. The data and the mathematic fitting result of the curve are shown in Fig 3.10. The fitting result shows that the shear force scales as $V^{4.7}$ (R^2 = 0.97), which is more dramatically than the theoretical value V^2 (R^2 = 0.48). This result indicates that increasing the applied voltage is an effective method to boost the holding force and the voltage plays more important roles than prediction. The deviation of the curve should be ascribed to the elimination of air gaps between the two electroadhesive pads under high external voltages.[4] Apart from the eliminated air gaps, the increased effective contact area (A) and the friction coefficient

(μ) under relatively high electric field strength (V/t) will also contribute to the generated shear force. The charge accumulation at the interface may also result in the large shear force. The clutch could be activated at 80 V though the generated force is lower than 5 N. It could provide an electroadhesive force of 58.14 ± 8.24 N at 140V, resulting in a shear force of 96.90 ±13.73 kPa, which is much higher than the previously reported values (23.8 kPa at 320 V).[4] The current change of the clutch with the increase of the voltage is also recorded (see Fig 3.10). The corresponding data are summarized in Table 3.3. When voltages increase from 80 to 140 V, the power consumption caused by the current leakage increases dramatically from 0.52 μW to 19.88 μW.

Table 3.3 Summary of the electroadhesive forces and current under different voltages

Voltage / V	80	90	100	110	120	130	140
$\overline{F}$ / N	4.33	11.23	24.42	29.01	48.11	50.54	58.14
STD / N	0.38	2.54	2.48	2.89	4.70	2.03	8.24
Current / nA	6.49	10.97	16.00	22.53	46.35	67.93	142.33
STD / nA	0.13	0.30	0.79	0.57	0.83	0.66	4.16
Power consumption / μW	0.52	0.99	1.60	2.48	5.56	8.83	19.88

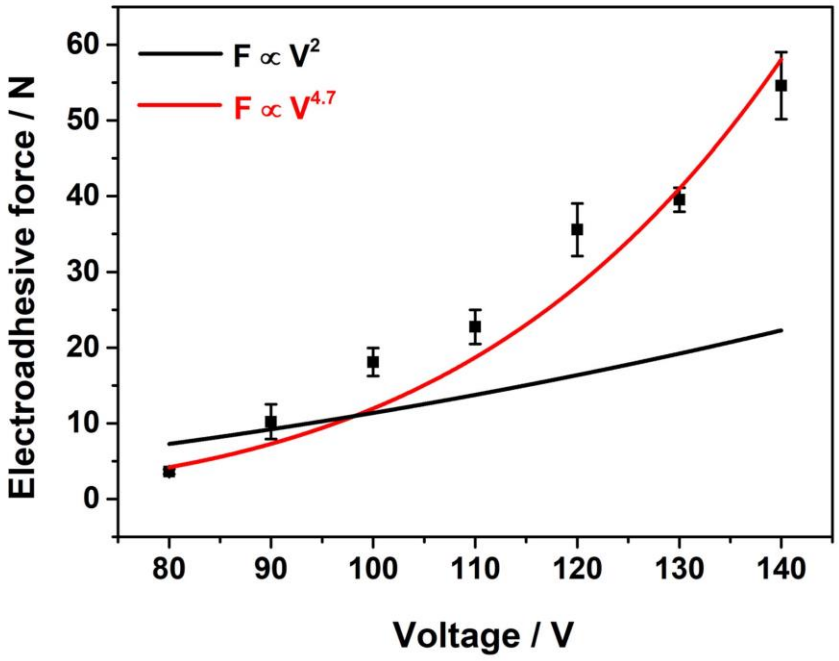

Fig 3.10 Relationship between voltage and electroadhesive force ($F = 4.75 \times 10^{-9} V^{4.7}$, $R^2 = 0.97$; $F = 1.10 \times 10^{-3} V^2$, $R^2 = 0.48$)

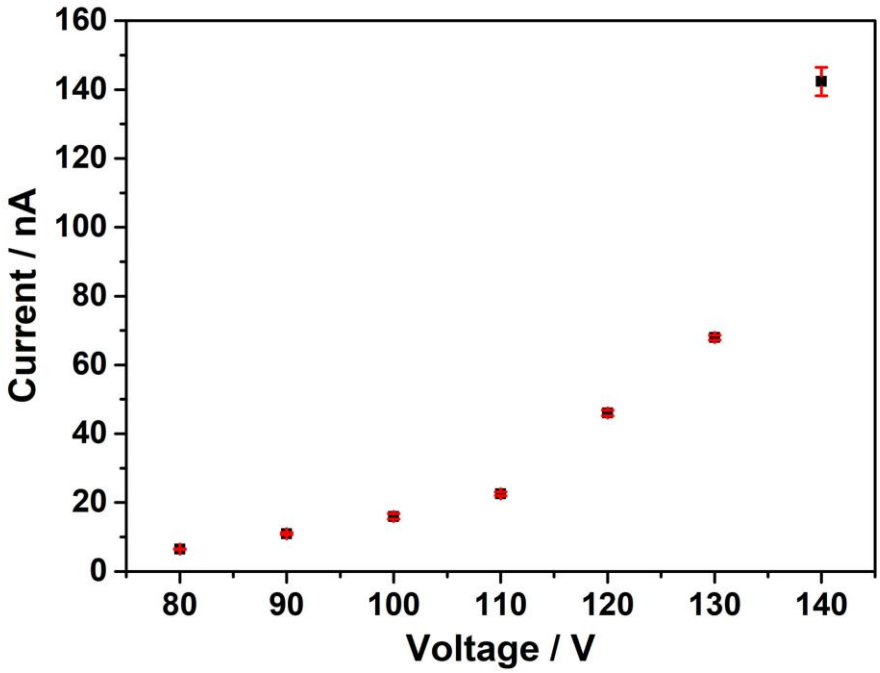

Fig 3.11 Relationship between the applied voltage and current in the clutch

3.3.4.2 A-F relationship

The relationship between the overlapping area and the produced shear force was studied at a fixed working voltage of 140 V and a dielectric thickness of 15.4 ± 1.5 μm. The data are summarized in Table 3.4 and the results are demonstrated in Fig 3.12. The slope of the linear-fitted curve is calculated to be 9.13 N/cm^2 (91.3 kPa) with $R^2 = 0.98$, suggesting the generated electroadhesive force increases almost linearly with the overlapping area.

Table 3.4 Summary of the electroadhesive force with different overlapping areas

A / cm^2	1	2	4	6
$\bar{F}$ / N	8.47	19.82	37.90	54.95
STD / N	0.79	1.96	4.84	7.99

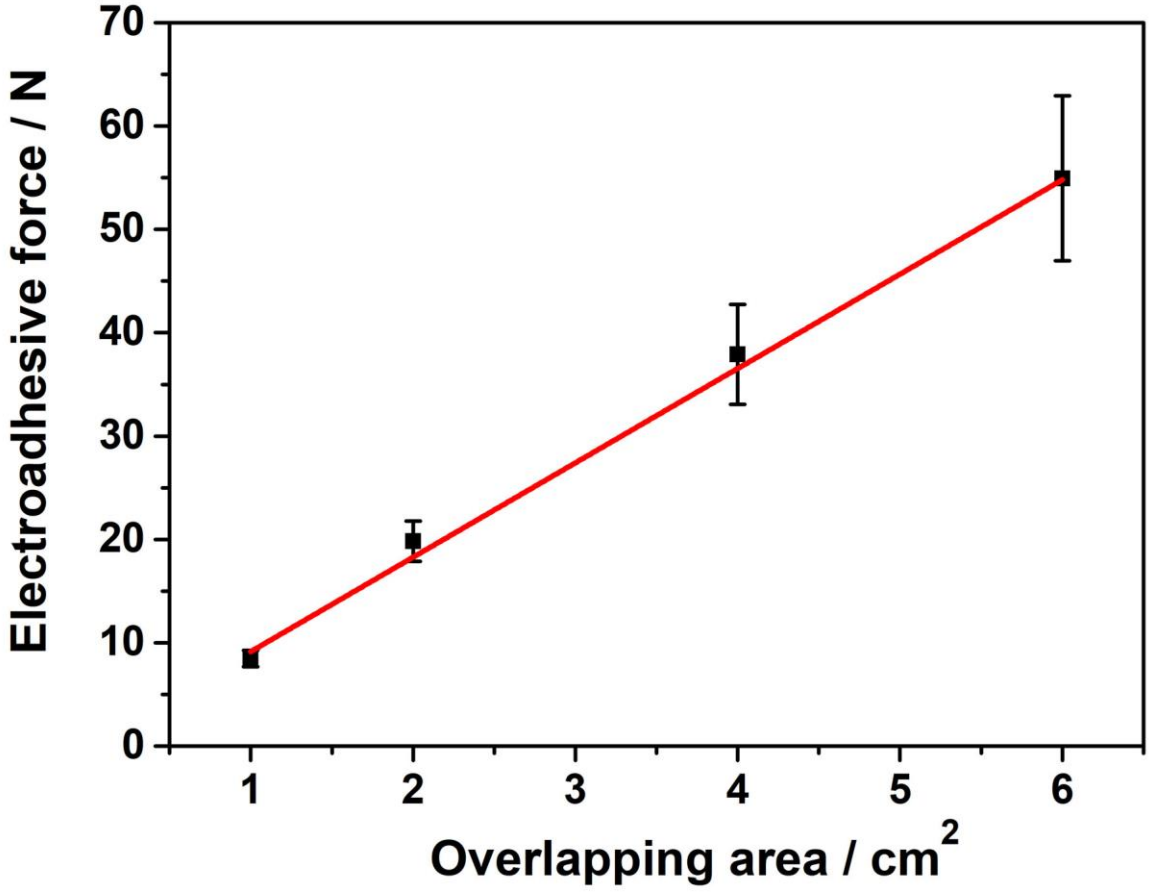

Fig 3.12 Relationship between the overlapping area and electroadhesive force (F = 9.13A, R^2 = 0.98)

3.3.4.3 t-F relationship

The maximum electrostatic force as a function of the total dielectric thickness has also been explored under a fixed voltage of 120 V and the overlapping area is set as 4 cm^2. The corresponding data are outlined in Table 3.5 and Fig 3.13. The best performance is 40.66 ± 2.70 N at 120 V with a total dielectric thickness of ~12 μm, resulting in a shear

force of 101.6 ± 0.68 kPa. According to Equation (2-1), the electroadhesive force should be proportional to $1/t^2$, however, the fitted curve shows that the generated force matches better with $1/t^{1.6}$ ($R^2 = 0.97$) than $1/t^2$ ($R^2 = 0.90$). It could be concluded that reducing the dielectric thickness is also a practical approach to obtain large electroadhesive force, though it is not as remarkable as expected. The reason behind should also be the minimized air gaps at the interface of the clutch under relatively high electrical field strength. The changes in the physical properties are also likely to result in the large shear force.

Table 3.5 Summary of the electroadhesive force with different dielectric thickness

t / μm	12	19	23	30
$\bar{F}$ / N	40.66	21.05	15.45	7.55
STD / N	2.70	0.20	1.15	1.11

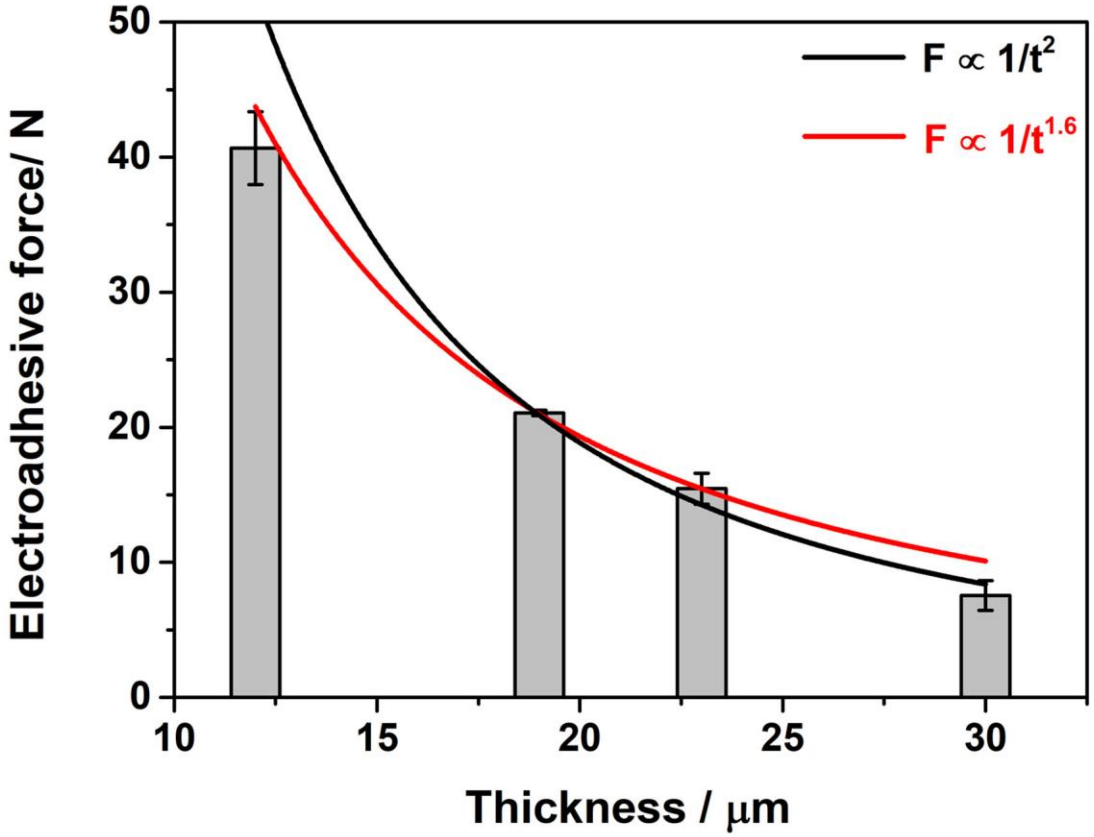

Fig 3.13 Relationship between dielectric thickness and electroadhesive force ($F = 2332/t^{1.6}$, $R^2 = 0.97$; $F = 7545/t^2$, $R^2 = 0.90$)

3.3.4.4 Response time

As demonstrated in the Experimental section, the engage time was defined as the time lapse required for the transition from the electrical signal to the mechanical signal. The working voltage and dielectric thickness were fixed at 140 V and 17.7 ± 2.6 μm, respectively. The engage time measured is 25.3 ± 1.2 ms, which is comparable with the

literatures (~20 ms)[1,4] and a typical picture is shown in Fig 3.14. The time duration between A point and B point is calculated as the engage time where A is the initial transition point of the electrical field and B is the starting point of the generated force. The release time measured is 324 ± 71 ms (see Fig 3.15) with the same clutch at a constant load of ~25 N and the overlapping area is 4 cm^2. A is the point when the power source is switched off and B is the point when the two electroadhesive pads separate from each other. The measured release time is much higher than the literature values, which are generally less than 15 ms.[1,4] This may be ascribe to the presence of the remnant polarization (P_r) of the PVDF-FS when the external electrical fields is removed since it is a kind of typical ferroelectric materials.[31–33] Vacuum adhesion may also exist since the PVDF-FS is much softer (Yong's modulus E < 0.4 GPa) than the other dielectric materials used for electroadhseive clutches (*e.g.* PI and PVDF composites, E > 2 GPa).[1,3,4]

Based on the theoretical model,[16,29,34] soft dielectric layer will minimize the air gaps and thus result in large shear forces. However, the soft nature of the dielectric materials seems to be detrimental to the fast response of the clutch and the impact is even more serious on the release time. A trade-off may exist between the electroadhesive force and response time and the material selection are thus significant for different application scenario.

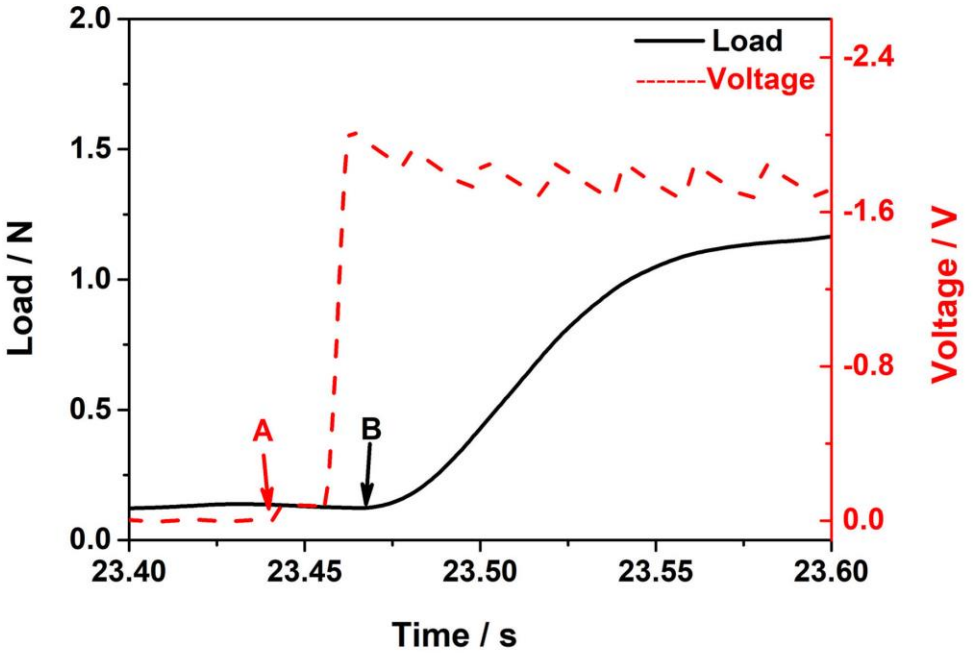

Fig 3.14 Engage time of the clutch

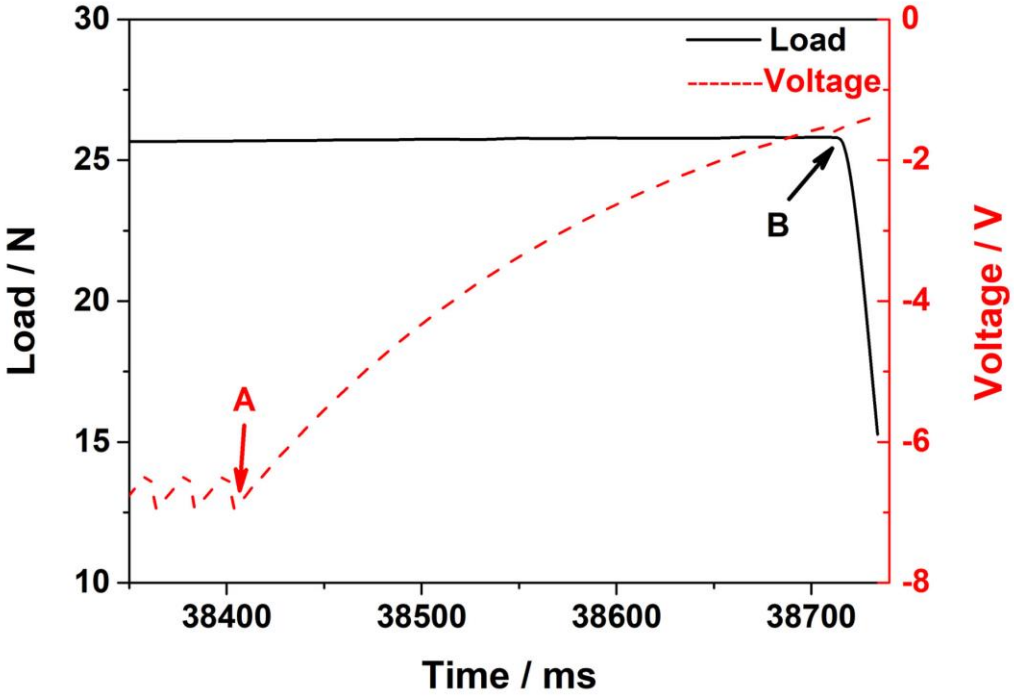

Fig 3.15 Release time of the clutch

3.3.4.5 Flexural rigidity

When the two electroadhesive pads are adhered with each other and act as if a pad of double thickness under an external electrical field, and the stiffness of the clutch is supposed to be increased. The flexural rigidity of the clutch under different applied voltages have been evaluated. The total thickness of the clutch was about 170 μm. The mass per unit area (W) of the clutch was measured to be 227 g/m^2 and the flexural rigidity was calculated by Equation (3-2) by using the ASMT standard D1388-08 (2002) method of bending length. The corresponding parameters and results are summarized in Table 3.6 and the voltage-stiffness variation relationship is shown in Fig 3.16. The results show that the flexural rigidity of the clutch rises with the increase of the applied voltage. When the voltage comes to 120 V, the rigidity is calculated to be 2.83 $mJ \cdot m^{-1}$, which almost doubles as compared with the non-engage clutch ($G = 1.43\ mJ \cdot m^{-1}$). This result may provide a novel strategy to accommodate the stiffness of the films in a certain range by simply adjusting the applied voltages.

Table 3.6 Data summary of the stiffness test

Voltage / V	c / mm	G / mJ·m^{-1}	G/G_0
0	60.50 ± 0.10	1.43	1.00
80	67.43 ± 0.15	1.98	1.38
100	71.93 ± 0.21	2.31	1.62
120	76.13 ± 0.12	2.83	1.98

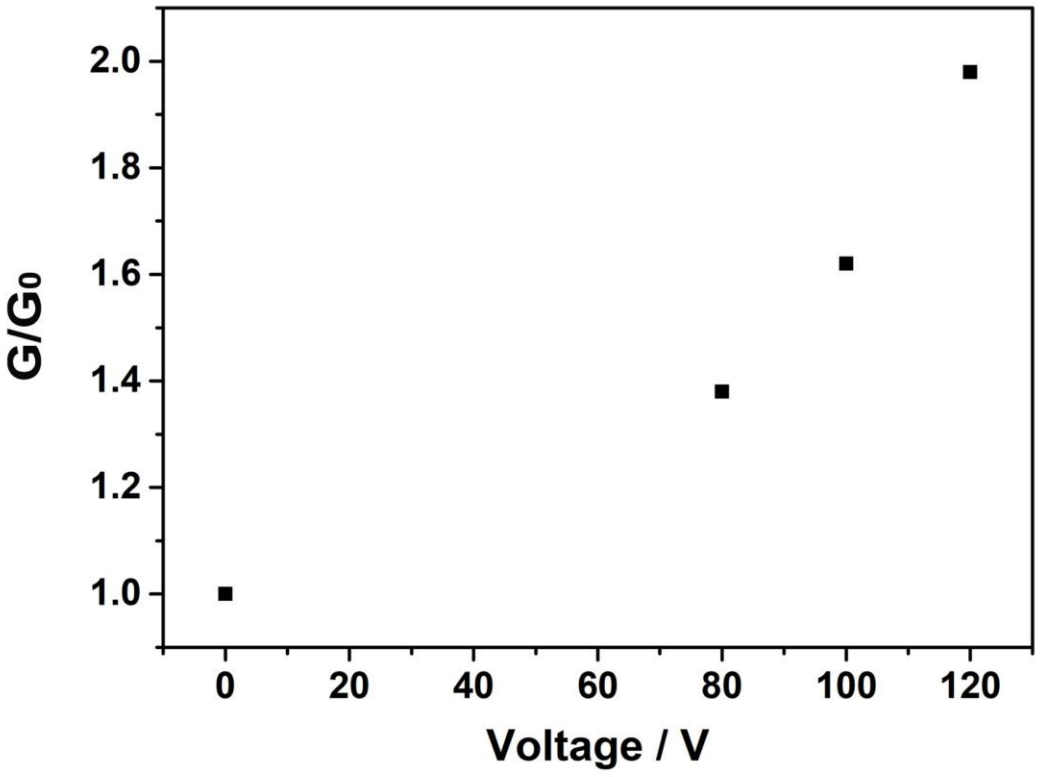

Fig 3.16 Relationship between voltage and stiffness change

3.3.4.6 Electroadhesion under AC square-wave voltage

To explore the electroadhesion behaviour of the symmetric clutch under an AC voltage, the clutch performance with a square wave output have been investigated for the first time. The peak and valley voltages were set at 100 V and -100 V respectively and hold for 1 s. The voltage was provided and recorded at a Keithley 2400 and the voltage profiles are shown in Fig 3.17. The overlapping area of the clutch was 6 cm^2 and the dielectric thickness was 17.7 ± 2.6 μm, which is the same with the clutch used in the V-F measurement. The clutch could generate a shear force of 24.02 ± 1.65 N, which is almost the same as measured electroadhesive force at 100 V DC voltage (24.42 ± 2.48 N). This result indicates the AC source could also be used to drive the electroadhesive clutch and could provide a comparable shear force with the DC source at the same voltage. The application scenes of the electroadhesive clutches will be remarkably broadened since AC source could also be used to drive the devices.

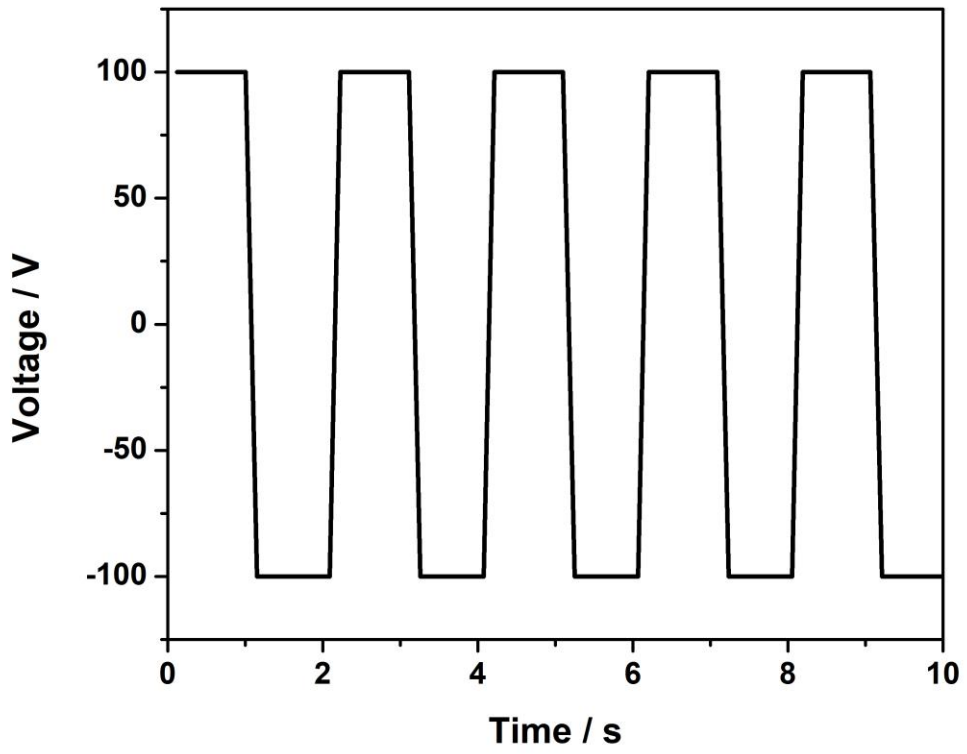

Fig 3.17 Voltage profile of the square-wave power supply

3.4 Conclusion and future works

To conclude, electroadhesive clutches based on high-*k* PVDF-FS polymers and flexible electrodes have been fabricated through blade coating and the clutch performance have been evaluated. The PVDF-FS dielectric layer exhibits a high dielectric constant of 48 and tan δ of 0.048 with a very smooth surface. The relationships between the external voltage, overlapping area, dielectric thickness and the generated electroadhesive force have also been explored. A shear force over 100 kPa could be generated by using a DC source of 120

V and power under 20 μW. The generated shear forces exhibit positive relation with the working voltage and overlapping area but a negative relation with the total dielectric thickness. The influence of the applied voltage turns out to be more significant among the three factors. The engage time and release time are ~25 ms and ~324 ms respectively. The symmetric clutches exhibit a relatively long release time due to the eliminated air gaps, changed physical properties of the electroadhesive pads under high electrical field strength and the charge accumulation. The stiffness change of the clutch has also been evaluated and the results show that the rigidity under 120 V increases 2-fold than the original one. This may pave the way towards novel design strategies for tuneable stiffness based on external voltages. The clutch is found to be able to work under AC square-wave voltage with comparable performance as DC voltage. The application scenarios of the electroadhesive clutches are expected to be remarkably expanded with AC source as the power supply.

However, when the holding force of the clutch becomes higher than 100 N, irreversible deformation or fracture may occur due to the limited mechanical strength of the dielectric layer, electrode and substrate. This issue could be addressed by utilizing multi-pair clutch or develop clutch with stronger materials. Textile-based clutch should be further explored to improve the performance by decreasing the surface roughness of the coatings. New theoretical models should also be proposed to explain the huge deviation of the experimental results and the current models. The physical properties of the dielectric and electrode materials should be taken into account.

References

[1] V. Ramachandran, J. Shintake, D. Floreano, *Adv. Mater. Technol.* **2019**, *4*, 1800313.

[2] S. Diller, C. Majidi, S. H. Collins, in *2016 IEEE Int. Conf. Robot. Autom.*, IEEE, **2016**, pp. 682–689.

[3] R. Hinchet, V. Vechev, H. Shea, O. Hilliges, in *31st Annu. ACM Symp. User Interface Softw. Technol. - UIST '18*, ACM Press, New York, New York, USA, **2018**, pp. 901–912.

[4] S. B. Diller, S. H. Collins, C. Majidi, *J. Intell. Mater. Syst. Struct.* **2018**, *29*, 3804.

[5] C. Li, L. Shi, W. Yang, Y. Zhou, X. Li, C. Zhang, Y. Yang, *Nanoscale Res. Lett.* **2020**, *15*, 36.

[6] F. Xia, R. Klein, F. Bauer, Q. M. Zhang, *MRS Proc.* **2003**, *785*, D5.8.

[7] R. J. Klein, J. Runt, Q. M. Zhang, *Macromolecules* **2003**, *36*, 7220.

[8] S. Ahmed, E. Arrojado, N. Sigamani, Z. Ounaies, in *Behav. Mech. Multifunct. Mater. Compos. 2015* (Ed.: N.C. Goulbourne), **2015**, p. 943206.

[9] R. J. Klein, F. Xia, Q. M. Zhang, F. Bauer, *J. Appl. Phys.* **2005**, *97*, 094105.

[10] M. A. Graule, P. Chirarattananon, S. B. Fuller, N. T. Jafferis, K. Y. Ma, M. Spenko, R. Kornbluh, R. J. Wood, *Science (80-.).* **2016**, *352*, 978.

[11] S. Baik, D. W. Kim, Y. Park, T.-J. Lee, S. Ho Bhang, C. Pang, *Nature* **2017**, *546*, 396.

[12] J. Jeong, J. G. McCall, G. Shin, Y. Zhang, R. Al-Hasani, M. Kim, S. Li, J. Y. Sim,

K.-I. Jang, Y. Shi, D. Y. Hong, Y. Liu, G. P. Schmitz, L. Xia, Z. He, P. Gamble, W. Z. Ray, Y. Huang, M. R. Bruchas, J. A. Rogers, *Cell* **2015**, *162*, 662.

[13] Y. Bi, Y. Liu, X. Zhang, D. Yin, W. Wang, J. Feng, H. Sun, *Adv. Opt. Mater.* **2019**, *7*, 1800778.

[14] X. Lin, M. Wu, L. Zhang, D. Wang, *ACS Appl. Electron. Mater.* **2019**, *1*, 397.

[15] X. Zhang, Y. Shen, Z. Shen, J. Jiang, L. Chen, C. W. Nan, *ACS Appl. Mater. Interfaces* **2016**, *8*, 27236.

[16] T. Nakamura, A. Yamamoto, *ROBOMECH J.* **2017**, *4*, 18.

[17] F. Xia, Z. Cheng, H. Xu, H. Li, Q. Zhang, G. J. Kavarnos, R. Y. Ting, G. Abdul-Sedat, K. D. Belfield, *Adv. Mater.* **2002**, *14*, 1574.

[18] B. Chu, *Science (80-.).* **2006**, *313*, 334.

[19] J. Xiao, X. Zhou, Q. M. Zhang, P. A. Dowben, *J. Appl. Phys.* **2009**, *106*, 044105.

[20] H. Xu, Z.-Y. Cheng, D. Olson, T. Mai, Q. M. Zhang, G. Kavarnos, *Appl. Phys. Lett.* **2001**, *78*, 2360.

[21] V. Bharti, Q. M. Zhang, *Phys. Rev. B* **2001**, *63*, 184103.

[22] W. Xia, J. Lu, S. Tan, J. Liu, Z. Zhang, in *Dielectr. Polym. Mater. High-Density Energy Storage*, Elsevier, **2018**, pp. 103–163.

[23] P. E. Aba-Perea, T. Pirling, M. Preuss, *Mater. Des.* **2016**, *110*, 925.

[24] M. Kobayashi, K. Tashiro, H. Tadokoro, *Macromolecules* **1975**, *8*, 158.

[25] K. Tashiro, M. Kobayashi, H. Tadokoro, *Macromolecules* **1981**, *14*, 1757.

[26] M. A. Bachmann, W. L. Gordon, J. L. Koenig, J. B. Lando, *J. Appl. Phys.* **1979**, *50*, 6106.

[27] L. Weng, P.-C. Liao, C.-C. Lin, T.-L. Ting, W.-H. Hsu, J.-J. Su, L.-C. Chien, *AIP Adv.* **2015**, *5*, 097218.

[28] W. Hu, V. B. F. Mathot, R. G. Alamo, H. Gao, X. Chen, in *Polym. Cryst. I From Chain Microstruct. to Process.*, **2016**, pp. 1–43.

[29] C. Cao, X. Sun, Y. Fang, Q.-H. Qin, A. Yu, X.-Q. Feng, *Mater. Des.* **2016**, *89*, 485.

[30] R. Liu, R. Chen, H. Shen, R. Zhang, *Int. J. Adv. Robot. Syst.* **2013**, *10*, 36.

[31] Prateek, V. K. Thakur, R. K. Gupta, *Chem. Rev.* **2016**, *116*, 4260.

[32] Y. Shen, D. Shen, X. Zhang, J. Jiang, Z. Dan, Y. Song, Y. Lin, M. Li, C. Nan, *J. Mater. Chem. A* **2016**, *4*, 8359.

[33] D. Cao, C. Wang, F. Zheng, L. Fang, W. Dong, M. Shen, *J. Mater. Chem.* **2012**, *22*, 12592.

[34] A. S. Chen, S. Bergbreiter, *Smart Mater. Struct.* **2017**, *26*, 025028.

Chapter 4 Asymmetric-structured electroadhesive clutches made from polyurethane, polyimide and polytetrafluoroethylene

4.1 Introduction

Asymmetric strategy is widely adopted in the design of energy converting and harvesting systems, including supercapacitors,[1–4] batteries,[5–7] soft actuators,[8,9] memory devices[10,11] and triboelectric nanogenerators (TENGs).[12–15] Rational design of asymmetric structures could improve the performance of the batteries and supercapacitors, which could enlarge the potential window, increase the cycle stability and energy density.[1,3,16] Asymmetric structure has also been widely used in TENGs to maximum the contact-induced opposite charges and could create large static electricity.[17] The triboelectrification charge densities of the common film[17] and fibrous[18] materials have been quantified for TENGs. Wang's research group developed an asymmetric TENG with an extremely high sustainable output open-circuit voltage (> 20 kV) based on negative electrified polyimide (PI) and positive electrified nylon films recently.[14] Yu and co-authors have also summarized the tendency of loss or gain electrons of some typical materials and the results are shown in Fig 4.1.[12] The ability of losing electrons decrease from the top to bottom of the figure, which means the polyurethane (PU) is easy to lose electrons and be positive charged while polytetrafluoroethylene (PTFE) tends to gain

electrons and be negative charged. The device structure of the TENG is similar with the electroadhesive clutch, which consists of two electrodes coated with thin-layer dielectric materials. And the charges at the interface of the two pads play dominant roles in the performance of TENGs and electroadhesive clutches.

However, as demonstrated in **Chapter 2**, current research on electroadhesive clutches are all in symmetric structures with the same dielectric materials at both positive and negative electrodes. The effect of electronegativity of the dielectric materials on the clutch performance have not been explored yet. In this chapter, we mainly investigatesthe influence of the electronegativity of the dielectric materials to the performance of the clutches. Clutches with both symmetric and asymmetric structures will be fabricated and their electroadhesive performance is to be evaluated.

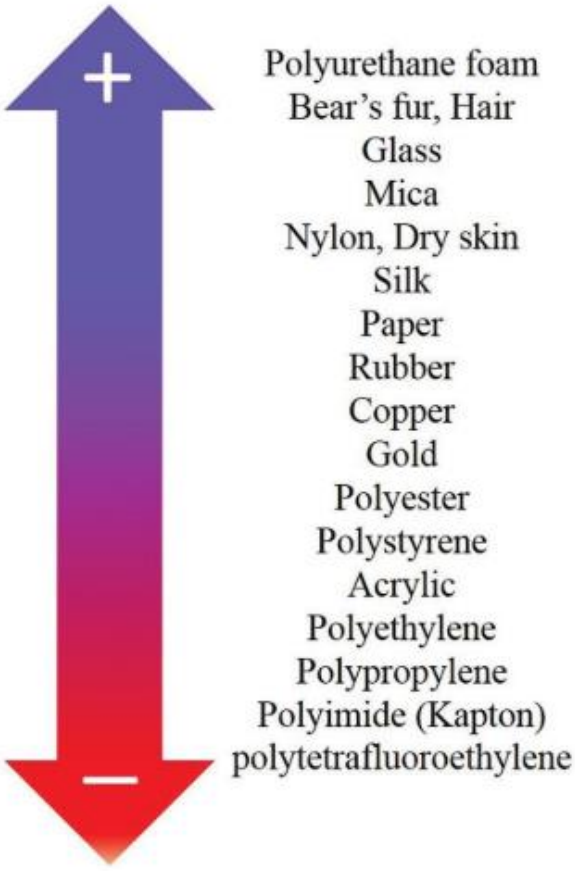

Fig 4.1 Tendency of lose (+) and to gain (−) electrons of polymers[12]

4.2 Experimental

4.2.1 Materials selection

According to Fig 4.1, PU is most likely to carry positive charges while PI and PTFE tend to carry negative charges among polymer materials. In this part, PU and PI or PTFE were used as the dielectric materials. Al/PVC was also used as the flexible electrode due to its smooth surface as demonstrated in Chapter 3. Since the PI and PTFE films with different

thickness have been well commercialized, robust conductive fabric with smooth adhesive layer was used directly. The adhesive layer of the fabric was also conductive and act as a part of the electrode.

The PU paint (1310B) and PTFE films were purchased from H.F Co. Ltd, Shenzhen. The PI films were purchased from Rayitek Co. Ltd, Shenzhen. The thickness of the PI films varies from 5 μm to 50 μm. PVC tape (Scotch, 65 μm), conductive fabric with adhesive layers (3M, 120 μm) and Al foil (Glad, 15 μm) were used directly. Silver paste (sigma) was diluted with small amount of isopropyl alcohol (IPA) to adjust the viscosity before printing. Solvents including IPA, acetone and ethanol were purchased from TCI chemicals and used without any further purification.

4.2.2 Materials characterization

Fourier-transform infrared spectroscopy (FTIR) was measured on a Perkin spectrum 100 FTIR spectrometer. The surface roughness was measured on a ZYGO laser interferometric non-contact profile system with sample size of 4 cm^2. Scanning electron microscope (SEM) images were taken on a JEOL Model JSM-6490. The mechanical properties and the performance of the clutches including the generated shear force and response time were measured on a Instron 5944. The high voltage direct voltage was provided by the RK2674A voltage withstand test instrument. The Agilent 4294A precision impedance analyzer was used to analysis the dielectric properties.

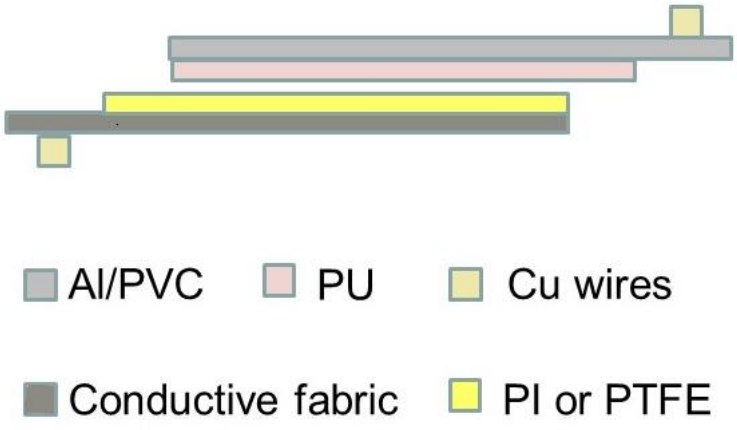

Fig 4.2 Schematic illustration of the device structure of the asymmetric electroadhesive clutch

4.2.2.1 Procedures for the sample preparation

The PU paint was used directly and the PU films with different thicknesses were directly blade coated on Al foils by different profile bars on a *k* control coater. The resultant films were cured at 65 ^{o}C for 3 hours and then the PVC tape was attached on the backside to protect the Al layers and improve the mechanical strength of the pads. The PTFE and PI films were directly stick on the conductive fabrics. The samples were cut into demanded sizes by a roller cutter. The device structure of the asymmetric elecctroadhesive clutches is demonstrated in Fig 4.2.

4.2.3 Clutch performance evaluation

The mechanical properties and the performance of the clutches including the generated shear force and response time were measured on a Instron 5944 with the same test system demonstrated in Fig 3.2 (Chapter 3). The high voltage direct voltage was provided by the RK2674A voltage withstand test instrument.

4.2.3.1 Procedures for the dielectric measurement

The measurement of the dielectric constant and loss were the same as the PVDF-FS films. The sample size was about 2 cm^2 and both sides of the films were coated with silver paste as the electrodes through screen printing. The capacitance and dielectric loss at different frequency were recorded by impedance analyzer and the relative dielectric constant was calculated by Equation (3-1).

4.2.3.2 Procedures for the mechanical measurement

The mechanical properties of the electrodes including the tensile strain, tensile stress and maxinum load were measured on a Instron 5944. The Load cell was moved with a constant speed of 10 mm/min. The samples size is 4 cm (width) multiple 4 cm (length) and each sample was measured 5 times to give the average value and standard deviation.

4.2.3.3 Procedures for the force measurement

The test system was also the same as the PVDF-FS-based clutches (see Fig 3.2). The direct-current (DC) voltage was provided by a high-voltage power source. When the two electroadhesive clutch was engaged under the applied electrical field, the load cell start to move with a constant speed. The speed was set at 40 N/min to minimize the experimental errors caused by the invalid contact and deformation of the two pads based on preliminary trials. The shear force was recorded as the maximum load before the slip of the two electroadhesive pads. Between each test, the surface of the clutches was wiped with ethanol and rested for around 5 mins to remove the residue charges at the interface of the clutch.[19] Each point was measured five times to obtain the average value and standard deviation. All measurements were conducted at 21 ^{o}C and relative humidity (RH) of 40% to 50%.

4.2.3.4 Procedures for the response time measurement

The instrument setup for the response time is the same as the symmetric clutches as demonstrated in Fig 3.2 (Chapter 3). The resistivities of R1 and R2 were increased to 0.5 MΩ and 15.0 MΩ respectively due to the relatively large voltage used in the test. Through the simple parallel circuit, the force sensor and voltage sensor were integrated into the Instron machine and the force and voltage could be synchronously measured. To measure the time needed for the engagement of the clutch, the upper fixture moved with a velocity of 2 mm/min, after a few seconds the voltage was turned on. The time needed from the

switch of voltage to the generation of the shear force is defined as the engage time. For the measurement of release time, the clutch was firstly engaged and a half of the maximum shear force was given. Then the voltage was turned off and the time between the power outage and the separation of the two pads is the release time. The only difference was that the load cell moved upwards at a constant speed of 0.001 N/min otherwise the holding force will decrease gradually.

4.3 Results and discussion

4.3.1 Electrode properties

The resistivity of the Al/PVC and conductive fabric was measured to be 0.30 ± 0.04 and 2.57 ± 0.06 $\Omega \cdot cm \cdot sq^{-1}$ with the total thickness of 80 μm and 120 μm. Both electrodes show excellent electrical conductivities. The fabric electrode exhibit much stronger tensile stress and holding force as compared with the film electrode. The typical strain-stress and strain-load relationships of the two electrodes were shown in Fig 4.3. The maximum load of the fabric electrode is ~ 280 N, which is about two times higher than the film electrode (~ 130 N). The mechanical and electrical properties of the electrodes were summarized in Table 4.1.

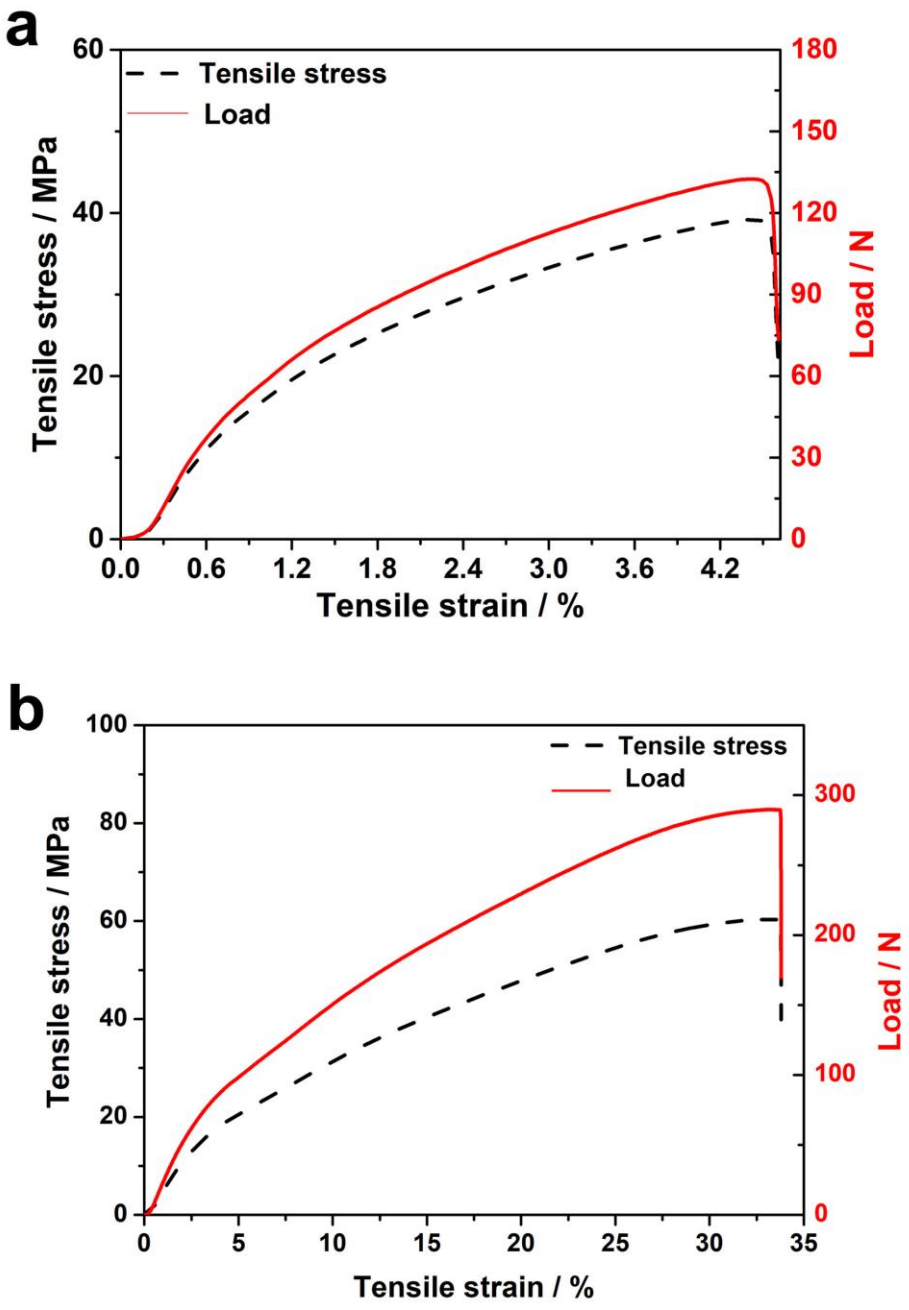

Fig 4.3 Strain-stress curves of the (a) Al/PVC and (b) conductive fabric electrodes

Table 4.1 Mechanical and electrical properties of the electrodes

	Resistivity / $\Omega \cdot cm \cdot sq^{-1}$	Tensile stress / Mpa	Maximum Load / N	E / MPa
Al/PVC	0.30 ± 0.04	39.13 ± 4.03	133.76 ± 11.14	1024.33 ± 73.65
Conductive fabric	2.57 ± 0.06	57.71 ± 1.98	281.75 ± 9.72	593.93 ± 23.97

4.3.2 Dielectric properties

The dielectric constant and dielectric loss of the PU, PI and PTFE have been evaluated by the impedance analyser and the results are shown in Fig 4.4. The dielectric constant of PI (~ 3.7) decreases slightly while the dielectric loss increases as the frequency increases. Considering the nature of the pure polymer materials, dipolar polarization should be the dominant polarization at the measured frequency range which matches the dielectric performance of PI.[20,21] The PTFE film exhibit almost constant dielectric constant of ~ 2.0 and dielectric loss lower than 0.005 due to its intrinsic non-polarity caused by the highly symmetric chemical structure.[22,23] PU exhibit the highest relative dielectric

constant of (4.64 at 1 kHz) as well as the highest tan δ (0.197 at 1 kHz) at low frequency due to the existence of the strong polar urethane groups.[24,25] The dielectric constant and loss decrease from PU, PI to PTFE, which are mainly determined by the molecular polarity.

Table 4.2 Dielectric properties of PU, PI and PTFE

	100 Hz		1000 Hz	
	ε_r	tan δ	ε_r	tan δ
PU	5.07	0.515	4.64	0.197
PI	3.72	0.007	3.70	0.007
PTFE	2.04	0.002	2.03	0.003

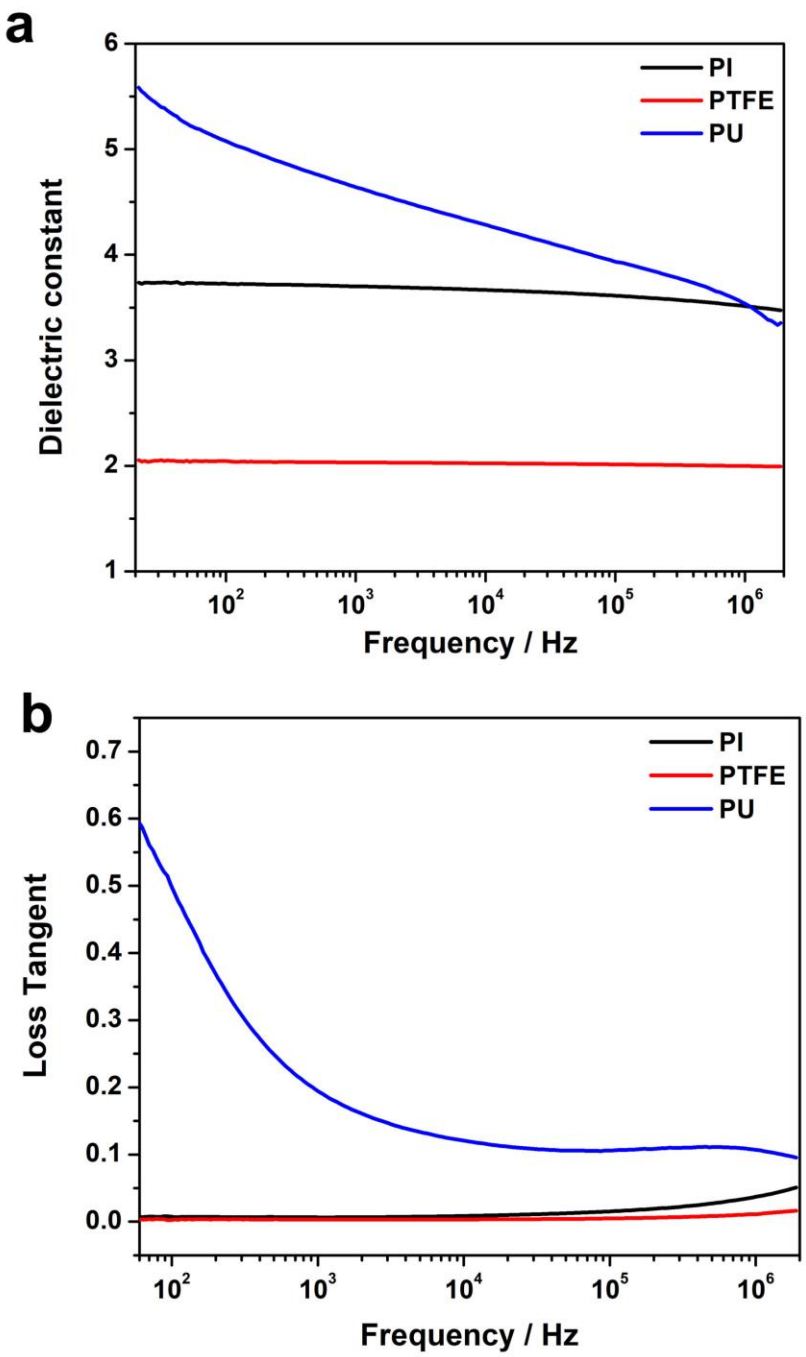

Fig 4.4 Frequency dependent relative dielectric constant and loss tangent of PU, PI and PTFE

4.3.3 Surface morphology

The surface morphologies of the three dielectric polymer films were characterized by the surface roughness. Sa, Sq and Sz refer to the arithmetical mean height, root mean square height and maximum height of the samples. The PU, PI and PTFE exhibit average surface roughness of 20 nm, 19 nm and 303 nm respectively. The roughness of PTFE films turns out to be much larger than PU and PI, which should be detrimental to the clutch performance.

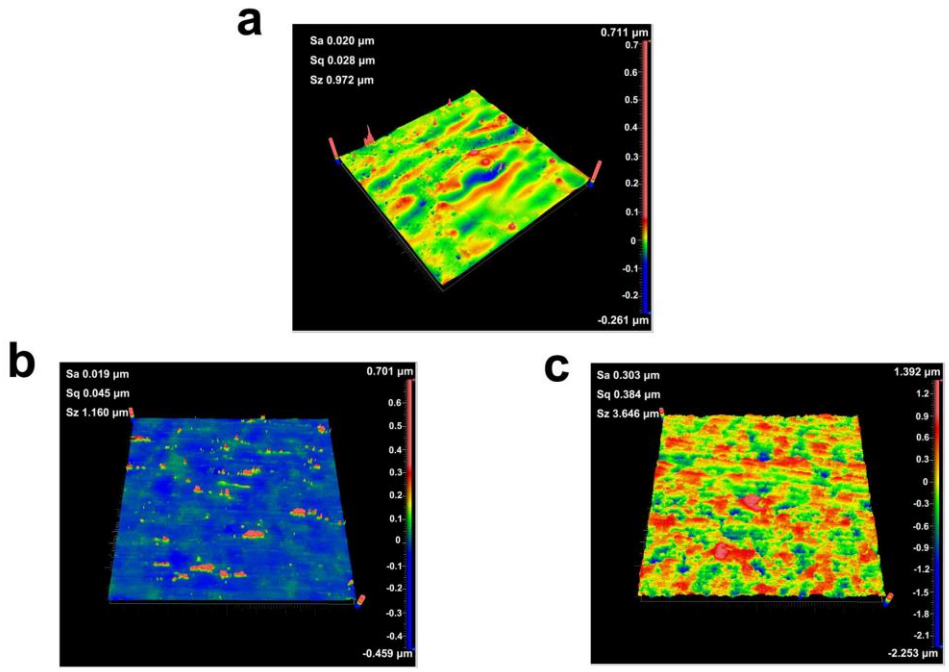

Fig 4.5 Surface roughness of the (a) PU on Al/PVC; (b) PI film on conductive fabric and (c) PTFE film on conductive fabric.

More detailed information was given by the SEM images (see Fig 4.6). No holes or wrinkles could be observed from the PU and PI samples while some grooves existed in the PTFE films. The friction coefficients of the PU, PI and PTFE were measured to be 0.50, 0.38 and 0.24.

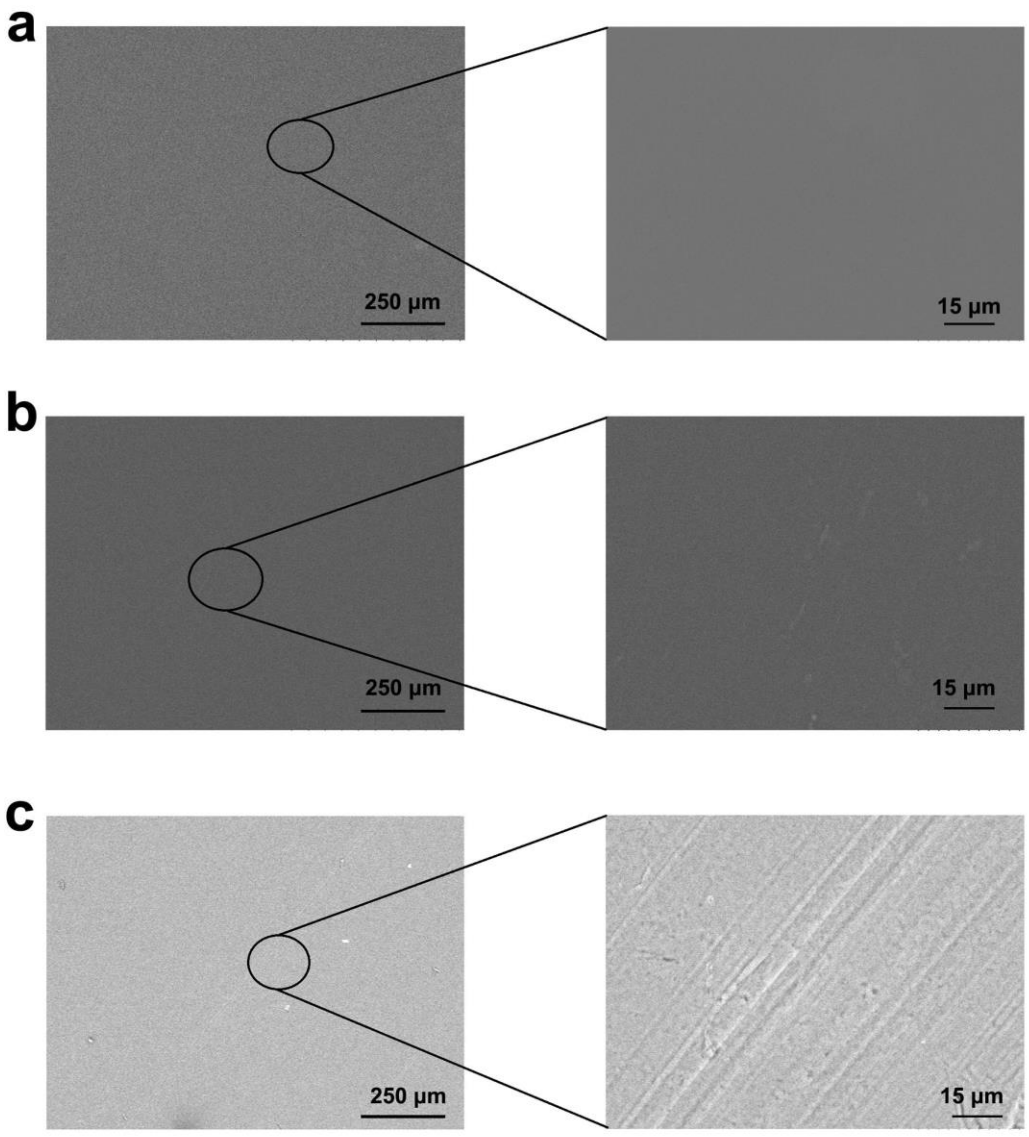

Fig 4.6 SEM images of the (a) PU on Al/PVC; (b) PI film on conductive fabric and (c) PTFE film on conductive fabric.

4.3.4 Preliminary study

4.3.4.1 Symmetric clutches based on PU, PI and PTFE

Based on the results of the materials characterization, it could be concluded that PI films exhibit relatively higher dielectric constant and smoother surface as compared with PTFE films though the electronegativity of PTFE films is higher than PI. Firstly, symmetric electroadhesive clutches based on PU/Al/PVC, PTFE/conductive fabric, PI/conductive fabric have been fabricated and their performance have been evaluated. The applied voltage was set at 500 V considering the relatively low dielectric constant. The total dielectric thickness and overlapping area of each clutch was 50 μm and 5 cm^2 respectively. The PU/PU clutch could generate a shear force as high as 80.27 ± 5.36 N and PI/PI could only provide an electroadhesive force of 11.11 ± 2.02 N. However, PTFE/PTFE clutch could not response at the same voltage. The corresponding data are described in Fig 4.7.

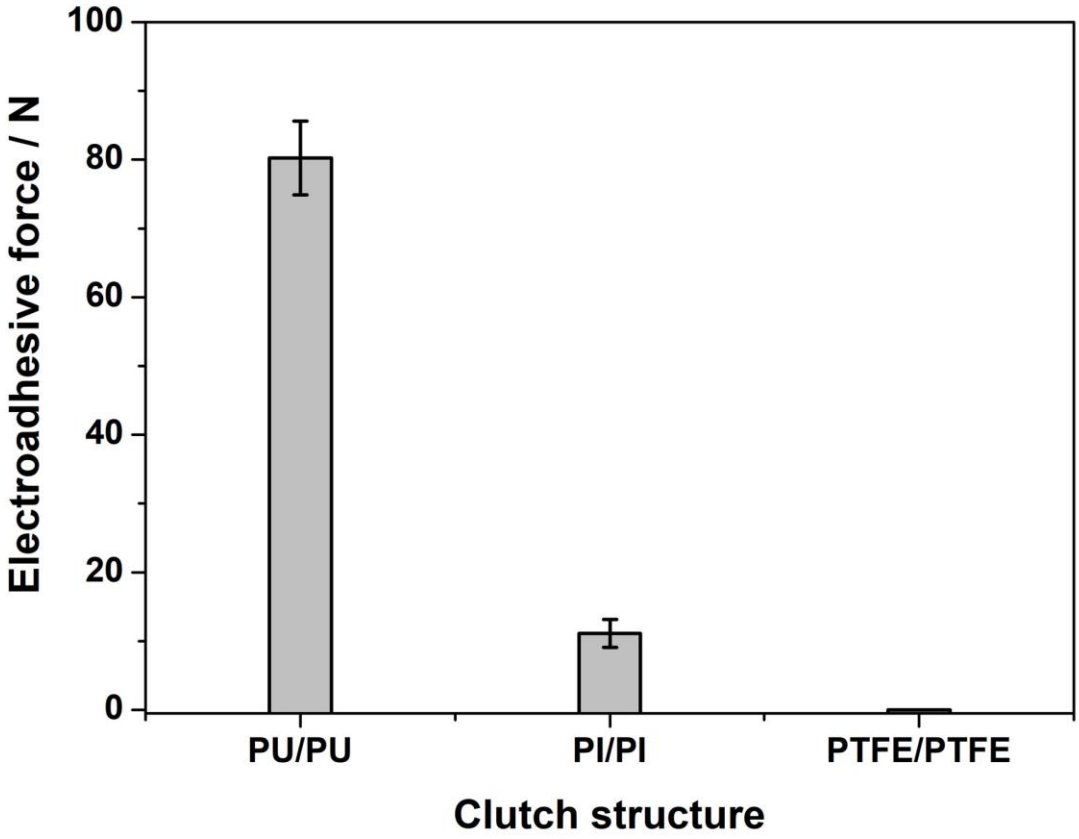

Fig 4.7 Generated electroadhesive force of different types of symmetric clutch

4.3.4.2 Asymmetric clutches based on PU and PTFE

Asymmetric clutches based on PU and PTFE were also prepared and the generated electroadhesive force was evaluated. The two kinds of connection to the power source, namely PU(P)/PTFE(N) and PU(N)/PTFE(P) were demonstrated in Fig 4.8, in which P and N represent that the corresponding dielectric material was connected to positive or negative electrode of the DC power. The dielectric thicknesses of the PU and PTFE layer

were ~ 25 μm. The electroadhesive force was also measured at 500 V and an overlapping area of 5 cm^2, which is the same as the symmetric clutch. The generated shear forces of the PU(P)/PTFE(N) and PU(N)/PTFE(P) clutches were measured to be 1.41 ± 0.16 N and 3.95 ± 0.39 N respectively (see Fig 4.9). The asymmetric clutches could response and generate relatively small shear forces as compared with the PU/PU symmetric clutch. The electroadhesive force increases about 2.8 times by simply reversing the anode and cathode. The difference in the asymmetric PU(P)/PTFE(N) and PU(N)/PTFE(P) clutches indicates that the negativity of the polymer materials could also contribute to the clutch performance. When the polarity of the induced charges matches the nature of the materials, that is, the induced charges are positive on PU and negative on PTFE, it will help to improve the generated holding force and vice versa.

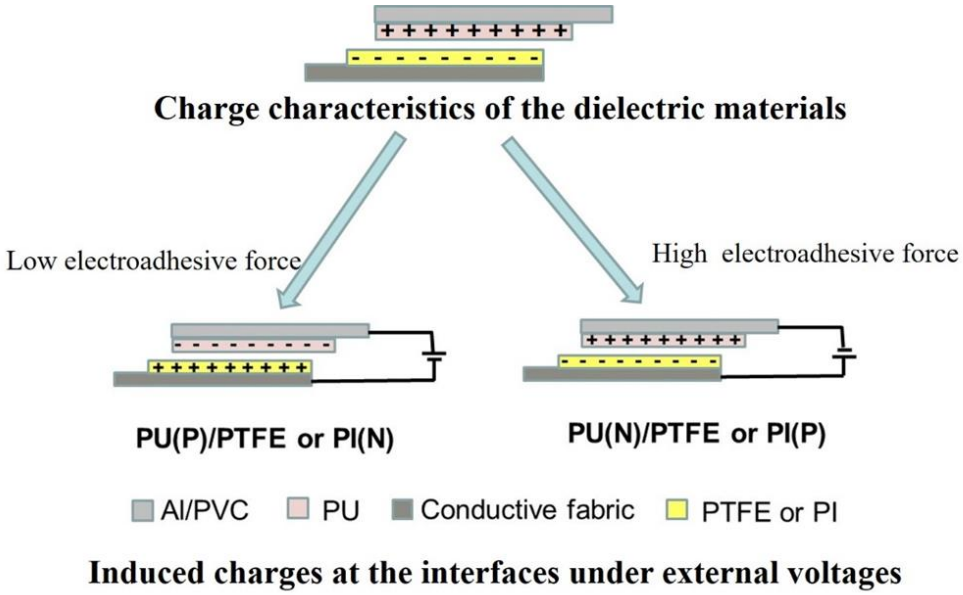

Fig 4.8 Schematic illustration for the different electroadhesive force of the two connection methods in asymmetric-structured clutches

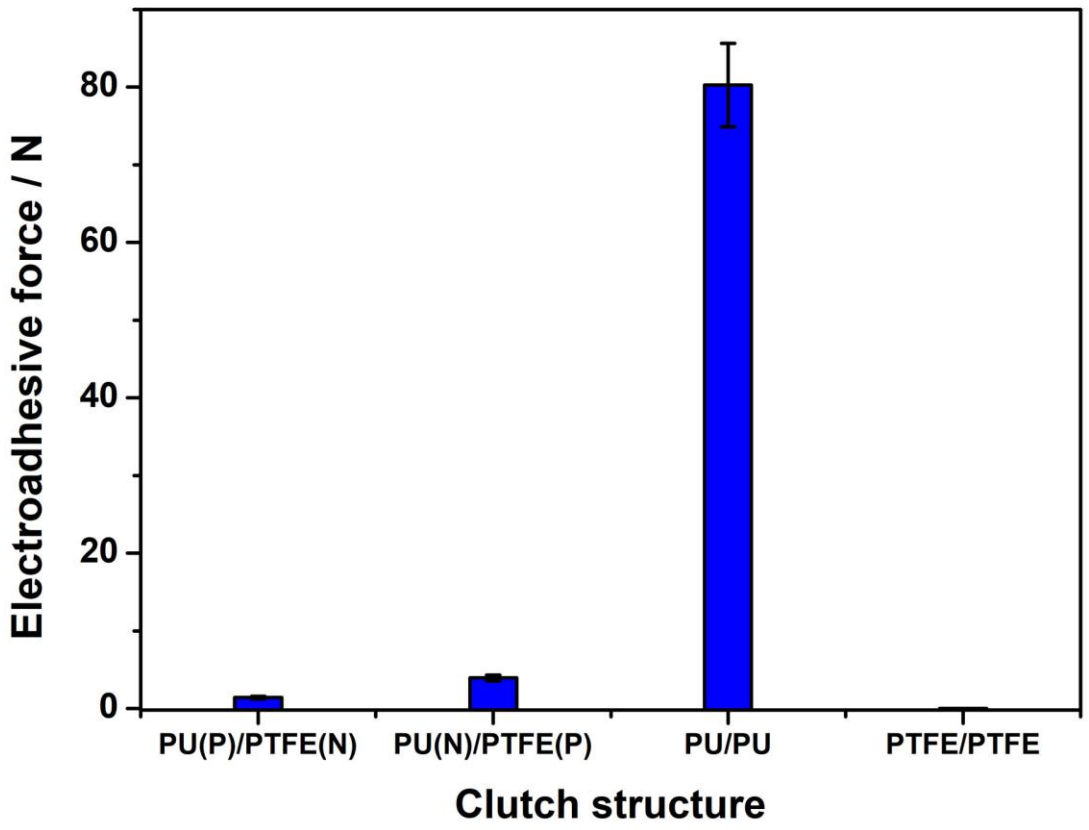

Fig 4.9 Electroadhesive forces of different clutches based on PU and/or PTFE

4.3.4.3 Asymmetric clutches based on PU and PI

PU(P)/PI(N) and PU(N)/PI(P) asymmetric clutches were also prepared (see Fig 4.7) and the generated electrostatic forces were measured. PU/PI based asymmetric clutches could provide larger shear forces than the PU/PTFE systems due to the relatively high dielectric constant, friction coefficient and smooth surface of PI, as discussed in previous sections. PU(N)/PI(P) could generate an electroadhesive force of 93.12 ± 5.06 N, which is higher

than PU/PU, PI/PI and PU(P)/PI(N) clutches, proving the advantages of using asymmetric materials and device structures. The results have been demonstrated in Fig 4.10.

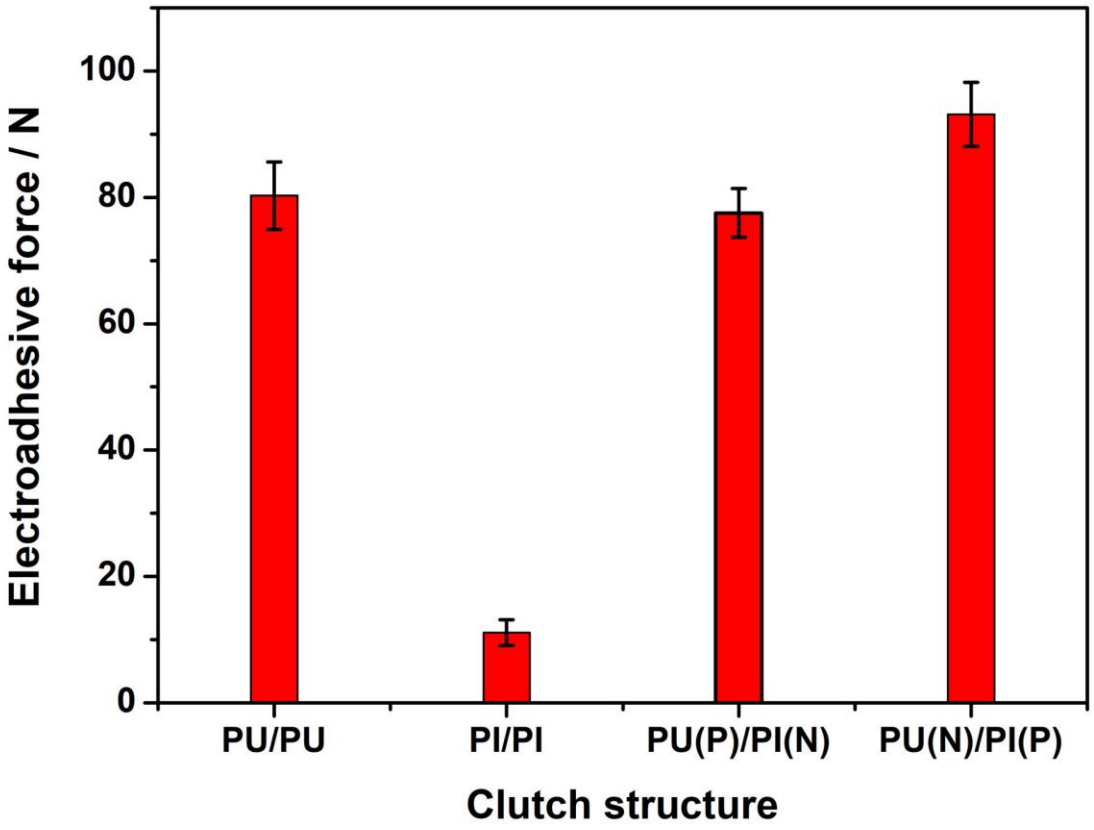

Fig 4.10 Electroadhesive forces of different clutches based on PU and/or PI

4.3.4.4 Summary

The generated electroadhesive force of symmetric and asymmetric clutches based on PU, PI and PTFE are summarized in Table 4.3. PU/PI asymmetric clutches could generate larger holding force as compared with the PU/PTFE clutches due to the higher dielectric constant and smoother surface of PI films. It could be observed that asymmetric clutches

with PU pad connected to negative pole could provide larger shear force than the clutches with PU at positive pole in both PI and PTFE systems. A shear force of 186.24 ± 10.12 kPa could be obtained at 500 V with the clutch structure of PU(N)/PI(P). Apart from the dielectric constant and surface morphology, the charge characteristics of the dielectric materials will also contribute to the final electroadhesive force of the clutch. When the polarity of the induced charges is in accordance with the charge characteristics of the dielectric materials, the generated shear force will increase due to the synergy effect.

Table 4.3 Clutch performance of symmetric and asymmetric clutches based on PU, PI and PTFE (E = 500 V, t = 50 μm, A = 5 cm^2)

		Positive electrode		
		PTFE	PI	PU
Negative electrode	PTFE	0	-	1.41 ± 0.16 N
	PI	-	11.11 ± 2.02 N	77.54 ± 3.86 N
	PU	3.95 ± 0.39 N	93.12 ± 5.06 N	80.27 ± 5.36 N

The PU/PU symmetric clutches exhibit unexpected high performance, which may arise from the intermolecular hydrogen bonding (H-bonding) of the PU chains.[26,27] A self-adhesive behaviour could also be observed in PU/PU clutches without external voltages. The two PU pads could adhere reversibly and repeatably under external forces (~ 50 N

for 5 s) and interestingly a similar adhesive phenomenon could be observed in PU/PI clutches while PU and PTFE films could not be stuck together at the same condition. The same test was also conducted on PU and another two polymer films, namely polyvinyl chloride (PVC) and polypropylene (PP). The PU/PVC and PU/PP could not adhere under pressure as well. PI could not adhere on PTFE, PVC and PP. Since the surfaces of the polymer films were wiped with ethanol before each test, electrostatic interactions between the films could be eliminated.[19]

The adhesion between the PU/PU and PU/PI are probably caused by the interfacial hydrogen bonding.[28,29] The photographs of the combined PU/PU and PU/PI films and the repeating units of the above-mentioned polymers as well as the possible H-bonding are shown in Fig 4.11. This should also be the main reason for the dramatically decrease in electroadhesive force of PU/PTFE clutches as compared with PU/PI and PU/PU clutches. The high performance of the symmetric PU/PU clutch and PU/PI asymmetric clutch should be ascribed to the combination of the electrostatic attraction and the intrinsic H-bonding. And the intrinsic charge characteristics of the dielectric materials also contribute to the generated electroadhesive forces in the asymmetric clutches.

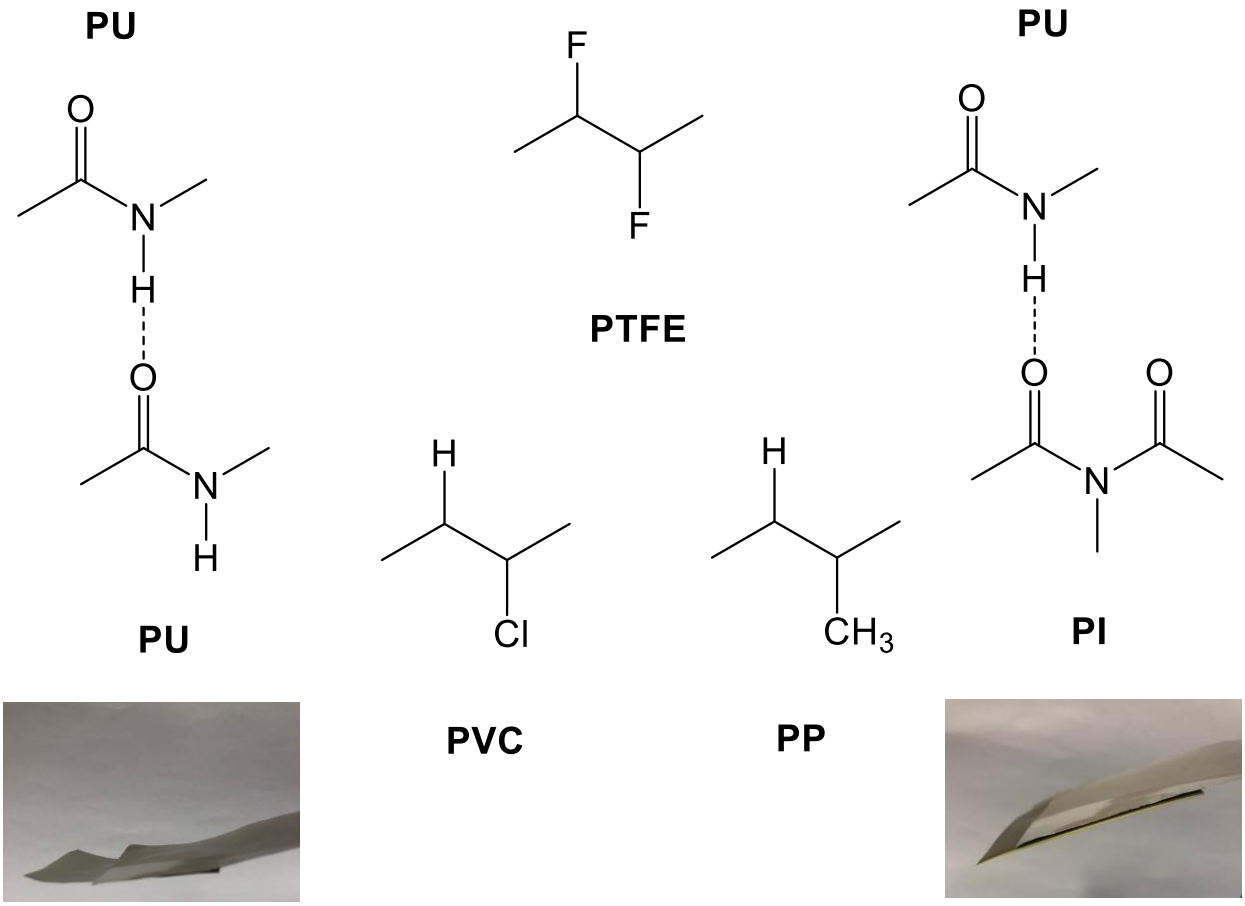

Fig 4.11 Chemical structures of the repeating units of PU, PI and PTFE and their adhesive behaviours based on H-bonding

4.3.5 Performance of asymmetric PU/PI clutches

Based on the preliminary study on the asymmetric clutches, PU(N)/PI(P) clutch exhibits the highest adhesive shear stress of 186.24 ± 10.12 kPa at 500 V and in this part more detailed clutch performance including the relationships between the external voltage,

dielectric thickness, overlapping area and the electroadhesive force, as well as the response time will be systematically investigated.

4.3.5.1 t-F relationship

Firstly, two asymmetric clutches with an identical total dielectric thickness of 75 μm were prepared with the combination of 50 μm PU, 25 μm PI and 25 μm PU, 50 μm PI, which were short for PU50PI25 and PU25PI50. Both clutches were activated at 500 V with overlapping areas of 5 cm^2. The PU50PI25 clutch could afford an electroadhesive force of 39.42 ± 2.64 N, while a holding force of 89.70 ± 3.46 N could be achieved by the PU25PI50 clutch (see Fig 4.12). This result indicates that reducing the thickness of the PU layer may be more effective to the improve the electroadhesive force. Asymmetric clutches with different thickness of PU layers and a PI film of 5 μm (PUXPI5, X is the thickness of PU layers, μm) have been tested as well. The overlapping area was also 5 cm^2 and the applied voltage was reduced to 300 V considering the relatively small dielectric thickness.

Clutches made from a PU film with a fixed thickness of 25 μm and PI films with variations in thickness ((PU25PIY, Y is the thickness of PI layers, μm)) have also been prepared and measured at the same condition. The actual thicknesses of the blade coated PU45, PU35 and PU25 were 47.60 ± 0.89, 36.80 ± 0.45 and 26.20 ± 1.79 respectively. All PI films were commercially available with standard deviations lower than ± 0.10 μm

in thickness. The results are shown in Fig 4.13. The electroadhesive force increases with the decrease of the dielectric thickness of PU and/or PI layers and a best performance of 98.65 ± 7.72 N (197.30 ± 15.44 kPa) at 300 V could be achieved by the PU25PI25 clutch, which is much higher than the previously reported values (23.8 kPa at 320 V).[30] The PU25PI25 clutch also exhibit a better performance than the PU35PI15 clutch. Reducing the dielectric thickness, especially the PU part, turns out to be an effective method to improve the performance of the asymmetric clutches.

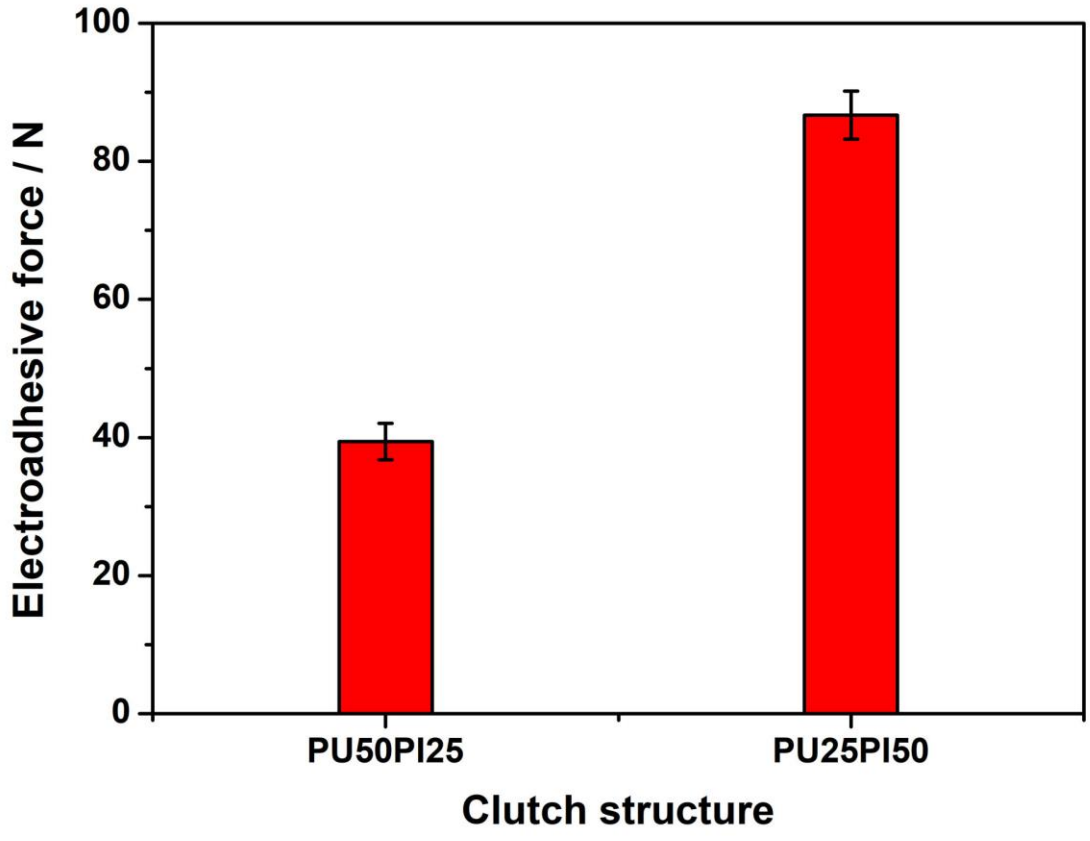

Fig 4.12 Electroadhesive forces of PU50PI25 and PU25PI50 clutches

Table 4.4 Summary of the electroadhesive force with different dielectric thickness (E = 300 V, A = 5 cm^2)

Thickness / μm	PU45PI5	PU35PI5	PU25PI5	PU25PI10	PU25PI25	PU25PI50
$\bar{F}$ / N	41.93	52.24	98.65	89.15	58.40	33.10
STD / N	4.37	0.84	7.72	4.39	4.94	3.23

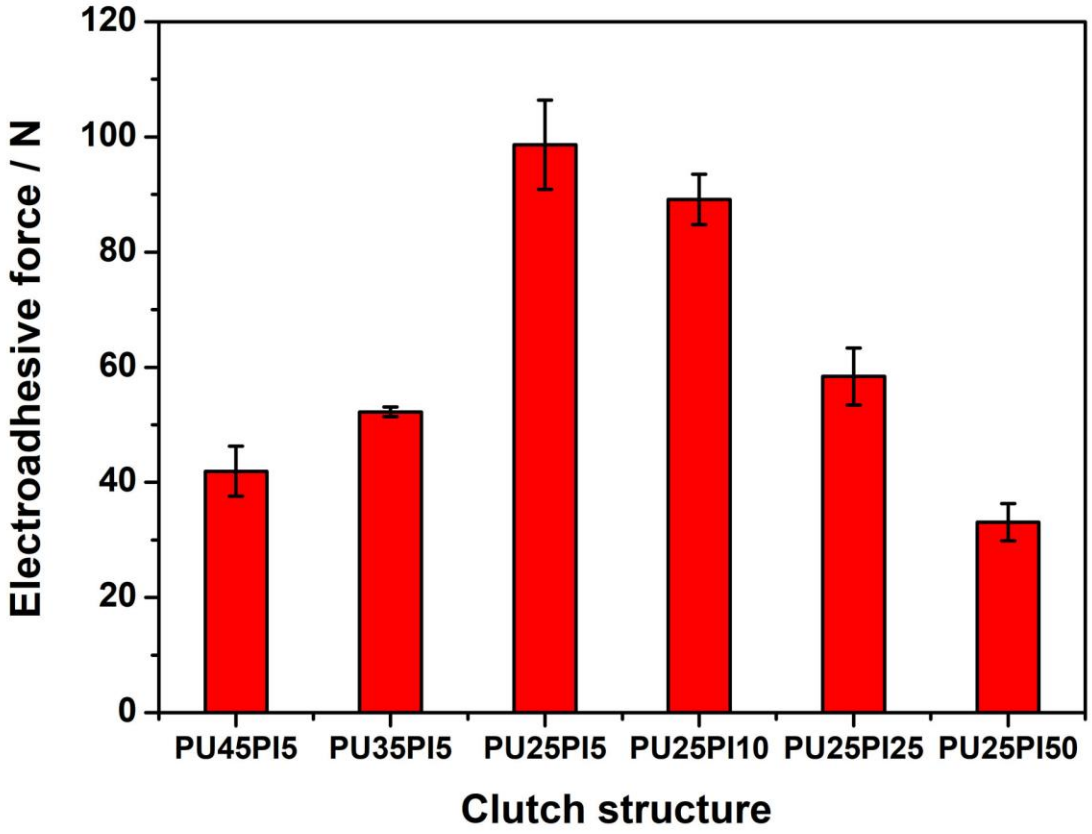

Fig 4.13 Electroadhesive forces of clutches with different thickness of PI and PU

4.3.5.2 V-F relationship

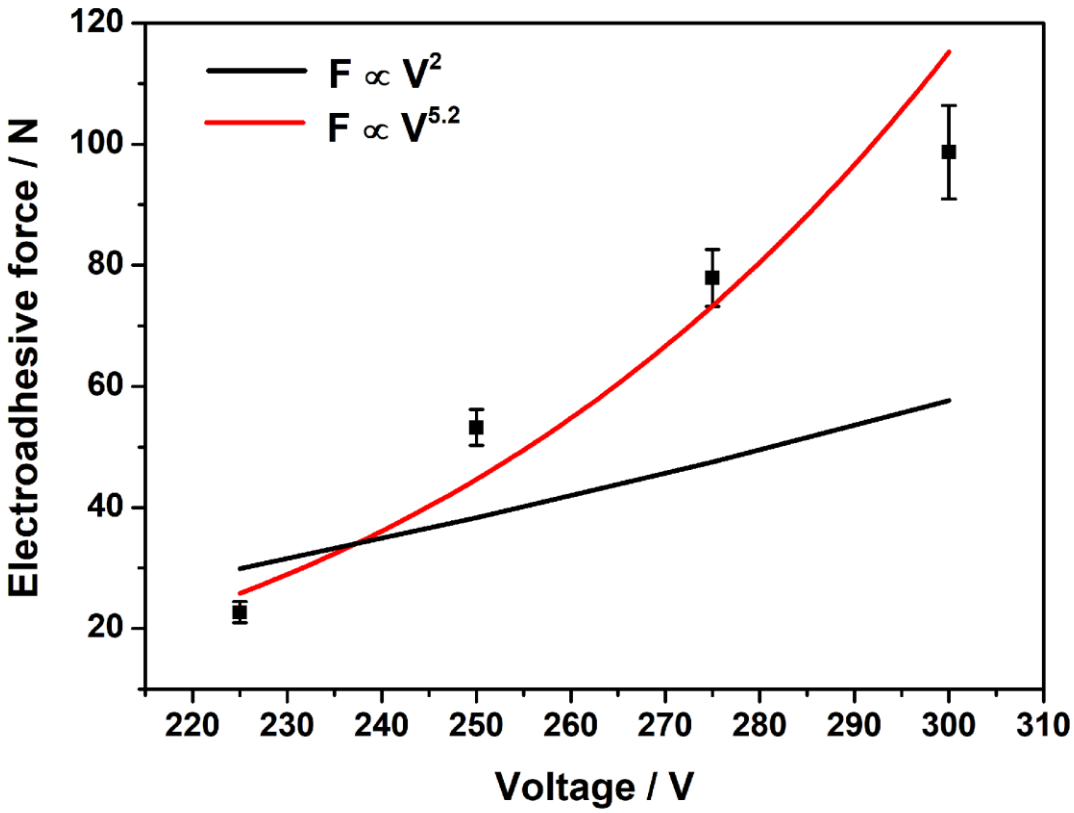

Fig 4.14 Electroadhesive forces of the clutches with different applied voltages ($F = 2.64 \times 10^{-11} V^{5.2}$, $R^2 = 0.93$; $F = 4.48 \times 10^{-3} V^2$, $R^2 < 0.1$)

To evaluate the V-F relationship, the asymmetric clutch exhibits the best performance was used which consisted of a 5-μm PI and a 25-μm PU layer. The overlapping area was also set at 5 cm^2. The clutch could response at 225 V with an electroadhesive force of 22.70 ± 1.74 N and provide a holding force of 98.65 ± 7.72 N (or shear stress of 197.30 ± 15.44 kPa) at 300 V. The corresponding data are summarized in Table 4.5 and the results are demonstrated in Fig 4.14 with fitted curves. The fitting results show that the

electroadhesive force increases as $V^{5.2}$ (R^2 = 0.93), which is much higher than the expected V^2.[31,32] The fitting result is similar with the PVDF-FS based symmetric clutch, in which F is proportional to $V^{4.7}$. The dominant reason should also be the elimination of air gaps between the electroadhesive pads under higher external voltages.[30] The changes in the physical properties of the electroadhesive pads under high electrical field strength the charge accumulation are also likely to result in the large shear force.

Table 4.5 Summary of the electroadhesive force of PU25PI5 under different external voltages (A = 5 cm^2)

Voltage / V	225	250	275	300
$\overline{F}$ / N	22.70	53.22	77.89	98.65
STD / N	1.74	1.74	4.70	7.72

4.3.5.3 A-F relationship

The relationship between the overlapping area and the produced shear force was studied at a fixed working voltage of 250 V and a clutch structure of PU25PI5. The data are summarized in Table 4.6 and the results are demonstrated in Fig 4.15. The slope of the linear-fitted curve is calculated to be 11.17 N/cm^2 (111.7 kPa) with R^2 = 0.99, suggesting an excellent linear relationship between the generated electroadhesive and the overlapping area.

Table 4.6 Summary of the electroadhesive force of PU25PI5 with different overlapping areas (E = 250 V)

A / cm^2	1	2	3	4	5
$\bar{F}$ / N	10.64	22.86	32.49	42.93	53.22
STD / N	0.89	0.59	4.14	3.49	2.96

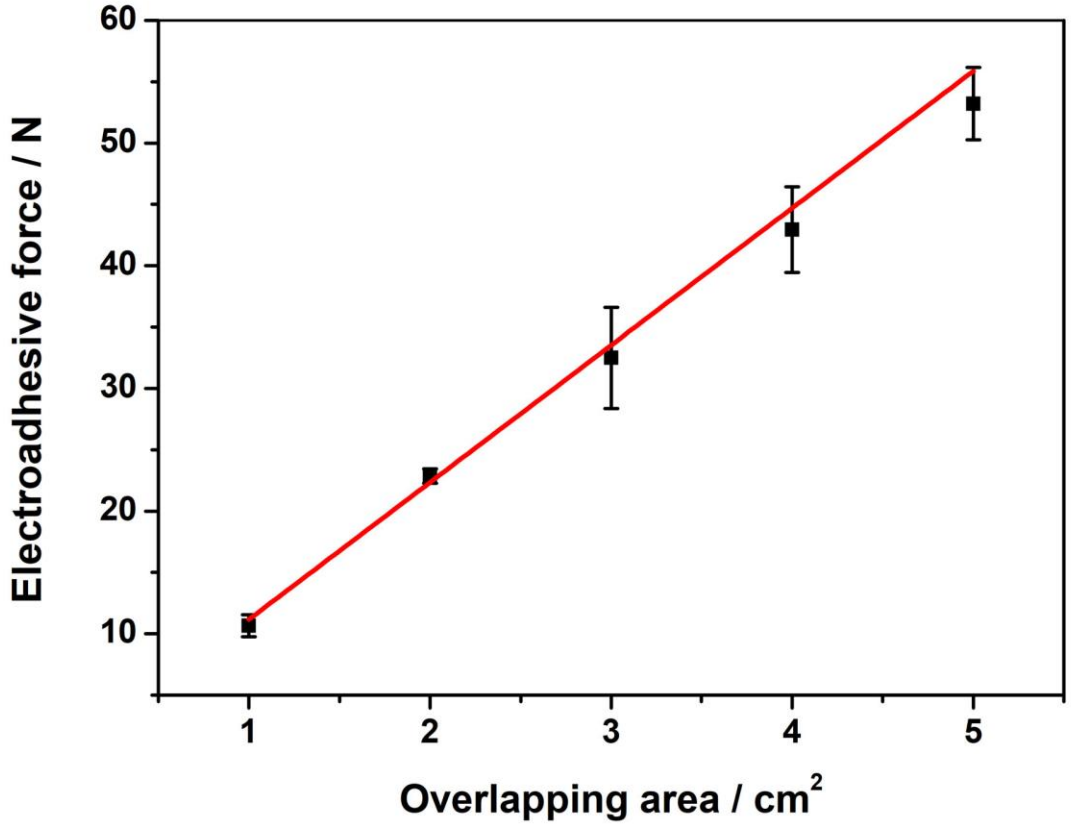

Fig 4.15 Relationship between the overlapping area and electroadhesive force (F = 11.17A, R^2 = 0.99)

4.3.5.4 Response time

The measurement method for the engage time is the same as the symmetric PVDF-FS clutches. The PU25PI5 clutch was used for the engage time measurement and the applied voltage was 250 V. The engage time measured is 20.2 ± 2.6 ms, which is comparable with symmetric clutch (25.3 ± 1.2 ms) and the literatures (~20 ms)[30,32] and a typical picture is shown in Fig 4.16. The time duration between A point and B point is calculated as the engage time where A is the initial transition point of the electrical field and B is the starting point of the generated force.

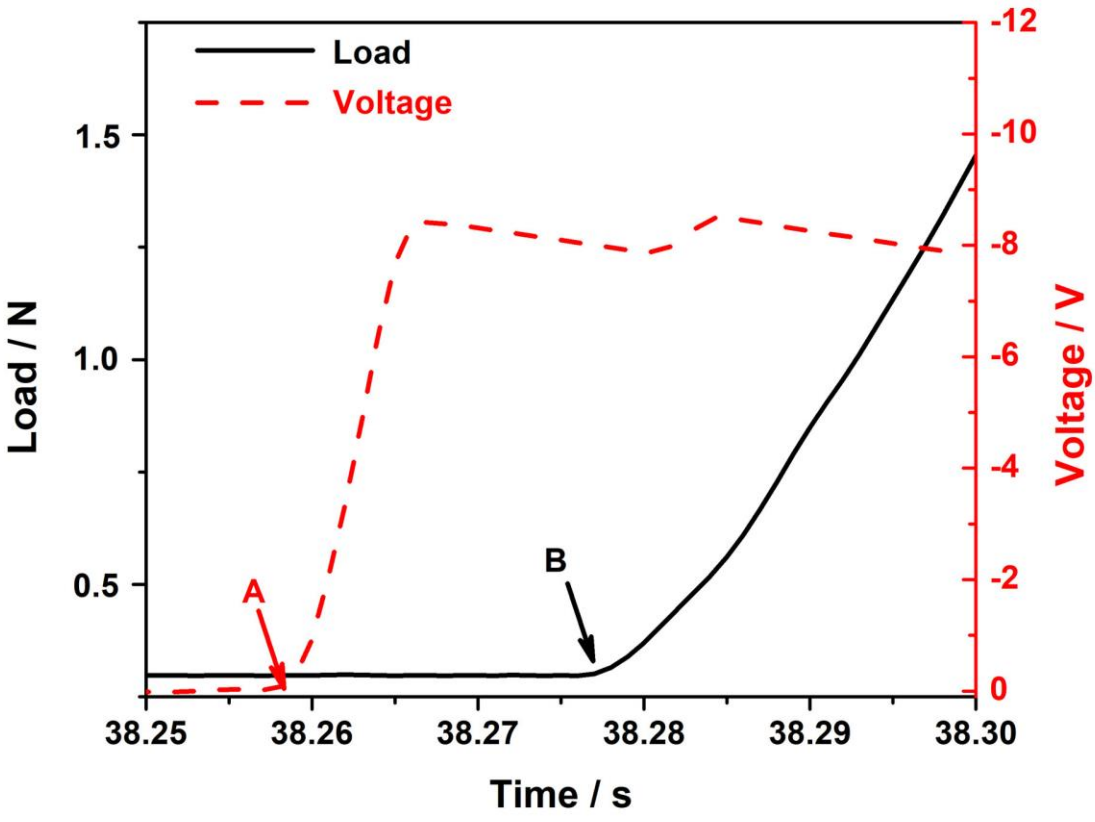

Fig 4.16 Engage time of the PU25PI5 clutch

However, the release time measured with the same clutch at a constant load of ~40 N and the overlapping area is 5 cm^2 is 926.8 ± 124.6 s, which means the clutch was still engaged even after the voltage was removed for ~ 15 min. This value is several-order higher than the symmetric PVDF-FS clutch (~ 324 ms) and the literatures (~ 15 ms).[30,32] The reason should be ascribe to the aforementioned H-bonding between PU and PI. The typical picture is given in Fig 4.17, where A is the point when the power source is switched off and B is the point when the two electroadhesive pads separate from each other.

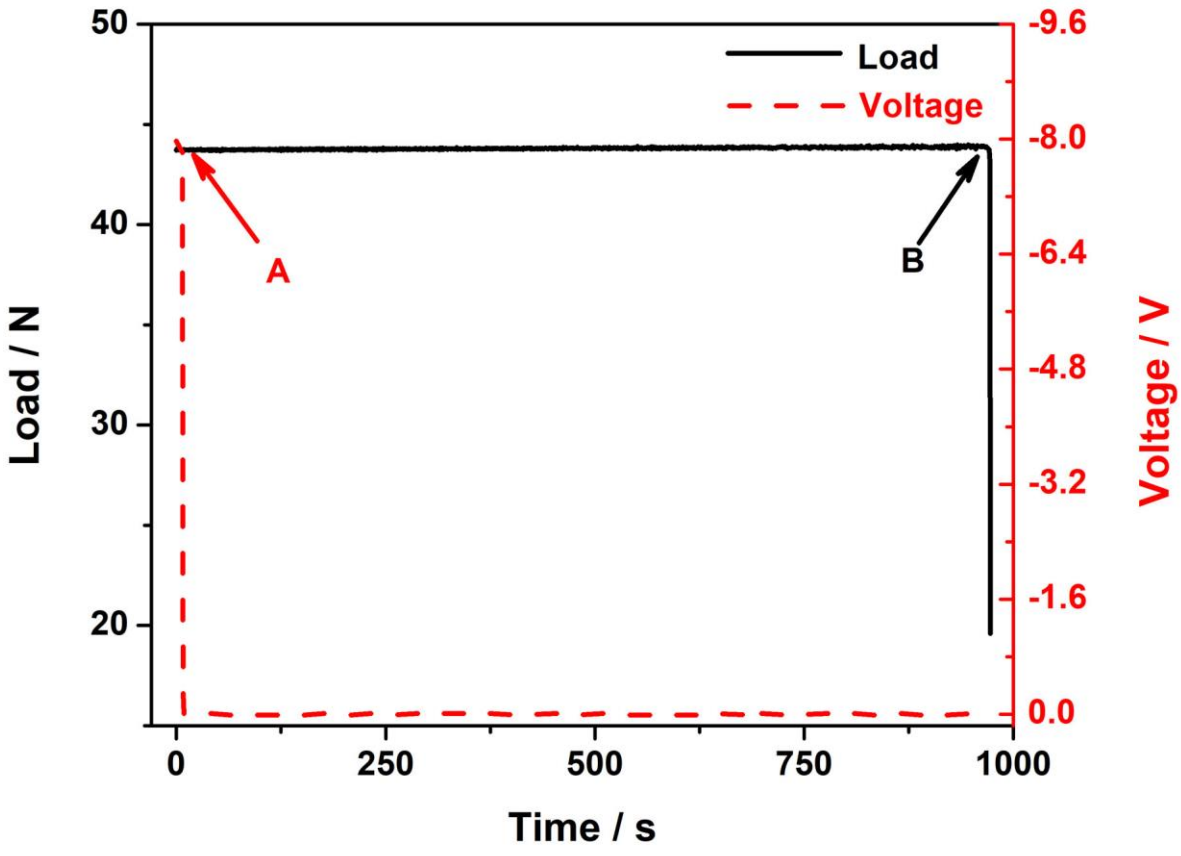

Fig 4.17 Release time of the PU25PI5 clutch

4.4 Conclusion and future works

Dielectric materials of opposite electron affinity may enhance the performance of current symmetric clutches by boosting the electrostatic attraction between the two surfaces in an asymmetric clutch. Hence, in Chapter 4, the first batch of asymmetric electroadhesive clutches made from PU, PI and/or PTFE is proposed, fabricated and evaluated. The effect of the charge characteristics of the dielectric materials on the clutch performance is investigated. A shear stress of 197.30 ± 15.44 kPa is generated at 300 V in around 20 ms by the asymmetric clutch made from polyurethane and polyimide active dielectric pads. When the induced charges match the charge characteristics of dielectric materials, it will give a boost to the final holding forces. For PU/PI clutches, reducing the dielectric thickness of PU and/or PU, increasing the working voltage and the overlapping area could effectively improve the generated electroadhesive force. Similar to the symmetric PVDF-FS clutch, the influence of the applied voltage turns out to be more significant among the three factors. In addition, the hydrogen bonds at the interface are found to contribute to the high electroadhesive stress. This chapter demonstrates an effective asymmetric and multi-mechanism strategy to develop high performance electroadhesive clutches with diverse materials selection. The high performance of the asymmetric PU/PI clutch originates from the integration of interfacial H-bonds, electrostatic attraction and charge characteristics of the dielectric materials. The release time is longer than 15 mins due to the abundant hydrogen bonds at the PU/PI interface. The long release time indicates it is necessary to develop the direct method where time and force are measured at the same time. The high performance of the asymmetric PU/PI clutch originates from the

integration of interfacial H-bonds, electrostatic attraction and charge characteristics of the dielectric materials. The long release time may be benefit for long-term used of clutches with reduced power consumption by intermittent or pulsed power supply, though it is undesired in fast-response application such as exoskeleton and haptic systems.

Future works could be focused on reducing the working voltage of the asymmetric clutches with the use of high-*k* materials with opposite charge affinity. Other adhesion mechanisms and material systems could be developed and incorporated into the asymmetric clutches. High-*k* materials with tendency of loss and gain electrons could also be developed.

References

[1] J. Yan, Z. Fan, W. Sun, G. Ning, T. Wei, Q. Zhang, R. Zhang, L. Zhi, F. Wei, *Adv. Funct. Mater.* **2012**, *22*, 2632.

[2] S. Zhu, L. Li, J. Liu, H. Wang, T. Wang, Y. Zhang, L. Zhang, R. S. Ruoff, F. Dong, *ACS Nano* **2018**, *12*, 1033.

[3] Y. Li, J. Xu, T. Feng, Q. Yao, J. Xie, H. Xia, *Adv. Funct. Mater.* **2017**, *27*, 1606728.

[4] L. Hou, Y. Shi, C. Wu, Y. Zhang, Y. Ma, X. Sun, J. Sun, X. Zhang, C. Yuan, *Adv. Funct. Mater.* **2018**, *28*, 1705921.

[5] X.-G. Yang, T. Liu, Y. Gao, S. Ge, Y. Leng, D. Wang, C.-Y. Wang, *Joule* **2019**, *3*, 3002.

[6] D. Koo, B. Kwon, J. Lee, K. T. Lee, *Chem. Commun.* **2019**, *55*, 9637.

[7] J. Zheng, W. Deng, Z. Hu, Z. Zhuo, F. Liu, H. Chen, Y. Lin, W. Yang, K. Amine, R. Li, J. Lu, F. Pan, *ACS Energy Lett.* **2018**, *3*, 65.

[8] B. Shin, J. Ha, M. Lee, K. Park, G. H. Park, T. H. Choi, K.-J. Cho, H.-Y. Kim, *Sci. Robot.* **2018**, *3*, eaar2629.

[9] Z. Zhang, L. Wen, L. Jiang, *Chem. Soc. Rev.* **2018**, *47*, 322.

[10] I. G. Baek, M. S. Lee, S. Sco, M. J. Lee, D. H. Seo, D.-S. Suh, J. C. Park, S. O. Park, H. S. Kim, I. K. Yoo, U.-I. Chung, J. T. Moon, in *IEDM Tech. Dig. IEEE Int. Electron Devices Meet. 2004.*, IEEE, **2004**, pp. 587–590.

[11] M.-J. Lee, C. B. Lee, D. Lee, S. R. Lee, M. Chang, J. H. Hur, Y.-B. Kim, C.-J. Kim,

D. H. Seo, S. Seo, U.-I. Chung, I.-K. Yoo, K. Kim, *Nat. Mater.* **2011**, *10*, 625.

[12] A. Yu, Y. Zhu, W. Wang, J. Zhai, *Adv. Funct. Mater.* **2019**, *29*, 1900098.

[13] B. Cheng, J. Ma, G. Li, S. Bai, Q. Xu, X. Cui, L. Cheng, Y. Qin, Z. L. Wang, *Adv. Energy Mater.* **2020**, *10*, 2000827.

[14] R. Lei, Y. Shi, Y. Ding, J. Nie, S. Li, F. Wang, H. Zhai, X. Chen, Z. L. Wang, *Energy Environ. Sci.* **2020**, *13*, 2178.

[15] Z. Ren, Z. Wang, Z. Liu, L. Wang, H. Guo, L. Li, S. Li, X. Chen, W. Tang, Z. L. Wang, *Adv. Energy Mater.* **2020**, DOI 10.1002/aenm.202001770.

[16] Z.-S. Wu, W. Ren, D.-W. Wang, F. Li, B. Liu, H.-M. Cheng, *ACS Nano* **2010**, *4*, 5835.

[17] H. Zou, Y. Zhang, L. Guo, P. Wang, X. He, G. Dai, H. Zheng, C. Chen, A. C. Wang, C. Xu, Z. L. Wang, *Nat. Commun.* **2019**, *10*, 1427.

[18] S. Liu, W. Zheng, B. Yang, X. Tao, *Nano Energy* **2018**, *53*, 383.

[19] T. Nakamura, A. Yamamoto, *ROBOMECH J.* **2017**, *4*, 18.

[20] X. Chen, H. Huang, X. Shu, S. Liu, J. Zhao, *RSC Adv.* **2017**, *7*, 1956.

[21] G. Qian, M. Hu, S. Zhang, M. Wang, C. Chen, J. Yao, *Polymers.* **2020**, *12*, 442.

[22] C. Pan, J. Zhang, K. Kou, Y. Zhang, G. Wu, *Int. J. Heat Mass Transf.* **2018**, *120*, 1.

[23] T. S. Sasikala, M. T. Sebastian, *Ceram. Int.* **2016**, *42*, 7551.

[24] T. Chen, J. Qiu, K. Zhu, J. Li, *Mater. Des.* **2016**, *90*, 1069.

[25] Y. Zhao, J.-W. Zha, L.-J. Yin, S.-T. Li, Y.-Q. Wen, Z.-M. Dang, *Polymer.* **2018**, *149*,

39.

[26] E. Ylgor, I. Ylgor, E. Yurtsever, *Polymer.* **2002**, *43*, 6551.

[27] J. Mattia, P. Painter, *Macromolecules* **2007**, *40*, 1546.

[28] Z. Jiang, M. O. G. Nayeem, K. Fukuda, S. Ding, H. Jin, T. Yokota, D. Inoue, D. Hashizume, T. Someya, *Adv. Mater.* **2019**, *31*, 1903446.

[29] H. R. Brown, *Annu. Rev. Mater. Sci.* **1991**, *21*, 463.

[30] S. B. Diller, S. H. Collins, C. Majidi, *J. Intell. Mater. Syst. Struct.* **2018**, *29*, 3804.

[31] S. Diller, C. Majidi, S. H. Collins, in *2016 IEEE Int. Conf. Robot. Autom.*, IEEE, **2016**, pp. 682–689.

[32] V. Ramachandran, J. Shintake, D. Floreano, *Adv. Mater. Technol.* **2019**, *4*, 1800313.

Chapter 5. Tuning dielectric properties through *in-situ* thermal reduction of GO in P(VDF-TrFE-CFE) matrix

5.1 Introduction

The experimental results of the P(VDF-TrFE-CFE) terpolymers based symmetric clutches (Chapter 3) show that the symmetric clutch could response at 80 V and the electroadhesive force is proportional to $V^{4.7}$, which deviates from the square relationship described in a classical model (Equation 2.1 in Chapter 2). High-*k* materials with dielectric constant over 1000 (specifically $48.2 * 2^{4.7} \approx 1253$) should be developed if the working voltage is expected to be halved.

Commonly used strategies for developing high-*k* materials mainly includes molecular modification,[1–3] doping of high-*k* ceramics[4–6] and conductive fillers.[7–11] However, molecular modification could only increase the dielectric constant several times, and doping of high-k materials could generally increase one-order at a large doping ratio (generally ~ 50 wt%). Doping with a few amounts of conductive fillers (generally below 5 wt%) turns out to be effective method to improve the dielectric constant several orders especially at low frequency range, where interfacial polarization plays a dominant role.

A few examples of special high-*k* systems based on dipolar polarization have also been reported.[12] Metal-based nanomaterials[13,14], and carbon-based materials (*e.g.* 0D carbon black,[15,16] 1D carbon nanotubes (CNT),[17,18] 2D graphene[19,20] and 3D graphene aerogel[21]) are generally used conductive materials for developing high-*k* polymer matrix composites (PMCs). Carbon-based materials have shown much better compatibility with polymers due to the residual hydrophilic groups and relatively low modulus as compared with metals.[7,17,22] Graphene with 2D flake-structure and anisotropic electrical properties make it promising as conductive fillers in high-*k* PMCs.[7,23] However, graphene (especially single-layer or few-layer graphene) tends to be aggregated and stacked due to the large surface free energy and the aggregation of graphene will decrease the dielectric constant and increase the dielectric loss.[24] GO which could be uniformly and homogeneously dispersed into polymer matrixes have widely used followed by *in situ* thermal or chemical reduction to obtain high-*k* but low loss reduced graphene oxide (RGO) or partially reduced graphene oxide (PRGO)-based PMCs.[9,25–27]

In this chapter, PRGO/PVDF terpolymer composites with tuneable dielectric properties by varying the thermal reduction times will be prepared for the first time. The dielectric and chemical properties of the composites will be fully characterized. The relationship between the dielectric properties (namely dielectric constant and loss) and reduction time and the doping ratio of the GO will be investigated. The preliminary study of the applications in electroadhesive clutches and clutch-type pressure sensors will also be conducted.

5.2 Experimental

5.2.1 Materials selection

PVDF-TrFE-CFE terpolymer has shown excellent dielectric properties as demonstrated in Chapter 3. GO could be easily and evenly dispersed into the polymer matrix by simply dissolved in organic solvents. The agglomeration of GO during the filming process will be greatly suppressed due to the high viscosity of the polymer solution.[7,24]

The P(VDF-TrFE-CFE) terpolymers (PIEZOTECH ® RT-FS) (PVDF-FS) were purchased form Arkema (French) and were used without any purification. The molar ratio of the VDF, TrFE and CFE was 64.8%, 27.4% and 7.8% respectively. GO was purchased from Times Nano (Jiangsu). PVC tape (Scotch, 65 μm) and Al foil (Glad, 15 μm) were used directly. Silver paste (sigma) was diluted with small amount of isopropyl alcohol (IPA) to adjust the viscosity before screen printing. Solvents including acetone, ethanol, tetrahydrofuran (THF), N, N-Dimethylformamide (DMF) and butyl acetate (BA) were purchased from TCI chemicals.

5.2.1.1 General procedures for the sample preparation

Taking 4 wt % GO/PVDF-FS composite as an example. 40 mg GO was firstly dissolved in 10 mL BA solution and the mixture was stirred for at least 4 hours to obtain brown GO solution. Then 1.00 g PVDF-FS powder was added into the GO solution and stirred for about 6 hours to give 4 wt % GO/PVDF-FS solution. Then blade coating on Al foil was

conducted on a *k* control coater with profile bars. The film was dried at 60 ^{o}C under vacuum for 2 hours to remove the solvents, followed by thermally reduction at 120 ^{o}C, which is a little bit lower than the melting point of PVDF-FS (~125 ^{o}C) for different times. For other doping ratio GO composites, the only difference is the weight of GO and it should be noticed that the GO must be dispersed first otherwise it could not be successfully dispersed with the increased solution viscosity. PVC tape was attached on the backside to protect the Al layers and improve the mechanical strength of the pads.

Pure RGO samples have also been prepared for comparison and typically 100 μL GO solution (10 mg/mL in BA) was drop on a clean glass substrate and then dried and thermal-reduced at the same condition with GO/PVDF-FS samples.

5.2.2 Materials characterization

The chemical properties and crystallinity of the RGO, GO/PVDF-FS and RGO/PVDF-FS were characterized by attenuated total reflection Fourier-transform infrared spectroscopy (ATR-FTIR), Raman spectrum and X-Ray diffraction (XRD). The dielectric properties including the dielectric constant and loss tangent at different frequencies were recorded by the impedance analyzer.

FTIR spectrum was measured on a Perkin spectrum 100 FTIR. XRD data were collected on a Rigaku SmartLab 9kW at 293 K. The Raman spectrum was recorded on a BaySpec's

Nomadic Raman microscope (λ_{exc} = 532 nm). The Keysight E4980A precision impedance analyzer was used to analysis the dielectric properties. The surface roughness of the dielectric layer and electrode was measured on a ZYGO laser interferometric non-contact profile system with sample size of 4 cm^2. Scanning electron microscope (SEM) images were taken on a JEOL Model JSM-6490. The resistivity of the electrode was measured on a ST-2258A four-probe tester. The current and voltage were measured on a Keithley 2400.

5.2.3 Pressure-current measurement

The testing system for the pressure-current relationship of the clutch-type device is demonstrated in Fig 5.1. The contact area of the load cell and sample is 1 cm^2. The clutch was fixed on the sample holder by PVC tapes to minimize the error caused by the move of the samples under load and unload process. And gaps are supposed to be exist due to the two pads are not adhered. The pressure was given by the Instron load cell with a constant speed of 3 mm/min and hold for 10 s at maximum load. The initial distance of the load cell and clutch is about 1 mm and may have some deviations for different tests. The constant direct voltage was provided by the Keithley 2400 and the current were also recorded at the same time. The peak current and pressure were recorded.

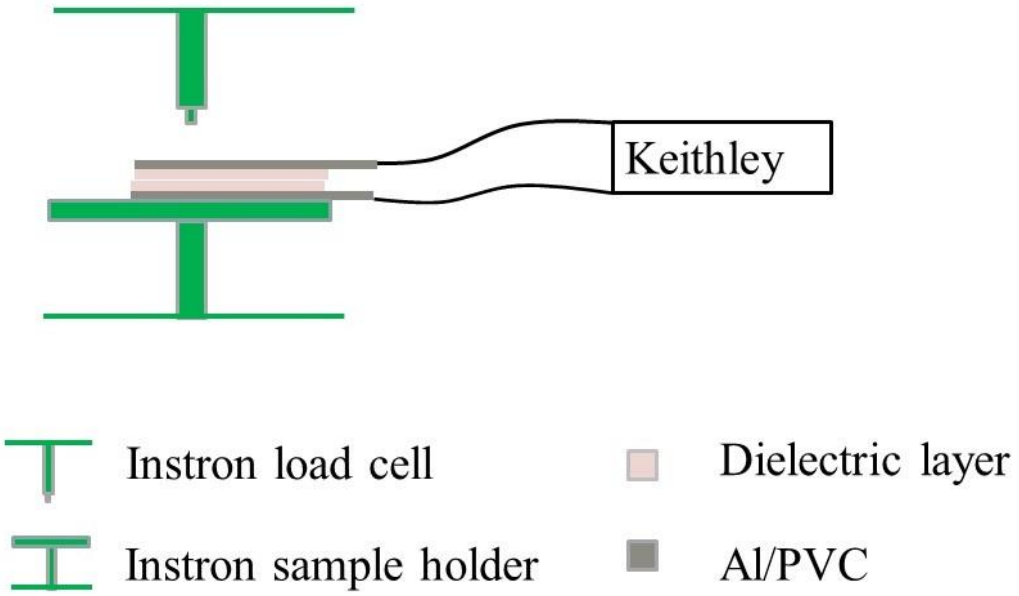

Fig 5.1 Schematic illustration of the test system

5.3 Results and discussion

5.3.1 Dielectric properties

5.3.1.1 Dielectric properties of PVDF-FS composites with different RGO concentration

The dielectric constant and dielectric loss of the PVDF-FS with different doping ratio have been firstly evaluated. All samples were thermally reduced under vacuum for 14 days. The results are shown in Fig 5.2 and the corresponding data are summarized in Table 5.1. 4 wt% PRGO/PVDF-FS exhibits a dielectric constant as high as 1480 with a

loss tangent of 0.283 at 100 Hz. Both dielectric constant and the dielectric loss increases significantly at low frequency range with the doping of RGO, which arises from the interfacial polarization between the conductive fillers and polymer matrixes.[28,29] The dielectric constant decreases dramatically with the frequency increases for all RGO doped samples and this is also typical in interfacial polarizations.[28,29] The dielectric loss of samples with RGO concentration below 8 wt% decreases firstly due to the interfacial polarizations are dominant at low frequency range and then the loss increases at high frequency area where electronic polarizations of the ferroelectric polymer matrixes play important roles.[30–32] While at high doping ratios (≥10 wt%), the dielectric loss exhibit a monotone decreasing as the frequency increases.

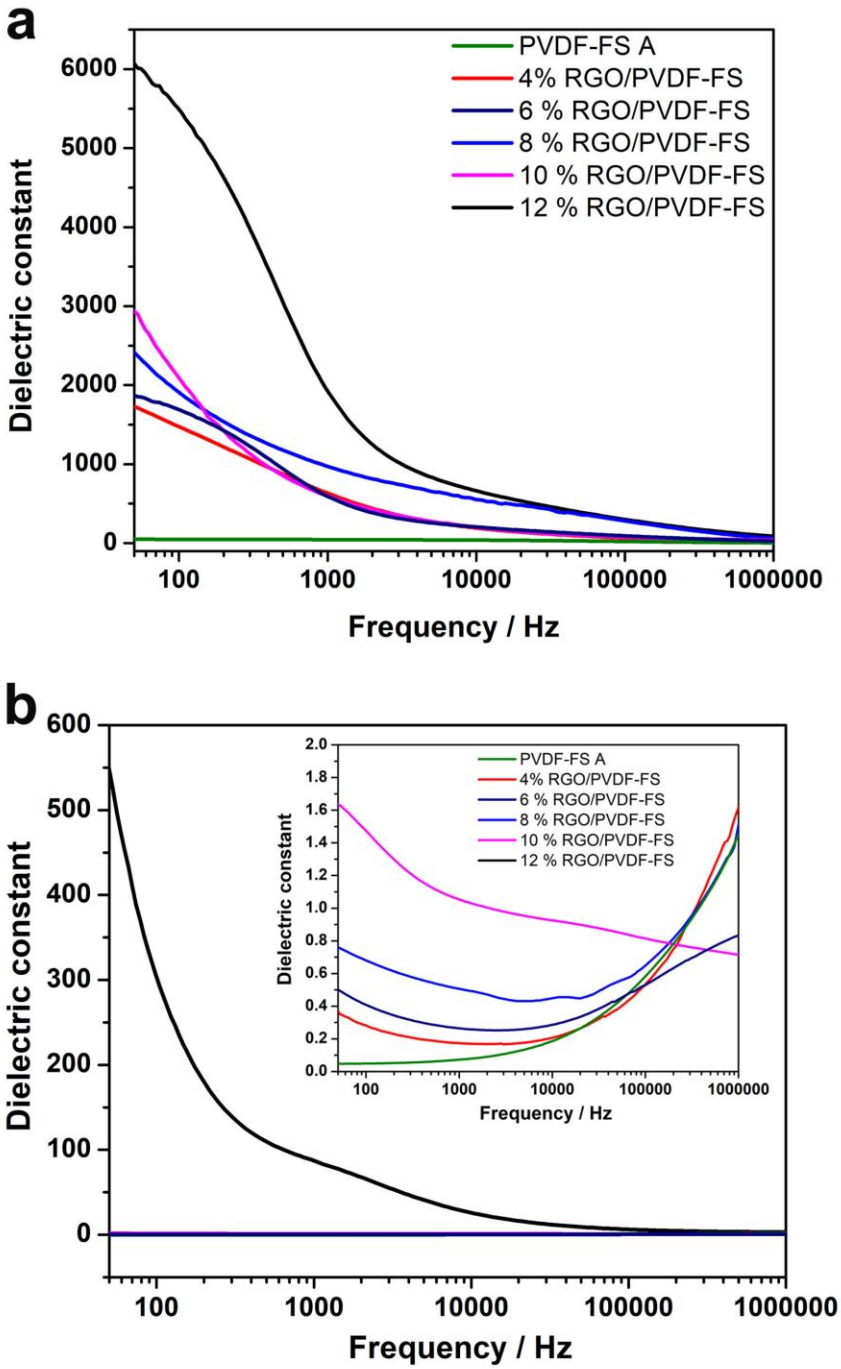

Fig 5.2 Frequency dependent relative dielectric constant and loss tangent of the RGO/PVDF-FS composites

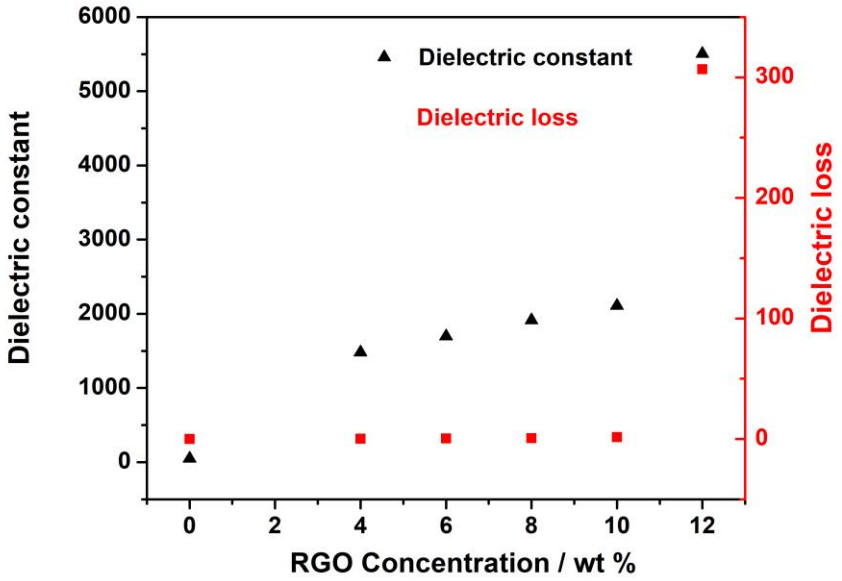

Fig 5.3 Frequency dependent relative dielectric constant and loss tangent of the RGO/PVDF-FS composites at 100 Hz

The relative dielectric constant reaches ~ 5500 at 100 Hz at RGO concentration of 12 wt% though the tan δ is higher than 300. Typical percolation transition could be found at 12 wt% RGO,[7,33] and the resistivity of the 12 wt% RGO/PVDF-FS was measured to be 61.98 ± 3.39 kΩ·cm/□, indicating that conductive pathway should formed at the high doping ratio. The resistivity of the 10 wt% RGO/PVDF-FS were also measured with a value of 2.58 ± 0.07 MΩ·cm/□, while for other samples the resistivity could not be measured by the four-probe tester. The dielectric constants and dielectric losses at 100 Hz of the samples were displayed in Fig 5.3, which could give a more intuitive concept for the percolation transition. The dielectric constant and loss did not show significant change

from 4 wt% to 10 wt% and transitions could be found for both dielectric constant and dielectric loss between 10 wt% and 12 wt% RGO/PVDF-FS.

Table 5.1 Dielectric properties of PVDF-FS with different doping ratio of RGO at 100 Hz

	100 Hz	
	ε_r	**tan δ**
PVDF-FS (A)	48.2	0.048
4 wt% RGO/PVDF-FS	1480	0.283
6 wt% RGO/PVDF-FS	1696	0.410
8 wt% RGO/PVDF-FS	1916	0.682
10 wt% RGO/PVDF-FS	2108	1.477
12 wt% RGO/PVDF-FS	5506	306.6

5.3.1.2 Dielectric properties of 4 wt% RGO/PVDF-FS composites with different reduction time

The dielectric constant and loss as a function of reducing time of 4 wt% RGO/PVDF-FS were also recorded in Table 5.2. Day 0 refers to the samples dried at 60 ^{o}C under vacuum for 2 hours and Day 1-14 means the dried sample was thermally reduced at 120 ^{o}C under vacuum for corresponding times. The relationship between the reducing time and dielectric constant were shown in Fig 5.4 and the dielectric constant and loss of the

samples were almost the same for Day 12-14, indicating the GO were fully reduced after 12 days at the abovementioned condition. Mathematic fitting of the dielectric constant from Day 1 to Day 12 has also been conducted and the result shows a relationship of $\varepsilon_r = 95.2D + 448$, with a R^2 of 0.99 where D is the reduction days. The dielectric loss increase monotonously as reduction time increases due to the increase in the conductivity of RGO.[33,34] This result indicates that continuous change of dielectric properties in a certain range could be realized through the *in situ* thermal reduction of GO in PVDF-FS matrix by simply varying the reduction time. This is the first example of continuous regulation of dielectric properties, to the best of our knowledge. With higher reduction temperature, both dielectric constant and loss are expected to be increased with a shorter time is needed to reach the equilibrium, as demonstrated in previous researches the RGO were reduced at 180 ^{o}C or 200 ^{o}C for several hours.[9,25,27]

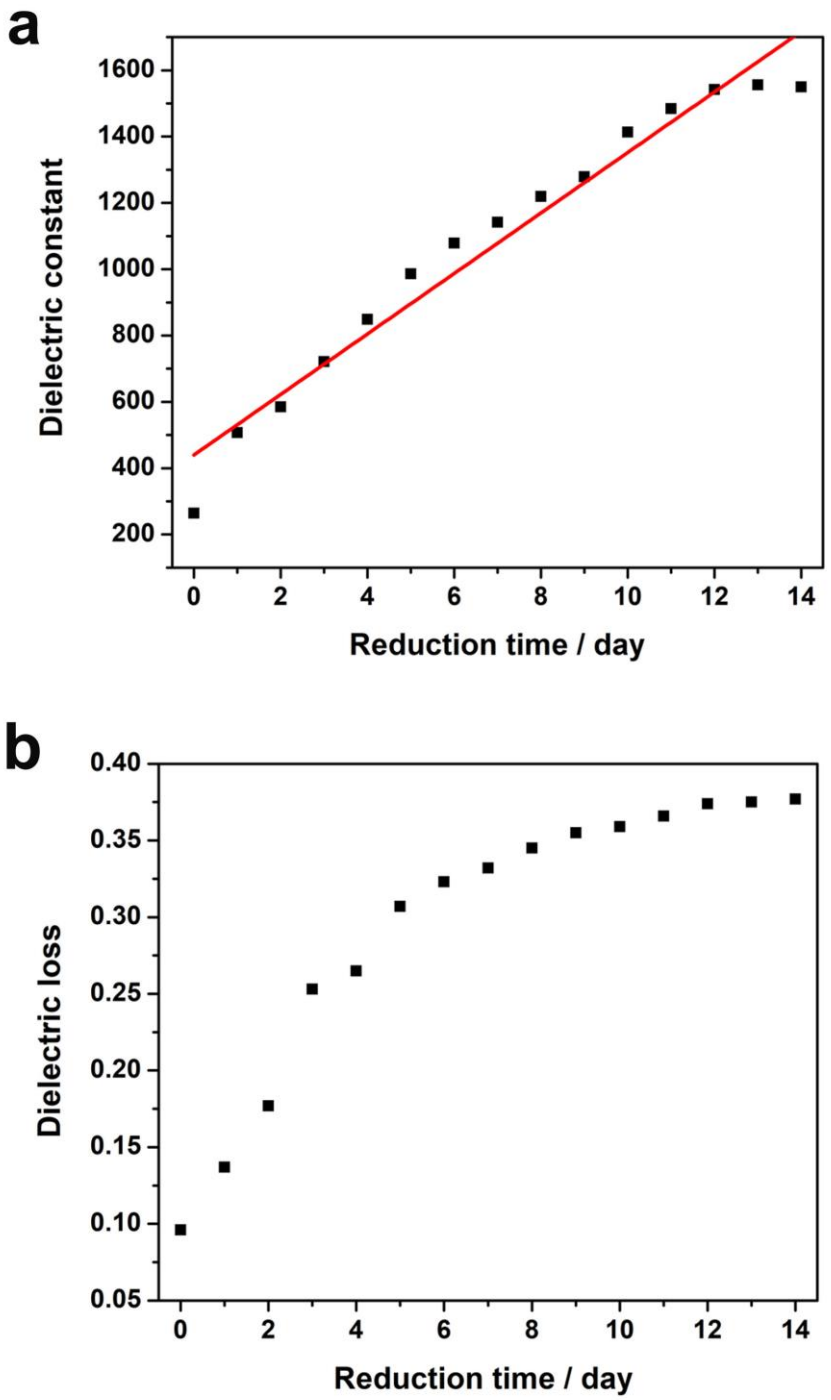

Fig 5.4 Reduction time dependent (a) relative dielectric constant (ε_r = 95.2D + 448, with a R^2 of 0.99) and (b) loss tangent of the 4 wt% RGO/PVDF-FS composites at 100 Hz

Table 5.2 Dielectric properties of 4 wt% RGO/PVDF-FS with different reduction times at 100 Hz

Day number	ε_r	tan δ
0	263.8	0.096
1	507.4	0.137
2	584.7	0.177
3	721.4	0.253
4	849.0	0.265
5	986.2	0.307
6	1079	0.323
7	1141	0.332
8	1219	0.345
9	1279	0.355
10	1413	0.359
11	1484	0.366
12	1542	0.374
13	1555	0.375
14	1550	0.377

5.3.2 Chemical properties

The FITR spectra of the 4 wt % GO/PVDF-FS and RGO/PVDF-FS are shown in Fig 5.5. Symmetric stretching of the all-trans (β phase) -CF_2 and -CH_2 vibration could be observed at 846 cm^{-1} and 1398 cm^{-1} respectively and the peak at 770 cm^{-1} should arise from the γ phase of the PVDF-FS.[35–37] These three peaks could be found for the annealed polymer, GO and RGO polymer composites and no peak shifts could be observed indicating there are no or very weak interaction between the conductive fillers and the polymer matrixes. In 4 wt% GO/PVDF-FS composites, two peaks at 2917 cm^{-1} and 2849 cm^{-1} could be found, which is typical peaks for C-H vibration from the -CHO groups of GO (see Fig 5.5b). And peaks at 1578 cm^{-1} and 1541 cm^{-1} should be assigned to the C=O from GO.[38] These four peaks could also observed at RGO/PVDF composites at the same wavenumbers with a lower intensities, indicating the oxygen-containing functional groups in GO were partially removed after the thermal treatment.

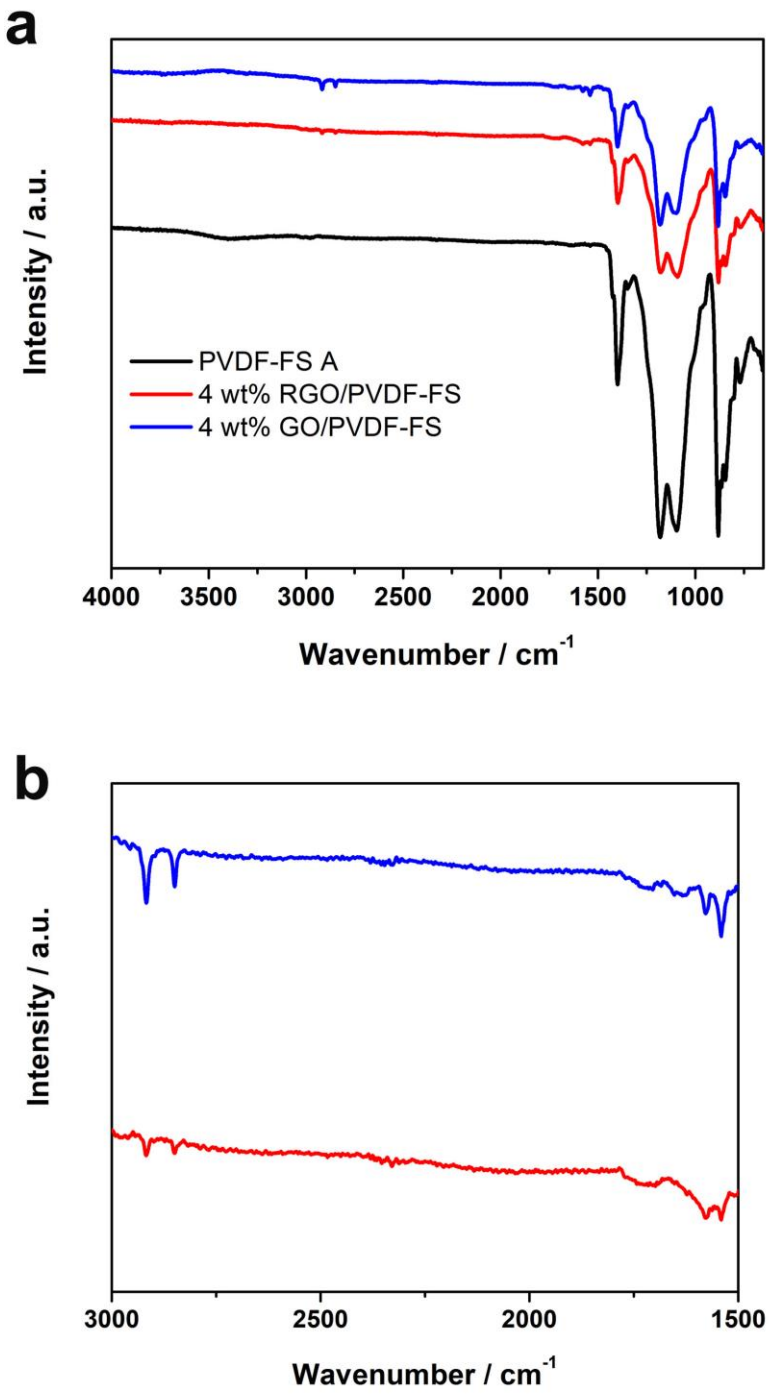

Fig 5.5 (a) FTIR spectra and (b) enlarged spectra of annealed PVDF-FS (PVDF-FS A), 4 wt% GO/PVDF and 4 wt% RGO/PVDF composites

The Raman spectra of the 4 wt % GO/PVDF-FS before and after reduction were also measured to characterize the reduction of GO, as shown in Fig 5.6. The D band at 1349 cm^{-1} of GP/PVDF-FS composite should be assigned to the breathing modes of the hexagonal rings, which is closely related to the edge defects.[38,39] The G band at 1599 cm^{-1} of GP/PVDF-FS composite should be assigned to the stretching of sp^2 carbons, which is related to the highly ordered graphite structures.[38,39] And the intensity ratio of D and G band (I_D/I_G) was calculated to be 0.90. After thermal reduction, the D band shift to 1354 cm^{-1} and G band shift to 1597 cm^{-1}, which is caused by the reduced domain size of sp^2 carbons. The I_D/I_G ratio of RGO also increases to 0.93 due to the restoration of sp^2 carbons after removal of oxygen-containing species.[27,38] The limited change in I_D/I_G ratio also indicates the relatively low degree of reduction. The broad and low peak at ~2700 cm^{-1} is assigned to the 2D band, indicating the GO and RGO are stacked as multilayers in the polymer matrixes.[39] And the brown films became dark after thermal reduction, as demonstrated in the photographs in Fig 5.6.

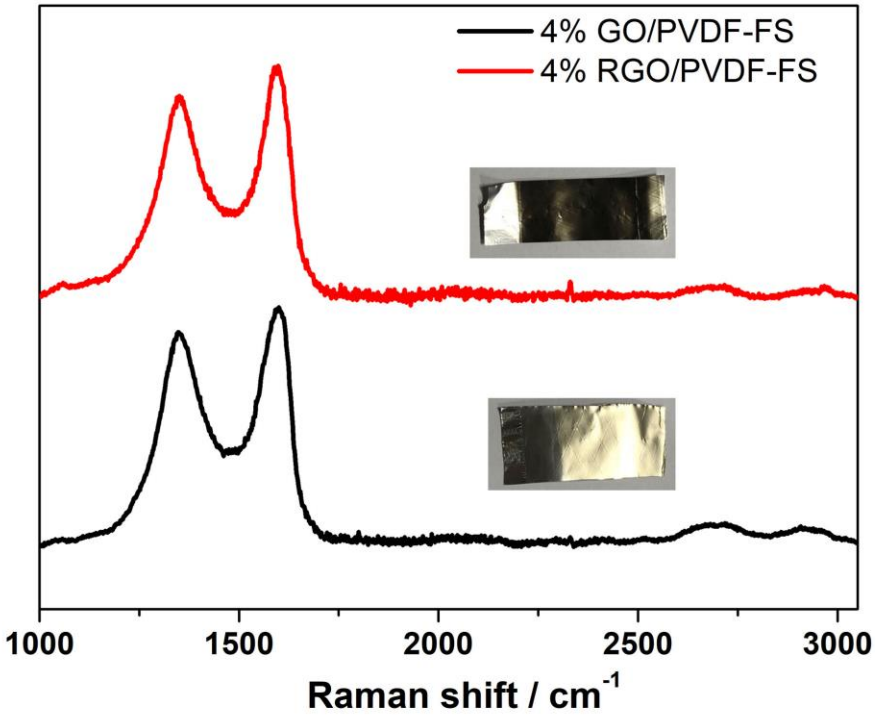

Fig 5.6 Raman spectra and photograph (insert) of 4 wt% GO/PVDF and 4 wt% RGO/PVDF composites

Table 5.3 Raman data of 4 wt% GO/PVDF-FS and R GO/PVDF-FS

	D band / cm^{-1}	**G band / cm^{-1}**	**I_D/I_G**
4% GO/ PVDF-FS	1349	1599	0.90
4% RGO/ PVDF-FS	1354	1597	0.94

The thermal reduction of GO is generally accompanied by the removal of oxygen-containing groups as gases (*e.g.* O_2, CO and CO_2) and is an exothermic reaction.[40,41] Reduction of GO is generally conducted at relatively high temperature (typically higher than 350 ^oC).[42] Considering the relative low reduction temperature and based on the results of FTIR and Raman spectra, it could be concluded that the GO in PVDF-FS polymers was not fully reduced, though it already reach the chemical equilibrium as demonstrated in the dielectric properties.

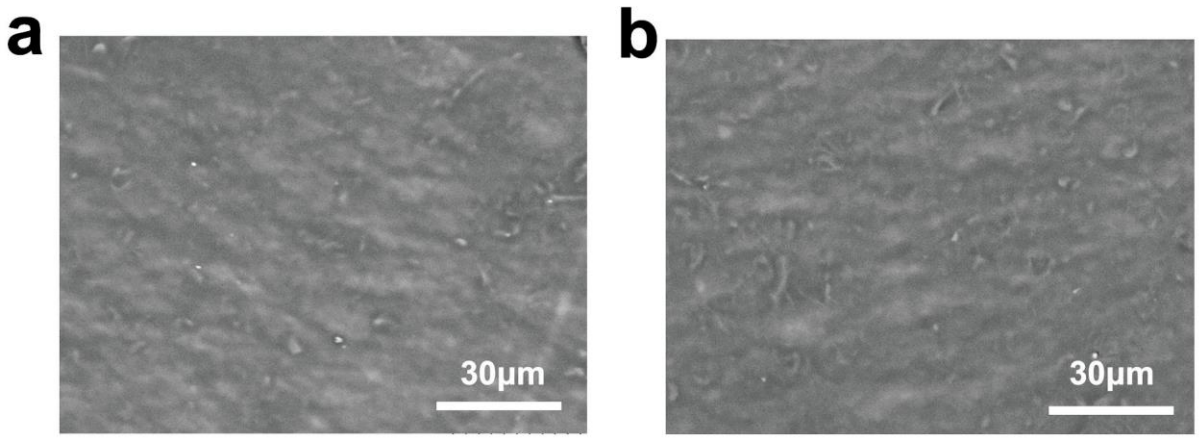

Fig 5.7 SEM images of the 4 wt% GO/PVDF-FS (left) and 4 wt% PRGO/PVDF-FS composites (right).

5.3.3 Surface morphology

The surface morphology of the 4 wt% GO/PVDF-FS and 4 wt% PRGO/PVDF-FS composites were characterized by SEM (see Fig 5.7). Both samples exhibit very smooth surfaces and no holes or wrinkles could be observed from the films.

5.3.4 Application study

5.3.4.1 Clutch performance

Firstly, symmetric clutches with total dielectric thickness of ~8 μm based on 4 wt% PRGO/PVDF-FS composites were fabricated and the clutch performance were evaluated. However, the clutch could not response under relatively low external electrical field (≤ 80 V) and breakdown of the dielectric layers were observed when the voltage went to 100 V. This result may suggest that the surface charges are dominant to the clutch performance other than the dielectric constant of the materials, since the mechanism for the huge increasement in the dielectric constant is the formation of microcapacitors in the 2D conductive nanomaterials filled composites.[23,43,44] The high performance of the asymmetric clutches in Chapter 4 also indicates the importance of the surface charges.

Interestingly, obvious current changes were observed during the experiments when the clutch was pressed by fingers. So systematic studies on the force-current of the clutch-type device were conducted.

5.3.4.2 Pressure sensing performance

The current change under a constant load of 50 N (500 kPa) was firstly investigated. The total dielectric thickness of the clutch was ~ 10 μm and the voltage was set at 2.5 V. The load profile and current changes (15 cycles) were recorded and are shown in Fig 5.8a. The proposed load profile was set as constant pressure at 500 kPa for 10 seconds, actual pressure which is a little different from the actual pressure, as shown in Fig 5.8b. The actual pressure turns out to be a crash mode, with maximum load at ~ 50 N and then decrease gradually.

The two small bulges indicate the contact and separation of the load cell and the clutch. It could be observed that the current changes almost the same as the load, making it possible for the real-time and dynamic monitoring of pressures as well as the contact and separation of external objectives. The 15 cycles give an average peak current of 751.1 ± 12.7 nA with a maximum pressure of 510.0 ± 3.0 N, while the current is lower than 1 nA without external pressure.

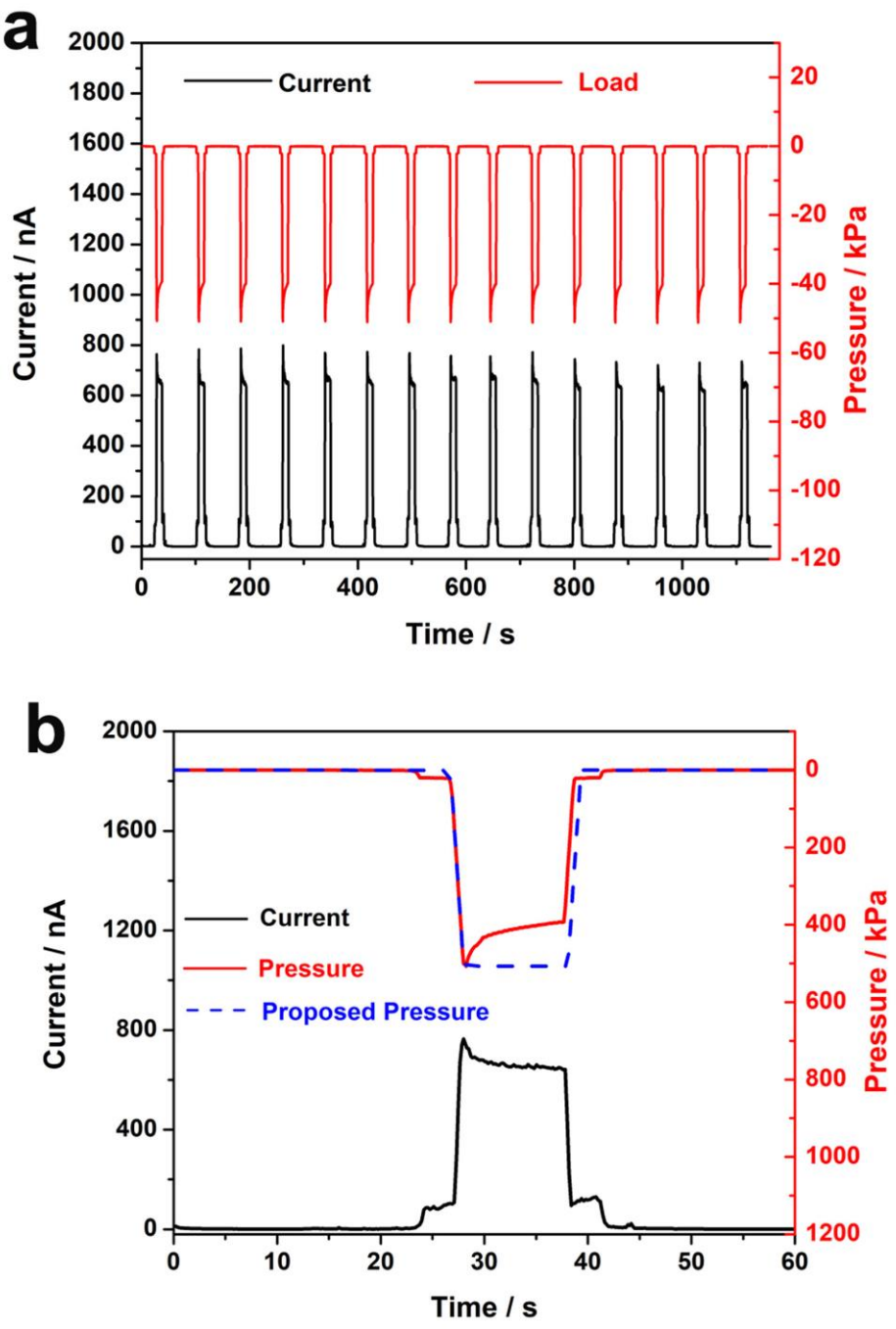

Fig 5.8 Current change of the clutch-type device under constant pressure of 500 kPa (a) 15 cycles and (b) 1 cycle with proposed load profile.

Then the current change under different external loads have also been investigated at 2.5 V with the same samples. Each load was tested for 5 times to give average current and standard deviations. All loads exhibit a similar force reduction after the crashed maximum loads and the peak currents at the maximum load are recorded and summarized in Table 5.4.

The current increases almost linearly with the pressure at relatively high-pressure range (100 kPa to 1 MPa) and the fitting result shows that I (nA) = 0.032 P (kPa) + 5.56 with a R^2 = 0.97 (see Fig 5.9a). The current change at medium pressure regime (10 kPa to 100 kPa)[45] have also been evaluated and the results are shown in Fig 5.9b. No obvious linearity is observed at medium pressure and when the pressure comes to lower than 10 kPa, the current change could be hardly observed. This result indicates the clutch-type sensors are preferred to be used under high-pressure range.

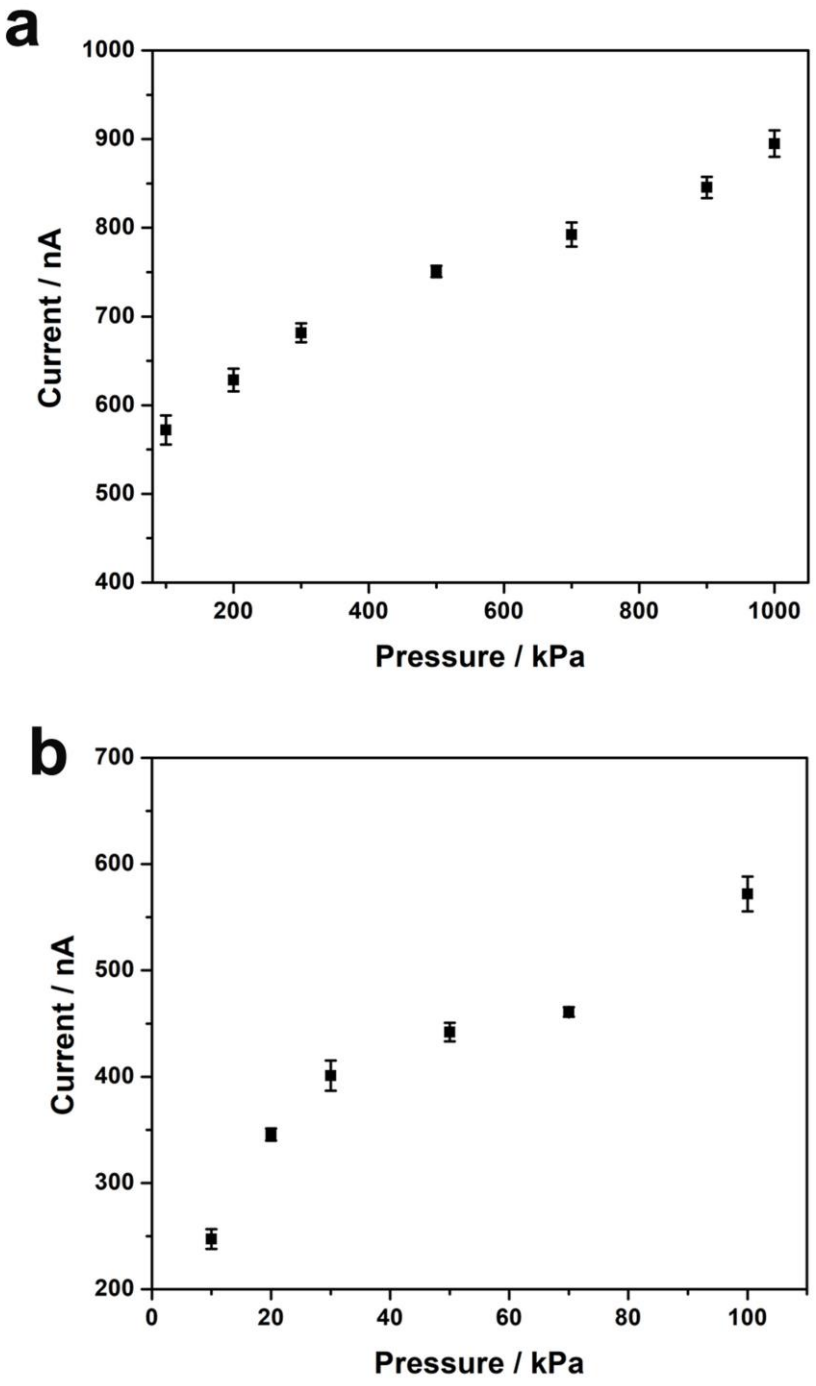

Fig 5.9 Current change of the clutch-type device under (a) high pressure and (b) medium pressure range

The long-term use of pressure sensor under was also conducted with a constant pressure of 300 kPa for 1800 s. The pressure profile and current were recorded in Fig 5.10. The applied pressure decreases dramatically from 313 kPa to 204 kPa during the first 100 seconds and then gradually decreases to 160 kPa at 1800 s. The current also exhibits the similar decreasing tendency but the drop of current is more significant from 677 nA at the beginning to 160 nA at ~ 200 s and then almost stay constant (151 nA at 1800 s), this is the typical characteristic of leakage current of capacitors.

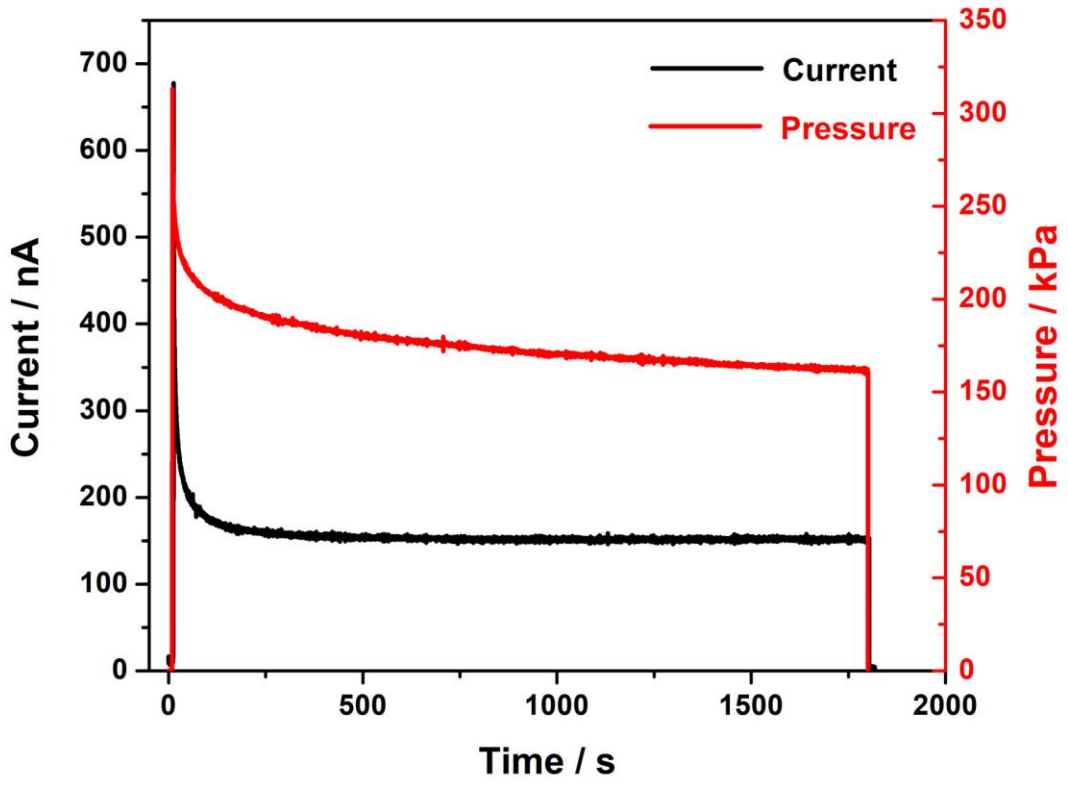

Fig 5.10 Current change of the clutch-type device for 1800 s

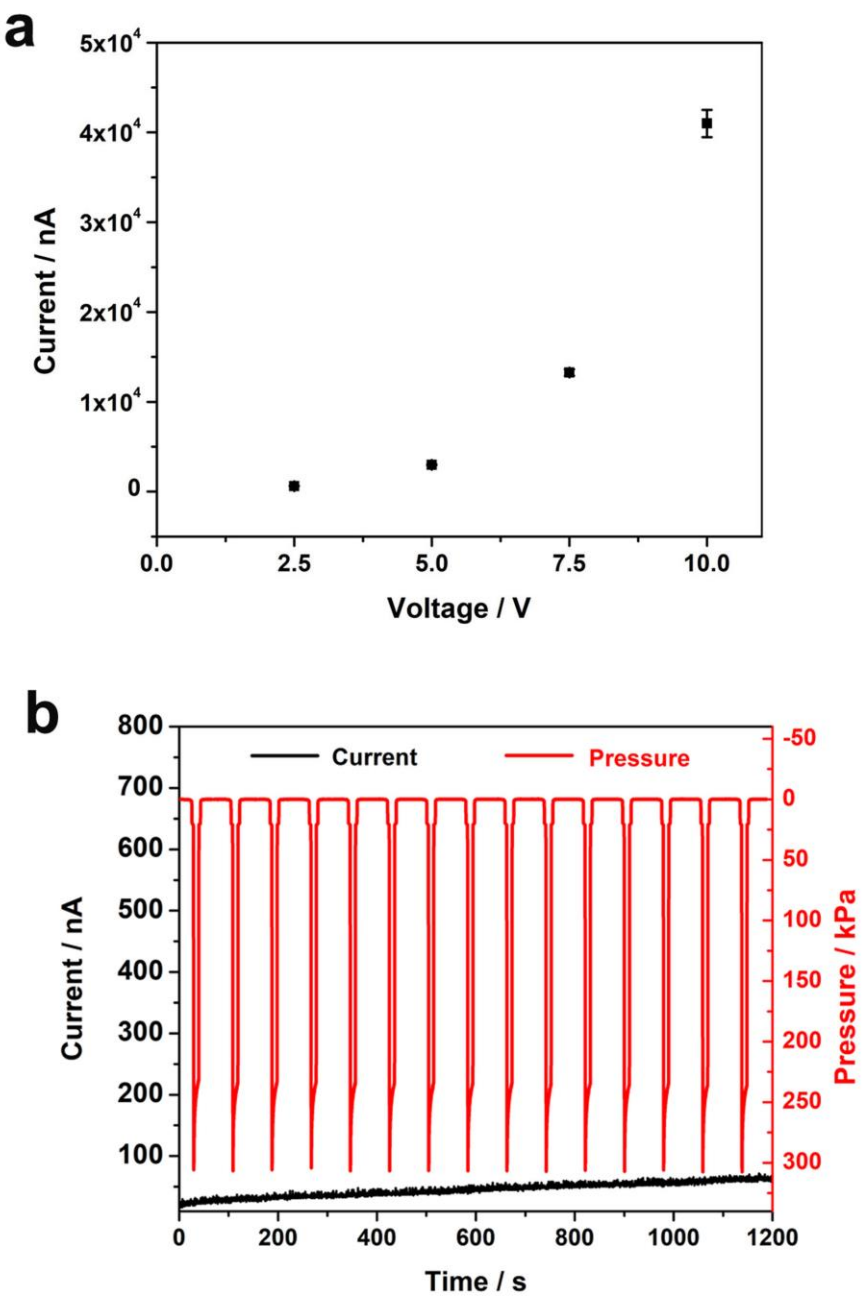

Fig 5.11 Current change of the clutch-type device under different voltage at 30 N (a). 2.5 – 10 V and (b). 0 V

Table 5.4 Current change under different pressures (V = 2.5 V, A = 1 cm^2)

Proposed pressure / kPa	**Pressure / kPa**	**Current / nA**
10	10.10 ± 0.09	247.2 ± 9.4
20	20.31 ± 0.22	345.4 ± 5.7
30	30.75 ± 0.03	401.0 ± 14.1
50	51.37 ± 0.23	441.62 ± 8.7
70	71.36 ± 0.26	460.9 ± 4.5
100	103.1 ± 0.5	572.0 ± 16.3
200	203.0 ± 0.5	628.4 ± 12.7
300	305.7 ± 1.0	679.2 ± 13.3
500	510.0 ± 3.0	751.1 ± 12.6
700	713.8 ± 0.6	791.2 ± 9.3
900	920.5 ± 1.4	845.8 ± 11.6
1000	1024 ± 1.4	883.2 ± 12.9

And then the current change with different voltages were investigated with a constant pressure of 300 kPa. The results are summarized in Table 5.5 and shown in Fig 5.11. It could be observed from Fig 5.11a that the current does not change linearly with the voltage at the same pressure. This result indicates that the working mechanism of the clutch-based sensor should not be resistance-type sensor, since the resistance is supposed to be constant at the same pressure and will increase linearly with the voltage. And the current increases gradually without applied voltage under the same load cycles, which may result from the charge accumulation at the interfaces.[46,47] And the sensor could not response when V = 0, indicating the current response is not caused by piezo or triboelectric effect (Fig 5.12).

Table 5.5 Current change under different voltages at P = 300 kPa

Voltage / V	**Current / nA**
2.5	679.2 ± 13.3
5.0	2983.2 ± 64.8
7.5	13262.8 ± 372.5
10	40998.8 ± 1518.2

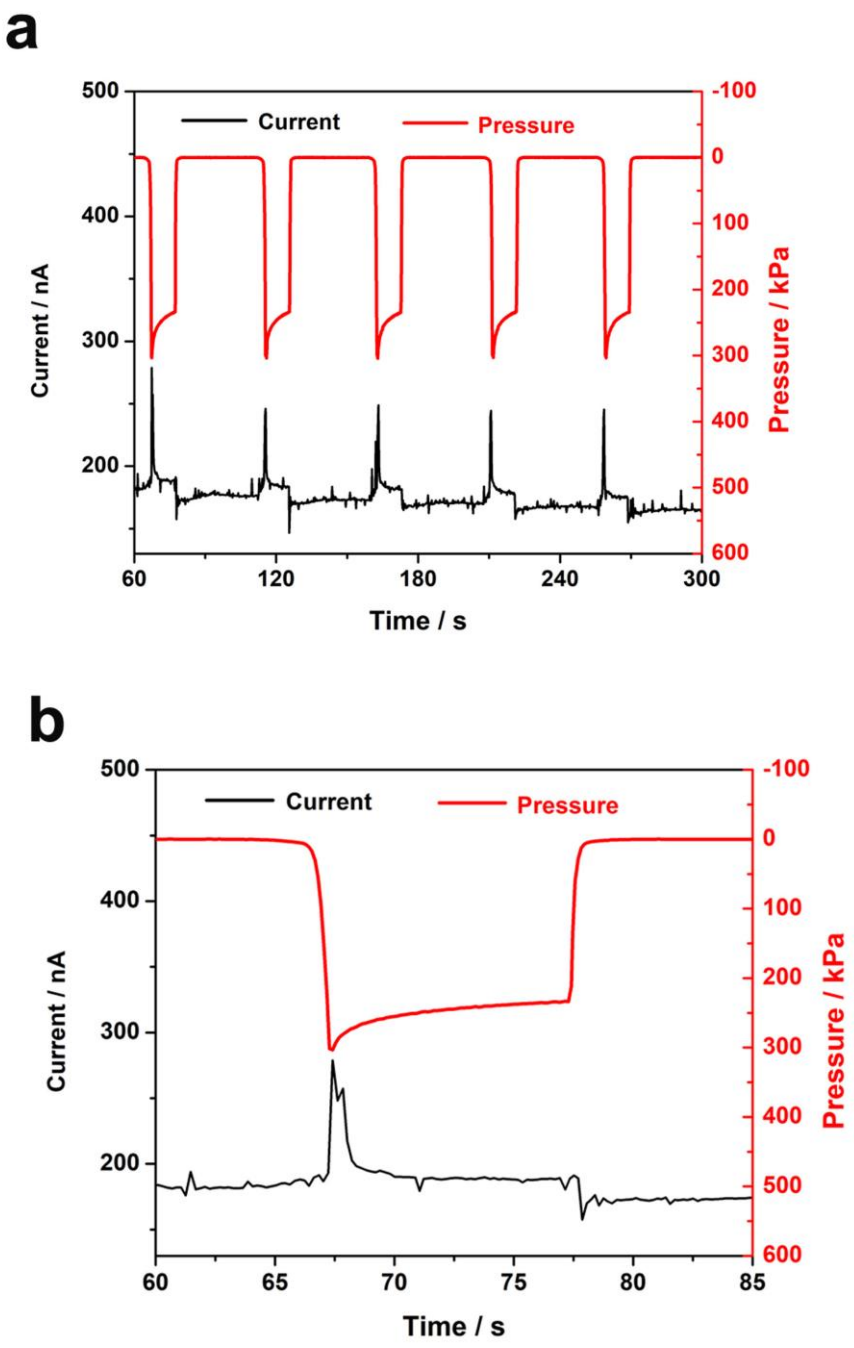

Fig 5.12 Current change of the PVDF-FS clutch at 300 kPa (V = 120 V, t = 10 μm.)

The sensing behaviour of the symmetric PVDF-FS clutch has been investigated as well. The total dielectric thickness is about 10 μm and a voltage of 120 V was given to engage the clutch. A pressure of 300 kPa was give periodically and the current change was recorded in Fig 5.12. Different from the PRGO/PVDF-FS composite, the pure polymer-based clutch exhibits capacitor-like behaviour, with a current decrease at the release of external pressure which arises from the discharging of capacitor due to the increase in dielectric thickness after removal of the pressure. This result inspires a multifunctional electroadhesive clutch strategy for wearable devices that could not only provide large holding forces but also allow real-time pressure monitoring and detection of contact and separation of external objectives.

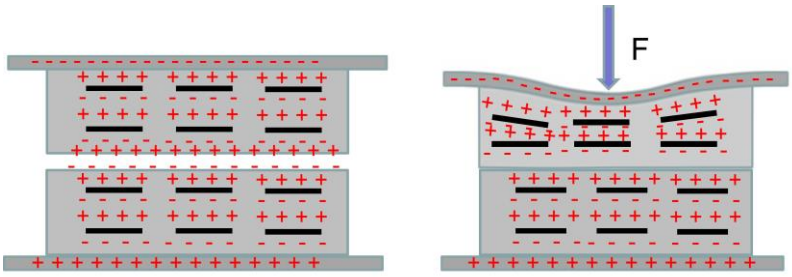

Fig 5.13 Proposed mechanism for the pressure sensing of PRGO/PVDF-FS composite

Since discharging current has not been found at 4 wt% PRGO/PVDF-FS based device (see Fig 5.8), capacitance change should not the mechanism for the current change as well. Possible mechanism is proposed based on the microcapacitor model[23,43,44] of the 2D conductive materials doped high-*k* PMCs. The conductive RGO nanoplates are

separated by the insulating PVDF-FS polymers and under an external force, the shape deformation of the composite films will lead to decreases in the distance between the two RGO "electrodes", as shown in Fig 5.13. The current is probably arised from the leakage current of the microcapacitors. And considering the ferroelectric nature of the PVDF-FS, the polarization direction will also change under external force and electrical field which will contribute to the current change as well.[48,49]

5.4 Conclusion and future works

To conclude, high-*k* polymer matrix composites based on *in situ* thermal reduction of GO in PVDF-FS terpolymers at 120 ºC under vacuum. 4 wt% PRGO/PVDF-FS exhibits a relative dielectric constant as high as 1480 with a tan δ of 0.283 at 100 Hz and the percolation threshold is near 12 wt%. The dielectric constant could be continuously tuned by simply varying the reduction time. The prototype application of the high-*k* composites in pressure sensing have been conducted. The current of the clutch-type pressure sensor changes with the applied voltages and external forces. The mechanism for the current response to external pressure is likely to be the leakage current from the microcapacitors in the high-*k* composites and the interfaces of the two pads. The sensing behaviour of the PVDF-FS based clutch may lead to multifunctional electroadhesive clutch which could provide holding force and dynamically sensing pressures simultaneously.

However, the high-*k* systems are not suitable for the clutch application, which may result from the relatively low dielectric strength and surface charges. Advanced theoretical models for the electroadhesive clutch should be established and the in-depth mechanism for the current change in the clutch-type devices should be further explored.

References

[1] M. Tian, H. Yan, H. Sun, L. Zhang, N. Ning, *RSC Adv.* **2016**, *6*, 96190.

[2] H. Sun, C. Jiang, N. Ning, L. Zhang, M. Tian, S. Yuan, *Polym. Chem.* **2016**, *7*, 4072.

[3] W. Xia, J. Lu, S. Tan, J. Liu, Z. Zhang, in *Dielectr. Polym. Mater. High-Density Energy Storage*, Elsevier, **2018**, pp. 103–163.

[4] M. Arbatti, X. Shan, Z.-Y. Cheng, *Adv. Mater.* **2007**, *19*, 1369.

[5] H. Zhang, M. A. Marwat, B. Xie, M. Ashtar, K. Liu, Y. Zhu, L. Zhang, P. Fan, C. Samart, Z. Ye, *ACS Appl. Mater. Interfaces* **2020**, *12*, 1.

[6] J. Castro, E. Rojas, T. Weller, J. Wang, in *2015 IEEE 16th Annu. Wirel. Microw. Technol. Conf.*, IEEE, **2015**, pp. 1–5.

[7] Z.-M. Dang, M.-S. Zheng, J.-W. Zha, *Small* **2016**, *12*, 1688.

[8] X. Huang, B. Sun, Y. Zhu, S. Li, P. Jiang, *Prog. Mater. Sci.* **2019**, *100*, 187.

[9] S. Liu, M. Tian, B. Yan, Y. Yao, L. Zhang, T. Nishi, N. Ning, *Polymer* **2015**, *56*, 375.

[10] Z. Chen, Y. Liu, L. Fang, P. Jiang, X. Huang, *Appl. Surf. Sci.* **2019**, *470*, 348.

[11] Y. Zhu, H. Yao, P. Jiang, J. Wu, X. Zhu, X. Huang, *J. Phys. Chem. C* **2018**, *122*, 18282.

[12] P. Ding, Y. Yang, Y. Wang, C. Liu, J. Yin, Y. Xia, A. Li, Z. Liu, *Appl. Phys. Lett.* **2019**, *114*, 053506.

[13] X.-Z. Tang, X. Li, Z. Cao, J. Yang, H. Wang, X. Pu, Z.-Z. Yu, *Carbon* **2013**, *59*, 93.

[14] Y. Zhang, Y. Wang, Y. Deng, M. Li, J. Bai, *ACS Appl. Mater. Interfaces* **2012**, *4*, 65.

[15] S. Kuester, C. Merlini, G. M. O. Barra, J. C. Ferreira, A. Lucas, A. C. de Souza, B. G. Soares, *Compos. Part B Eng.* **2016**, *84*, 236.

[16] J. Zhu, J. Shen, S. Guo, H.-J. Sue, *Carbon* **2015**, *84*, 355.

[17] Z. Zeng, H. Jin, M. Chen, W. Li, L. Zhou, Z. Zhang, *Adv. Funct. Mater.* **2016**, *26*, 303.

[18] Y. Chen, H.-B. Zhang, Y. Yang, M. Wang, A. Cao, Z.-Z. Yu, *Adv. Funct. Mater.* **2016**, *26*, 447.

[19] Y. Chen, Y. Wang, H.-B. Zhang, X. Li, C.-X. Gui, Z.-Z. Yu, *Carbon* **2015**, *82*, 67.

[20] S. Wu, R. B. Ladani, J. Zhang, K. Ghorbani, X. Zhang, A. P. Mouritz, A. J. Kinloch, C. H. Wang, *ACS Appl. Mater. Interfaces* **2016**, *8*, 24853.

[21] Z. Wang, N. M. Han, Y. Wu, X. Liu, X. Shen, Q. Zheng, J.-K. Kim, *Carbon* **2017**, *123*, 385.

[22] H. Sun, H. Zhang, S. Liu, N. Ning, L. Zhang, M. Tian, Y. Wang, *Compos. Sci. Technol.* **2018**, *154*, 145.

[23] M. H. Al-Saleh, *Nanotechnology* **2019**, *30*, 062001.

[24] J. Wang, X. Wang, C. Xu, M. Zhang, X. Shang, *Polym. Int.* **2011**, *60*, 816.

[25] H. Tang, G. J. Ehlert, Y. Lin, H. A. Sodano, *Nano Lett.* **2012**, *12*, 84.

[26] J. Guan, C. Xing, Y. Wang, Y. Li, J. Li, *Compos. Sci. Technol.* **2017**, *138*, 98.

[27] X.-J. Zhang, G.-S. Wang, W.-Q. Cao, Y.-Z. Wei, M.-S. Cao, L. Guo, *RSC Adv.* **2014**, *4*, 19594.

[28] C. Wu, X. Huang, G. Wang, X. Wu, K. Yang, S. Li, P. Jiang, *J. Mater. Chem.* **2012**, *22*, 7010.

[29] W. Li, Z. Song, J. Qian, Z. Tan, H. Chu, X. Wu, W. Nie, X. Ran, *Carbon* **2019**, *141*, 728.

[30] J. Xiao, X. Zhou, Q. M. Zhang, P. A. Dowben, *J. Appl. Phys.* **2009**, *106*, 044105.

[31] H. Xu, Z.-Y. Cheng, D. Olson, T. Mai, Q. M. Zhang, G. Kavarnos, *Appl. Phys. Lett.* **2001**, *78*, 2360.

[32] V. Bharti, Q. M. Zhang, *Phys. Rev. B* **2001**, *63*, 184103.

[33] N. Yousefi, X. Sun, X. Lin, X. Shen, J. Jia, B. Zhang, B. Tang, M. Chan, J.-K. Kim, *Adv. Mater.* **2014**, *26*, 5480.

[34] H. Luo, X. Zhou, C. Ellingford, Y. Zhang, S. Chen, K. Zhou, D. Zhang, C. R. Bowen, C. Wan, *Chem. Soc. Rev.* **2019**, *48*, 4424.

[35] M. Kobayashi, K. Tashiro, H. Tadokoro, *Macromolecules* **1975**, *8*, 158.

[36] K. Tashiro, M. Kobayashi, H. Tadokoro, *Macromolecules* **1981**, *14*, 1757.

[37] M. A. Bachmann, W. L. Gordon, J. L. Koenig, J. B. Lando, *J. Appl. Phys.* **1979**, *50*, 6106.

[38] N. M. S. Hidayah, W. Liu, C. Lai, N. Z. Noriman, C.-S. Khe, U. Hashim, H. C. Lee, in *AIP Conf. Proc. 1892*, **2017**, p. 150002.

[39] A. C. Ferrari, D. M. Basko, *Nat. Nanotechnol.* **2013**, *8*, 235.

[40] K. Yin, H. Li, Y. Xia, H. Bi, J. Sun, Z. Liu, L. Sun, *Nano-Micro Lett.* **2011**, *3*, 51.

[41] R. Larciprete, S. Fabris, T. Sun, P. Lacovig, A. Baraldi, S. Lizzit, *J. Am. Chem. Soc.* **2011**, *133*, 17315.

[42] M. Acik, G. Lee, C. Mattevi, M. Chhowalla, K. Cho, Y. J. Chabal, *Nat. Mater.* **2010**, *9*, 840.

[43] J. Shang, Y. Zhang, L. Yu, B. Shen, F. Lv, P. K. Chu, *Mater. Chem. Phys.* **2012**, *134*, 867.

[44] F. He, S. Lau, H. L. Chan, J. Fan, *Adv. Mater.* **2009**, *21*, 710.

[45] Y. Zang, F. Zhang, C. A. Di, D. Zhu, *Mater. Horizons* **2015**, *2*, 140.

[46] W. He, W. Liu, J. Chen, Z. Wang, Y. Liu, X. Pu, H. Yang, Q. Tang, H. Yang, H. Guo, C. Hu, *Nat. Commun.* **2020**, *11*, 1.

[47] Y. Noguchi, Y. Miyazaki, Y. Tanaka, N. Sato, Y. Nakayama, T. D. Schmidt, W. Brütting, H. Ishii, *J. Appl. Phys.* **2012**, *111*, 114508.

[48] J. Wu, H.-Y. Chen, N. Yang, J. Cao, X. Yan, F. Liu, Q. Sun, X. Ling, J. Guo, H. Wang, *Nat. Electron.* **2020**, *3*, 466.

[49] M. Y. Zhuravlev, Y. Wang, S. Maekawa, E. Y. Tsymbal, *Appl. Phys. Lett.* **2009**, *95*, 052902.

CHAPTER 6 Conclusions and future works

6.1 Conclusion

Flexible clutches are essential components for wearable systems where there is a need for a flexible and low-power mean to dynamically block or coupling motions. However, current research on electroadhesive clutches is still limited. Systematic and comprehensive study on electroadhesive clutches is thus of significant importance. In this thesis, the main objective of the thesis is to develop electroadhesive clutches with large shear force at a relatively low working voltage. This thesis presents a systematic study about electroadhesive clutches based on high-*k* materials and flexible electrodes. The mechanical and electrical properties of the electrodes as well as the surface morphology and dielectric properties of the dielectric materials have been characterized. The clutch performance has been evaluated with a comprehensive investigation of dielectric thickness-force, voltage-force, overlapping area-force relationships and response time. Multifunctional and mutli-mechanism clutches have also been investigated. The major conclusions are summarized as follows:

1. Symmetric electroadhesive clutches based on PVDF-FS terpolymers have been prepared through blade coating. The clutch could response at 80 V and the electroadhesive force increases dramatically with the increase of applied voltage. A shear stress over 100 kPa could be generated at 120 V (DC) and power

consumption below 20 μW. The engage time and release time are ~25 ms and ~324 ms respectively. The relatively long release time is like to be caused by the eliminated air gaps under high electrical field strength, changed physical properties of the electroadhesive pads under high electrical field strength and the charge accumulation.

2. The flexural rigidity of the symmetric clutch under 120 V increases about 2-times than the non-engaged state. The electroadhesive force under an AC square-wave voltage has also been evaluated and the AC-driving clutch exhibits a comparable shear stress as DC voltage.

3. Asymmetric electroadhesive clutches based on PU/PI, PU/PTFE have been fabricated and the influence of the charge characteristics of the dielectric polymers on the generated electroadhesive force has been investigated. The electroadhesive force will be increased when the polarity of the induced charges is the same as the charge characteristics of dielectric materials. A shear stress of ~ 200 kPa could be generated for the asymmetric PU25/PI5 clutch at 300 V with an engage time of ~ 20 ms. The release time is longer than 15 mins due to the formation of abundant hydrogen bonds at the PU/PI interface. In addition, the hydrogen bonds at the interface are found to contribute to the high electroadhesive stress.

4. The generated shear force in both symmetric and asymmetric clutches exhibit positive relation with the working voltage and overlapping area but a negative relation with the total dielectric thickness. The influence of the applied voltage turns out to be more significant among the three factors.

5. High-*k* polymer matrix composites with tunable dielectric properties based on *in situ* thermal reduction of GO in PVDF-FS terpolymers have been developed for the first time. By varying the reduction time of GO, almost linear change in dielectric constant has been observed at 100 Hz. The GO has been proved to be partially reduced (PRGO) at the relatively low reduction temperature of 120 ^{o}C. PRGO/PVDF-FS exhibits a relative dielectric constant as high as 1480 with a tan δ of 0.283 at 100 Hz with a doping ratio of 4 wt% and the dielectric constant and loss increase with the increasing doping ratio of GO. The percolation threshold is observed near 12 wt%.

6. A preliminary application study of the high-*k* PRGO/PVDF-FS composites-based clutch-type pressure sensor has been demonstrated. The current of the clutch-type pressure sensor changes with the applied voltages and external forces. The mechanism for the current response to external pressure is likely to be the leakage current from the microcapacitors in the high-*k* composites and the interfaces of the two pads.

6.2 Future works

There are still some deficiencies in the thesis due to the limited time, resource and equipment and future works could be focused on the following parts:

1. More comprehensive theoretical models should be proposed for both symmetric and asymmetric clutches. Based on the experimental results, the electroadhesive

force is proportional to $V^{4.7}$ and $V^{5.2}$, which is far away from the V^2 based on current theory. Apart from the working voltage, overlapping area and dielectric thickness, surface roughness, mechanical properties, shape deformation and the charge accumulation of the dielectric materials under electrical fields and the charge characteristics should also be considered.

2. Novel material and electrode systems and smart device structure should be developed to further reduce the working voltage to a safe value (≤ 36 V for wearable systems). And current clutches are still in planar-structure, other structures such as 1D fiber or yarn-based clutches could be developed for better integration in wearable systems. Apart from the dielectric materials, ionic elastomer or gels may also be used to lower down the driving voltage and for different applications. Asymmetric clutches based on high-*k* materials with different electron affinity could also be developed.

3. The performance of the PRGO/PVDF-FS composites-based pressure sensors could be further improved with optimized material selection and device structure. High-*k* systems with higher dielectric constant but lower dielectric loss should be developed, and other applications of the high-*k* composites should also be explored.

4. Apart from proving large shear force, the functionality of the electroadhesive clutches should be further explored and clutches with other mechanisms should also be developed to improve the clutch performance as well as expand the application scenario of the clutch.

5. Wearable systems based on electroadhesive clutch should be developed with integration of human motion-based energy harvesting systems.